A Feasibility Study of Magnetorheological Elastomers for a Potential Application in Prosthetic Devices

Ívar Guðmundsson

Faculty of Industrial Engineering, Mechanical Engineering and Computer Science
University of Iceland
2011

A Feasibility Study of Magnetorheological Elastomers for a Potential Application in Prosthetic Devices

Ívar Guðmundsson

60 ECTS thesis submitted in partial fulfillment of a *Magister Scientiarum* degree in Mechanical Engineering

Advisors
Fjóla Jónsdóttir
Christophe Lecomte
Ketill Heiðar Guðmundsson

Faculty Representative
Ragnar Sverrisson

Faculty of Industrial Engineering, Mechanical Engineering and Computer Science
School of Engineering and Natural Sciences
University of Iceland
Reykjavik, September 2011

A Feasibility Study of Magnetorheological Elastomers for a Potential Application in Prosthetic Devices.
Magnetorheological Elastomers in Prosthetics
60 ECTS thesis submitted in partial fulfillment of an M.Sc. degree in Mechanical Engineering

Faculty of Industrial Engineering, Mechanical Engineering and Computer Science
School of Engineering and Natural Sciences
University of Iceland
VRII, Hjarðarhagi 2-6
107 Reykjavík
Iceland

Telephone: 525 4600

Bibliographic information:
Ívar Guðmundsson, 2011, *A Feasibility Study of Magnetorheological Elastomers for a Potential Application in Prosthetic Devices*, M.Sc. thesis, Faculty of Industrial Engineering, Mechanical Engineering and Computer Science, University of Iceland.

Printing: Háskólaprent
Reykjavík, September 2011

Abstract

This work presents a study on the feasibility of incorporating magnetorheological elastomer (MRE) springs in prosthetic devices. MREs are composite materials that consist of micron-sized magnetizable particles embedded in a non-magnetizable elastomer matrix. They have the property of dynamically varying their mechanical properties, notably their stiffness, under the influence of a magnetic field.

The motivating application for this project is a prosthetic foot with an adaptive stiffness MRE spring. The design considerations include high stiffness, large deformations and a wide range between the off-state and on-state stiffness. An initial study of the manufacturing process of MREs is presented and the experimental test setup described. A prototype of a variable stiffness spring is designed and built, based on the initial experimental results and the requirements of a prosthetic foot. An MRE variable stiffness spring is found to have various implications in prosthetic devices, providing real-time controllable stiffness of the devices.

Útdráttur

Þessi ritgerð lýsir athugun á því hvort raunhæft sé að nota segulvirka elastómera til þess að gera stífni stoðtækja breytilega. Segulvirkir elastómerar eru samsett efni þar sem segulvirkar agnir eru blandaðar út í ósegulvirkt burðarefni. Þeir hafa þann eiginleika að geta breytt stífni sinni séu þeir bornir undir segulsvið.

Sérstaklega er litið til notkunar á segulvirkum elastómerum í gervifótum. Gervifætur eru almennt framleiddir misstífir eftir þyngd notandans og virkni í daglegu lífi en fýsilegt þykir að geta framleitt fót sem hefur stýranlega stífni. Aðferðir við framleiðslu segulvirkra elastómera eru kannaðar ásamt því hvernig mæla má stífni þeirra með og án segulsviðs. Sýni eru framleidd og stífnieiginleikar þeirra mældir með sérsmíðuðum búnaði. Frumgerð gormbúnaðar með segulvirkum elastómer er hönnuð og smíðuð með tilliti til þeirrar stífni sem búnaðurinn þarf að hafa með og án segulsviðs auk þeirra færslna sem búast má við í gervifótum. Slíkur búnaður er talinn hafa notkunarmöguleika í stoðtækjum þar sem hægt verður að stýra stífni þeirra í rauntíma.

Table of Contents

List of Figures ..... **vii**

List of Tables ..... **xi**

Abbreviations ..... **xiii**

Acknowledgements ..... **xv**

1 Introduction **1**
1.1 Motivation and background 1
1.2 Overview of the thesis 2

2 MRE technology **3**

3 Fabrication **7**
3.1 Sample fabrication 7
3.2 Particle distribution 9

4 Testing **13**
4.1 Testing setup 13
4.2 Testing Results 16

5 Prototyping **25**
5.1 Design 25
5.2 Testing and improvement 30
5.3 Further design proposals 35

6 Conclusions **39**
6.1 Discussion 39
6.2 Proposals for future work 39

References **41**

Appendix **43**

List of Figures

Figure 2.1: Schematic of MR materials..... 3

Figure 2.2: Schematic of a magnetic circuit 4

Figure 2.3:Absolute change in modulus vs. MFD for MREs with different particle concentration [1]. 5

Figure 3.1: Schematic showing the magnets, mold and MRE sample with aligned particles. 8

Figure 3.2: MRE Sample 8

Figure 3.3: Sample torn apart along 3 planes, showing the alignment of particles along the magnetic flux lines 9

Figure 3.4: SEM photo of a freeze-fractured sample of silicone-based MRE, showing slight horizontal column structures and a large agglemorate. Magnification: 2000x..... 10

Figure 3.5: SEM photo of a torn-apart sample of a silicone-based MRE. Magnification: 600x..... 11

Figure 3.6: SEM photo of a knife-cut sample of silicone-based MRE, showing a slight horizontal tendence of the CIP particles. Magnification: 1000x..... 11

Figure 3.7: Photo of a silicone sample, taken through an optical microscope...... 12

Figure 3.8: Photo of a polyurethane sample, taken through an optical microscope. 12

Figure 4.1: Schematic of the testing apparatus. Isometric section view. 14

Figure 4.2: Magnetic flux density vector sum of the testing apparatus as presented by the FEM program. 14

Figure 4.3: Flux lines through the testing apparatus and MRE sample as presented by the FEM program. 15

Figure 4.4: Testing rig 15

Figure 4.5: Fracture at high strain 16

Figure 4.6: Off-State and on-state stiffness of the samples at 15% strain 17

Figure 4.7: Photo of two polyurethane samples (upper no. 14, lower no. 15), taken through an optical microscope. 18

Figure 4.8: Compression testing results for an isotropic sample (blue: off-state, red: on-state) and an aligned sample (green: off-state, black: on-state) 19

Figure 4.9: Comparison of the off-state and on-state elastic modulus vs. strain of sample no.2. 20

Figure 4.10: Absolute MR effect - The difference between off-state and on-state elastic modulus vs. strain. 20

Figure 4.11: Relative MR effect - The relative difference between off-state and on-state elastic modulus vs. strain 21

Figure 4.12: Comparison of the off-state and on-state spring rate vs. strain of sample no. 2. 21

Figure 4.13: The difference between off-state and on-state spring rate vs. strain 22

Figure 4.14: The relative difference between off-state and on-state spring rate vs. strain 22

Figure 5.1: The Re-Flex Rotate™ prosthetic foot. 26

Figure 5.2: Axisymmetric cross-section schematic of the magnetic circuit in the Rheo Knee. 27

Figure 5.3: Magnetic flux density in the RheoKnee® [20] 28

Figure 5.4: Isometric cross section of an MRE spring 29

Figure 5.5: A prosthetic foot with an MRE spring used on the vertical axis. 30

Figure 5.6: Flux lines of the magnetic circuit in the RheoKnee 31

Figure 5.7: Magnetic flux density in the RheoKnee 31

Figure 5.8: Flux lines in the RheoKnee® when steel blades are replaced by MR fluid. 32

Figure 5.9: Magnetic flux density in the RheoKnee when steel blades are replaced by MR fluid. 32

Figure 5.10: Magnetic flux density of the MRE spring. 33

Figure 5.11: Magnetic flux density of the MRE spring with no gap. 34

Figure 5.12: Magnetic flux density of the MRE spring with smaller hole. 34

Figure 5.13: Magnetic flux density with a larger coil and higher current . a) The whole MRE Spring unit. b) A closer look of the MRE section 35

Figure 5.14: Various placements of MRE springs within prosthetic feet. a) Vertical axis b) Basic wedging idea c) Vertical wedge d) Heel wedge

e)Vertical/Heel wedge f) Heel/toe wedge g) MRE springs within an inert elastic medium 36

Figure 5.15: Various designs for MRE springs [18]. a) MRE with shear strain applied b) MRE in tension/compression c) MRE in compression. 37

List of Tables

Table 3.1: Properties of CIP [14, 16]. 7

Table 4.1: MRE samples and measuring results at 15 % strain. 17

Abbreviations

CIP: Carbonyl Iron Powder

FEM: Finite Element Modeling

MFD: Magnetic Flux Density

MR: Magnetorheological

MRE: Magnetorheological Elastomers

Off-state: In the absence of a magnetic field

On-state: Under the influence of a magnetic field

PU: Polyurethane

SEM: Scanning Electron Microscopy

T: Tesla

Acknowledgements

Firstly, I would like to thank my advisors, Dr. Fjóla Jónsdóttir, Dr. Ketill Heiðar Guðmundsson and Product Lead Engineer Christophe Lecomte. Special thanks go to Engineer Freygarður Þorsteinsson for the initial idea of using MREs in prosthetics and for his advice. Additionally I would like to thank all the staff at Össur that provided practical advice, equipment, time and craftsmanship. Jóhannes Brandsson at Spennubreytar ehf. has my gratitude for helping with designing and winding a large electric coil and Dr. Birgir Jóhannesson at the Innovation Center Iceland for operating the Scanning Electron Microscope. This project was funded by the Icelandic Centre for Research and by Össur.

1 Introduction

1.1 Motivation and background

One of the most important design goals of prosthetic devices is to provide the appropriate level of stiffness for the user. However, this is not as simple as constructing a fixed stiffness device for a specific person. Ideally, the stiffness of the device would change dynamically in response to his or her current demands. A variable stiffness prosthetic device would mean improved quality of life for the amputee, as the device changes its characteristics in response to the current activity level. High stiffness is required in more demanding tasks while low stiffness is more convenient while at rest or moving casually.

A variable stiffness prosthetic device can be constructed using various mechanical methods, which may require cumbersome mechanisms and manual interference of the user. Another method of varying the stiffness would be to use an adaptive, controllable smart material, such as magnetorheological elastomers (MREs). This is a class of composite materials that consist of micron-sized magnetizable particles embedded in an inert elastomer matrix. Typically, a carbonyl iron powder is mixed with silicones, polyurethanes or natural rubber. MREs change their mechanical properties, notably their stiffness, dynamically when subjected to a magnetic field and the response from low to high stiffness is almost instantaneous [1, 2]. Proposed applications of MREs include automotive bushings [3] and vibration absorbers [4] as well as actuators [5]. However, existing commercial applications are rare and the development and characterization of the materials are yet in the early stages. The application proposed in this paper is to use MRE materials for a dynamically adaptable stiffness prosthetic device, specifically a carbon-fiber prosthetic foot.

The behavior of MREs under the influence of a magnetic field has been studied by a number of research groups, see for example [1, 6-12]. In order to describe this behavior, terms like the MR effect are used, which is the difference or the ratio between an elastic modulus with applied magnetic field (on-state) and the same modulus with no field applied (off-state). Factors that affect the MR effect include the initial elastic modulus of the matrix, the particles' magnetic properties, size and concentration, the alignment of particles within the matrix and the use of additives for better matrix-particle interaction. The reported results differ considerably, based on the materials and methods used. In the literature, MREs with initial off-state elastic modulus from around 100 kPa to a few MPa are found to increase their stiffness considerably, even more than 100% [7, 9, 10]. Some researchers have reported that the MR effect depends on strain amplitude [1]. However, considerable MR effect has been found for large strains of up to 100% [13]. The effect of cyclic deformation on MREs has been investigated by Zhang et al. [13], who finds the fatigue properties of the MREs to be significantly affected by the particle concentration. Keeping a low particle concentration could be needed to maintain decent mechanical strength.

MREs under the influence of a magnetic field can deform because of inter-particle magnetic forces, an effect called magnetostriction. For example, Diguet [8] has found deformation of up to 9,2 % in an MRE with low off-state elastic modulus. The deformation was found to be dependent on the aspect ratio of the MRE sample, decreasing with increased thickness of the MRE. Although it may have promising implications in actuators, the effect of magnetostriction can affect the feasibility of using MREs as spring members in structures if the applied strains are of similar or less magnitude as the strains induced.

A comprehensive characterization of MREs is currently not available and bulk MRE material is, to this date, not commercially available. Motivation through new applications could be the key for further development and optimization of the materials, their characterization and stable manufacturing.

1.2 Overview of the thesis

In this thesis, the feasibility of integrating magnetorheological elastomers in prosthetic devices is studied. A particularly motivating application is considered - a variable stiffness spring in a prosthetic foot. The goal is to investigate some basic characteristics of the MRE composite, make proposals for application methods and to make a first prototype.

Chapter 2 serves as an introductory chapter to acquaint the reader with the technology of MR Elastomers. In Chapter 3, the fabrication process of silicone- and polyurethane based MREs with micron-sized iron particles is described. Chapter 4 contrains a description of the equipment and methods for investigating the MR effect, followed by testing results for cylindrical MRE specimens. Chapter 5 describes the prototyping of one particular design of an MRE spring that has potential application in prosthetics. Further application possibilities in lower limb prosthetics are then discussed. Chapter 6 concludes the thesis with discussion and proposals for future work.

2 MRE technology

Magnetorheological materials are a class of smart materials of which some mechanical properties can be controlled by an external stimulus. These materials are further classified into MR fluids and MR elastomers and other classes, such as, MR gels and foams. They all are composites constituting of magnetizable particles within a non-magnetizable medium. When magnetic field is applied, the particles become magnetized, resulting in inter-particle forces. These forces affect the mechanical properties of the composite as a whole, giving the MR fluids a controllable yield stress while the MR elastomers have a controllable elastic modulus. Figure 2.1 shows a schematic of MR materials.

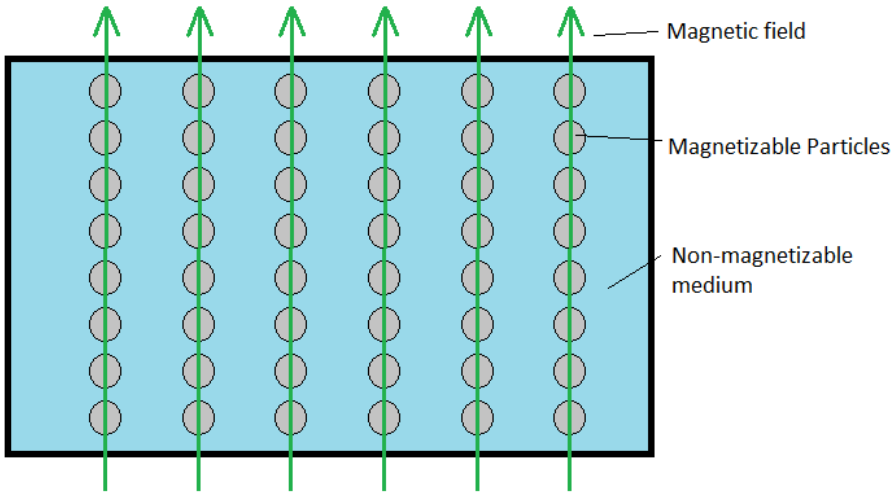

Figure 2.1: Schematic of MR materials

Research on MR materials was first published by Rabinow 60 years ago [14], but interest in the technology started to develop after the commercialization of computer processors. MR technology has more implications when coupled with automatic control systems considering the quasi-instantaneous response of the materials to the magnetic field. While MR fluids have found commercial applications in dampers, breaks and clutches, no device utilizing MREs has been commercialized [15]. Therefore, MR elastomers have undergone much less research than MR fluids.

Although no commercially available technology utilizes MREs, a number of research groups have investigated their behaviour. For a non-magnetizable medium or matrix material, silicones, natural rubbers and polyurethanes are most commonly used. The magnetizable particles ideally have a high magnetic permeability and low remnant magnetization. Magnetic permeability is a measure of how much a material is magnetized under a magnetic field. Remnant magnetization describes how much magnetization remains in the material after it ceases to be under magnetic field. Carbonyl iron powders are generally preferred as particles, with particle size usually on

the order of a few microns. To produce MREs, the CIP is mixed with the matrix material and the composite allowed to cure [15].

Stiffness is the mechanical property that undergoes most change when a magnetic field is applied on an MRE. To describe how effectively an MRE changes this property, the term MR effect is used. The MR effect can be either the relative change in elastic modululs or the absolute change. A number of factors have been shown to affect how great the MR effect will be. The absolute MR effect has been shown to be independent on the nominal stiffness of the matrix material itself [11]. This means that using a softer matrix material will allow for a greater relative MR effect. Curing the material under magnetic field will align the particles in chained structures along the magnetic flux through the material. After the matrix material is cured, this is the lowest energy state for the particles to be in when under the influence of a magnetic field. Thus, deforming the MRE in on-state will require that the particles go to a higher energy state, resulting in magnetic forces. Research has shown that MREs with aligned particles show more MR effect than MREs with an isotropic distribution of the particles [15]. The off-state stiffness of a composite of particle-loaded elastomer increases as the particle concentration increases. As the off-state stiffness increases, a decrease in MR effect is to be expected. The optimal particle concentration has been predicted to be 27 % with a mathematical model [2] which has been confirmed with both earlier and more recent modeling and experimental results [1, 10].

To make full use of the smart qualities of MREs, a suitable magnetic circuit has to be present to apply magnetic field.

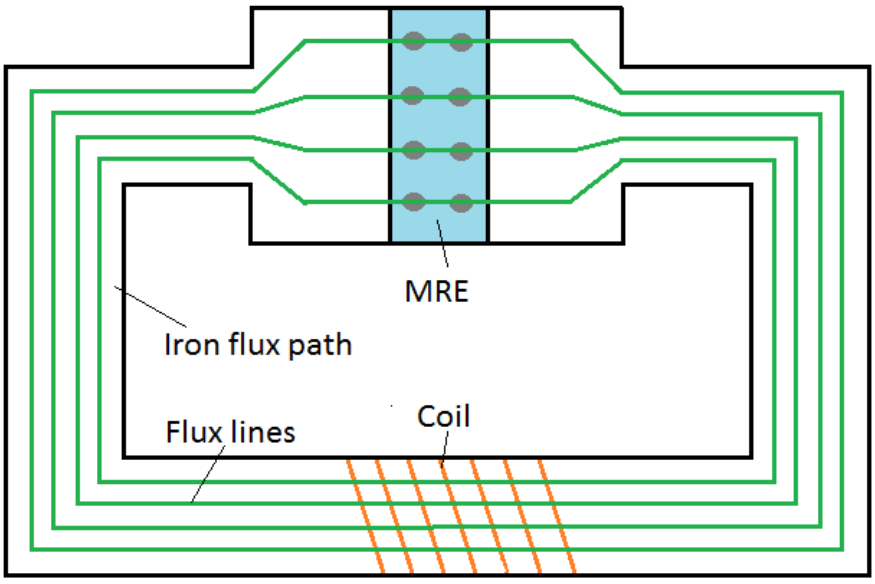

Figure 2.2: Schematic of a magnetic circuit

A schematic of a magnetic circuit can be seen in Figure 2.2. The basic function of such a circuit is that the current through the turns of the coil induce a magnetic field H which has strength according to equation (1),

$$H = \frac{NI}{L} \qquad (1)$$

Here, N represents number of turns in the coil, I represents electrical current and L is length of the coil. The coil is wound around a core made of material with high magnetic permeability, typically iron. High magnetic permeability, μ, means that high magnetic flux density, B, is induced in the core by the magnetic field H. This can be seen in equation (2)

$$B = \mu H \qquad (2)$$

The magnetic flux density is a measure of magnetic flux per unit area and is schematically represented in Figure 2.2 as the density of the flux lines. Its unit is the Tesla (T). Magnetic flux density can be induced in the iron core up to a certain value of saturation, typically around 2,1 T. Surrounding the structure, air has negligible magnetic permeability and thus the magnetic flux is directed along the iron structure with practically no flux leakage. As the cross-sectional area of the flux path increases, so decreases the magnetic flux density. Given a certain MFD in the iron core, lets say 2,1 T, if the cross-sectional area increases by a factor of 3 the MFD will decrease to 0,7 T. If the MRE has iron particles with the same saturation value as the core, at a concentration of 33%, then the effective cross-sectional area will decrease again by a factor of 3 and the particles will be saturated with an MFD of 2,1 T. The MFD through such an MRE will still be measured at 0,7 T. Figure 2.3, adapted from a study by Jolly [1], shows how MREs with more particle concentrations have higher saturation MFD.

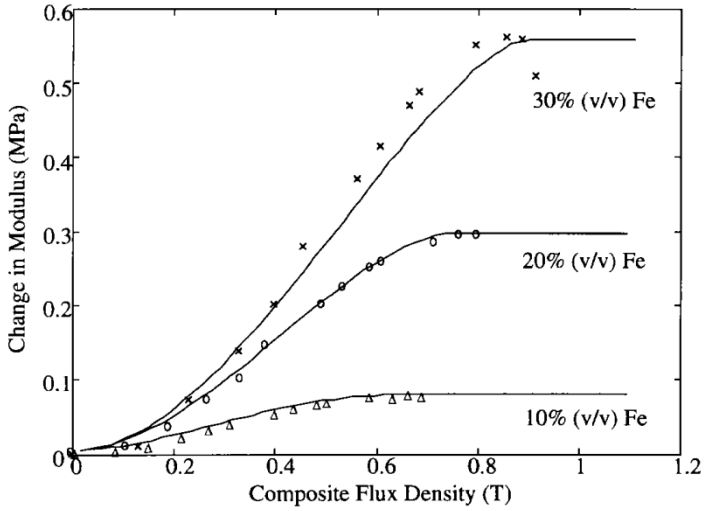

Figure 2.3:Absolute change in modulus vs. MFD for MREs with different particle concentration [1].

The above analysis is a simplification. In reality, a flux leakage to the surroundings may be expected, especially at the coupling between iron and MRE since the permeability of MRE is considerably lower than that of iron. Furthermore, the permeability of materials is usually not constant. Instead, the relationship between B and H is described with a nonlinear B-H curve.

3 Fabrication

3.1 Sample fabrication

For the MRE material testing, cylindrical samples with height 20 mm and diameter 25 mm were fabricated, using two different types of matrix materials and two types of iron particles. The first matrix material was Wacker Dental ADS 931 two-component silicone. The second was Axson UR/5801/5825 Polyurethane Casting Resin. The choice of the Wacker silicone elastomer was based on the convenient in-house availability of the material during the research period. However, the high viscosity of the uncured material as well as its extremely short curing time (approximately 1 hour) reduced the workability and made the mixing of particles difficult. Therefore, the polyurethane was also used for comparison. The polyurethane has much lower uncured viscosity and the mold time is 24 hours, thus allowing for the proper mixing of the particles, as further described below.

The particles used were BASF CM and BASF CC carbonyl iron powder. Their properties are shown in Table 3.1. The CM particles are somewhat larger and according to previous research they should be able to provide a larger MR effect [12]. In all the samples fabricated, a particle volume fraction of 27% was used. This particle concentration has been shown to be optimal in terms of the acquired MR effect [2].

Table 3.1: Properties of CIP [14, 16].

Grade	Min. Iron content [g/100g]	Coating	Max. Carbon content [g/100g]	Oxygen content [g/100g]	Particle size d 50 [μm]	Tap density [g/cm^3]
CM	99,5	None	0,03	0,10 - 0,25	7,0 - 9,5	3,7 - 4,4
CC	99,5	Silicated	0,05	0,18 - 0,35	3,8 - 5,3	3,9 - 4,3

The fabrication methods for the silicone and the polyurethane differed, depending on the curing properties of the material.

For the silicone the method was as follows:
First, the appropriate mass of each silicone component and carbonyl iron powder was put into beakers. The iron powder was thoroughly mixed into each silicone component by kneading for a few minutes. Then the components were poured into a mixing syringe. The mixing syringe was used to mix the components together and thrust the mixed silicone into the aluminum mold. The mold was then immediately placed in between two 50mm x 50mm x 25mm Neobdymium magnets.

An improved method of fabrication was used for the polyurethane:
The longer curing time of the polyurethane gave more time for mixing operations. First the CIP was mixed into the UR 5801 with a high-shear mixer for about 5 minutes. Then a Sonicifier2000 ultrasonic machine was used for 3 minutes for the purpose of splitting agglomerated CIP particles. This method is used by Össur to prevent agglomeration in MR fluids. The UR 5825 was then mixed into the blend of UR5801 and CIP and all

thoroughly mixed with a high-shear mixer for 2 minutes. The blend was then placed in vacuum of -1 bar for degassing, for 5 minutes, until no new bubbles were seen forming on the surface. The blend was then poured into the mold, the mold further degassed in -1 bar vacuum for 2 minutes and the mold then placed between the magnets as was done with the silicone. The polyurethane samples were left to cure for 24 hours before releasing them from the mold and then left to fully cure for at least 72 hours before any mechanical testing was performed.

Figure 3.1 shows a schematic of the sample inside the mold between the magnets and the alignment of the particles resulting from the magnetic field. Figure 3.2 shows an MRE sample.

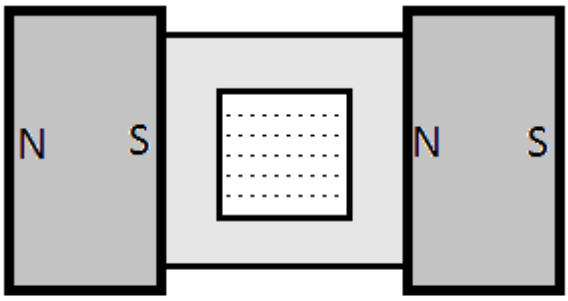

Figure 3.1: Schematic showing the magnets, mold and MRE sample with aligned particles.

Figure 3.2: MRE Sample

The magnetic flux density was measured with a Tel Atomic Smart Magnetic Sensor at one side of the aluminum mold, between the mold and the magnet. The magnetic flux

density varied from 0,5 T at the edge of the mold to 0,57 T in the middle of the cross-section. A magnetic flux density of this magnitude was considered sufficient to align the particles along the direction of flux.

3.2 Particle distribution

Flux density of over 0,5 T was thought to be sufficient to align the carbonyl iron particles in columnar structures along the direction of flux. This anisotropy in the alignment was confirmed by tearing samples apart along three perpendicular planes, whereas two of them were parallel to the flux lines and one was perpendicular to the flux lines. As seen in Figure 3.3, when tearing along the flux lines, the samples went apart along the intended plane. On the contrary, when tearing perpendicularily to the flux, the sample cracked perpendicular to the intended plane so the crack developed along the flux. This indicates that the anisotropic distribution of the particles with aligned structures along the flux lines dominates the cracking or tearing behaviour of the sample over the internal forces of the matrix material. This behaviour was confirmed both in silicone- and polyurethane samples.

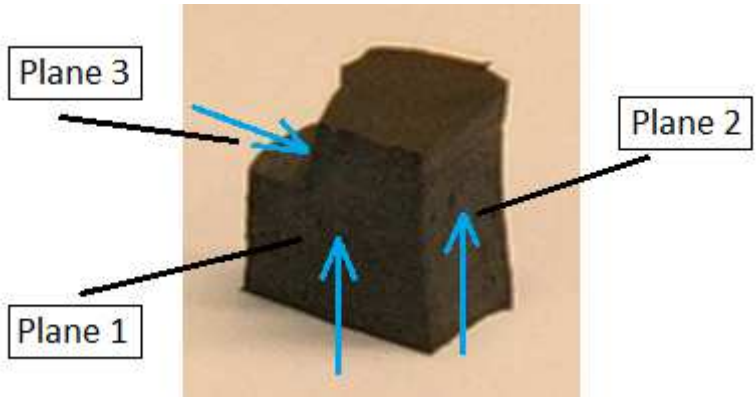

Figure 3.3: Sample torn apart along 3 planes, showing the alignment of particles along the magnetic flux lines

To further investigate the distribution of the particles within the matrix, scanning electron microscopy was considered. However, the columnar structures of the particles have been shown to be undetectable by inspection when the particle concentration is high, as shown in a study by Boczkowska [17]. At low concentration the particles align themselves in very distinctive columns but when the particle concentration is near to 30% vol./vol. it becomes impossible to distinguish between a highly anisotropic distribution and a slightly less anisotropic distribution by eye. In that same study by Boczkowska, the anisotropy of the particle distribution was assessed with an image analysis which showed good results [17]. For the porposes of this study it was therefore deemed that SEM photography, would not be suitable for assessing wheather the alignment differs between methods and materials used. The image analysis method should be kept in mind for possible further studies.

Although not suitable for comparison between fabrication methods, a few SEM photos were taken of silicone-based samples to investigate the particle distribution. Three methods were used to prepare samples for the SEM photography.

- Freeze-fracturing. The samples were frozen in liquid nitride and broken in two with a hammer.
- Tearing-apart. The samples were torn apart with hands.
- Knife-cutting. The samples were cut with a surgical knife

The surface of each sample was then gold-plated.

Figure 3.4, Figure 3.5 and Figure 3.6 show images for freeze-fractured, torn-apart and knife-cut samples, respectively. The freeze-fracturing method in Figure 3.4 is considered to give the clearest portrait of the particles and their distribution. The tearing-apart method results in a rather unclear picture (Figure 3.5). The surface seems to be rough, made up of loose particles and vacant holes of silicone, where particles have been pulled out. Similarly, for the knife-cut method, the black dots seen in Figure 3.6 are vacancies of particles that ended up on the other side of the knife's cut. Some anisotropy, represented by slightly horizontal columnar structures can be seen from all the three photos, the clearest being Figure 3.4, where columns have been marked with yellow lines.

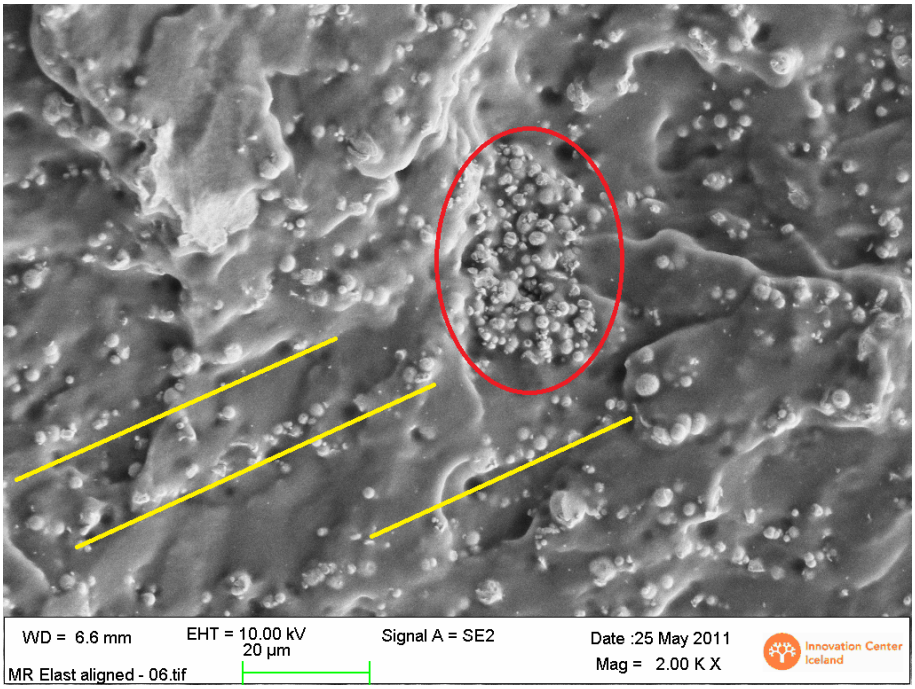

Figure 3.4: SEM photo of a freeze-fractured sample of silicone-based MRE, showing slight horizontal column structures and a large agglemorate. Magnification: 2000x

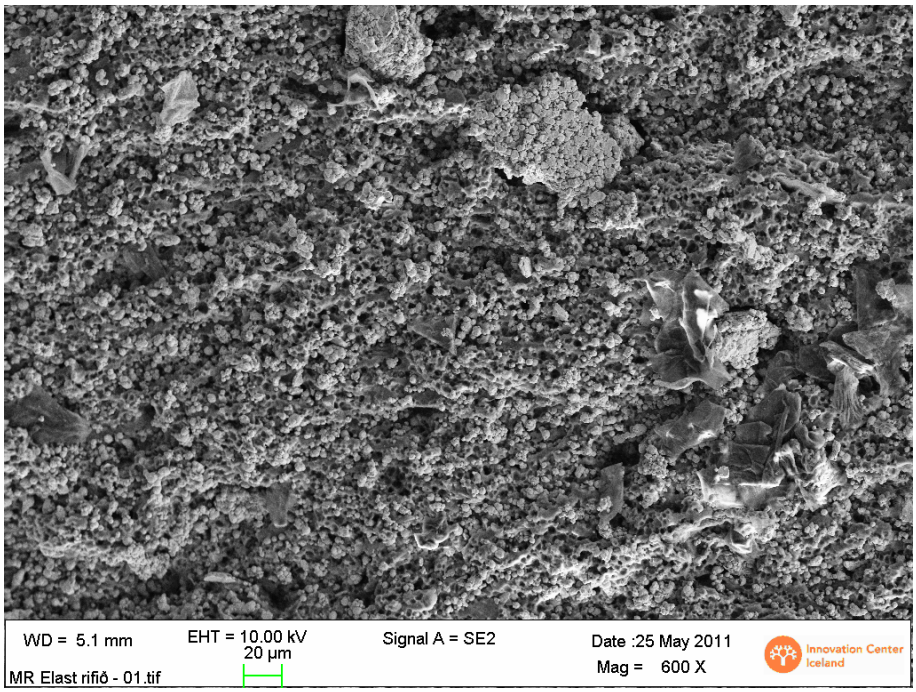

Figure 3.5: SEM photo of a torn-apart sample of a silicone-based MRE. Magnification: 600x

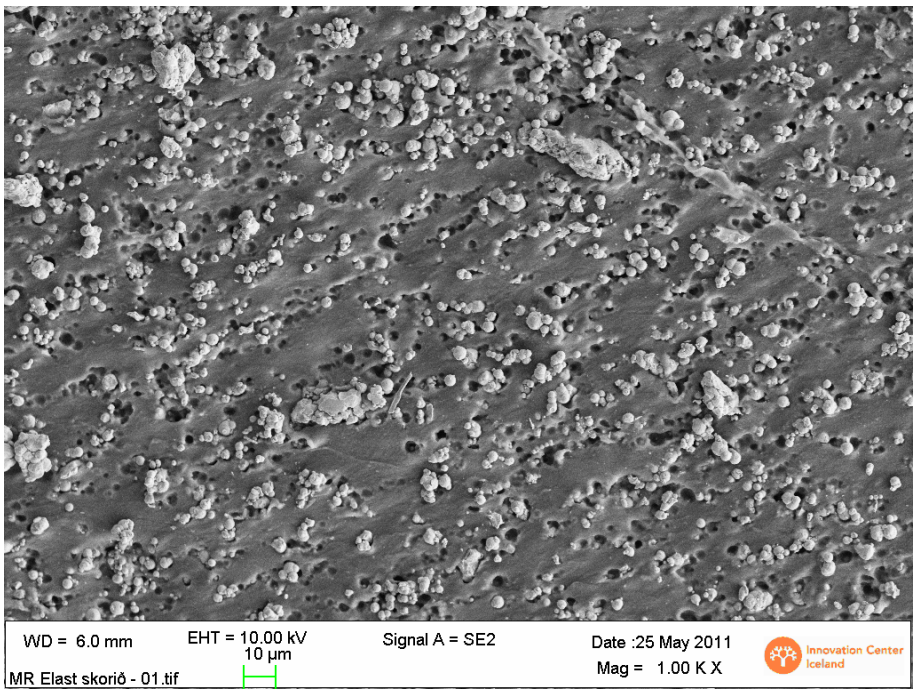

Figure 3.6: SEM photo of a knife-cut sample of silicone-based MRE, showing a slight horizontal tendence of the CIP particles. Magnification: 1000x

In addition to showing anisotropy in particle distribution, Figure 3.4 shows a large agglomerate of particles, marked with red. A high number of large agglomerates were seen across the SEM sample, which was silicone-based. A comparison was made of the agglomeration of particles in silicone samples and polyurethane samples. Figure 3.7 and Figure 3.8 are photos, taken through the lense of an optical microscope, showing the

cross-section of a silicone-based sample and a polyurethane-based sample respectively. Glares of white can be seen on the silicone-based sample where light is reflected from large agglomerates while the agglomerates appear much smaller on the polyurethane-based sample. This is considered to be a result of a better fabrication method for the polyurethane, as described in last section, including the splitting of agglomerates with sonic waves.

Figure 3.7: Photo of a silicone sample, taken through an optical microscope.

Figure 3.8: Photo of a polyurethane sample, taken through an optical microscope.

4 Testing

For the purpose of evaluating the MR effect obtainable with the materials and methods described above in chapter 3, the samples were tested in axial compression and their load-displacement curves investigated. The compression mode was chosen over shear or tension, based on the results from the study of Albanese-Lerner, which indicated that compression would yield the strongest MR effect [18]. Measurements were made on a total of 17 samples, with either silicone or polyurethane as matrix material and BASF CM or BASF CC carbonyl iron particles. Samples had either an aligned or isotropic particle distribution. Special testing apparatus was built to apply magnetic field for the on-state compression testing.

4.1 Testing setup

For testing the stiffness of the MRE samples under magnetic field, a testing apparatus was built. Prior to it‘s construction, a study was made to ensure that it would meet its purpose, which was to ensure a uniform magnetic flux through the MRE sample, with an MFD of about 0,6 to 0,7 T. According to the reports of other research groups, such testing apparatus would consist of a large copper coil, surrounded by a steel frame, and steel grips that would direct the magnetic flux through the MRE sample, which would be placed in the middle of the coil [10, 19]. Furthermore, the coil would consist of approximately 5000 turns of 20 AWG copper wire [19]. Suitable DC current through the coil was presumed to be on the order of magnitude of 1 Ampere to avoid excess heating.

An axisymmetric finite element model was built to aid the design of the testing apparatus and to evaluate the MFD attainable. The model included B-H curves of the materials, which represent their nonlinear magnetic bahaviour. The B-H curves for the steel and MR elastomer were the same as used by Jonsdottir et al. in a finite element study of an MR fluid device [20]. Specifically, for the MR elastomer, a B-H curve of an MR fluid (Lord MRF-336AG) was used, since no B-H curve was found for an MRE. The assumption was made that the magnetic properties of the MR elastomer would be similar to those of the MR fluid. This assumtion was based on the fact that the magnetic properties of the materials of which an MRE consists are similar to those of an MR fluid. Furthermore, the proportions of the composites‘ materials are similar, as well as their on-state particle distribution. Therefore, the best approximation to a B-H curve for an MRE would be that of an MR fluid. These approximations were considered to give results that should be accurate enough for the purposes of aiding the design of the testing apparatus.

Figure 4.1 shows a schematic of the chosen design of the testing apparatus. The coil is 70mm long with inner radius 27mm, outer radius 174mm and 5548 windings of 20 AWG copper wire. 66 Volts are needed to run a current of 1 Ampere through the coil. A cylindrical steel construction around the coil and steel grips direct the magnetic field uniformly through the MRE sample. The thickness of the steel construction is 12 mm. Figure 4.2 and Figure 4.3 show the MFD vector sum and magnetic flux lines in the

testing apparatus, as presented by the finite element program. It could be seen from the model that this design would yield sufficiently uniform magnetic flux with density of 0,69 T at the surface of the MRE sample.

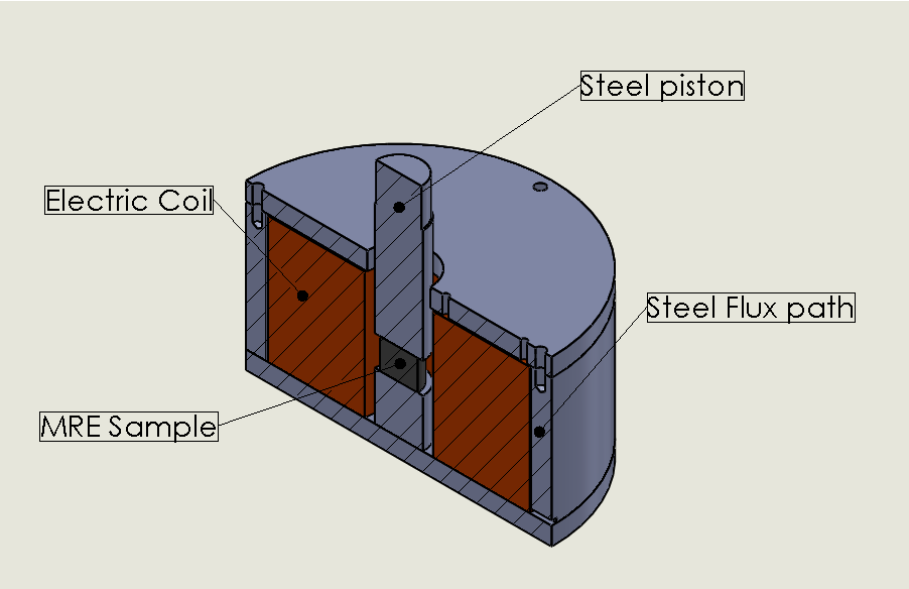

Figure 4.1: Schematic of the testing apparatus. Isometric section view.

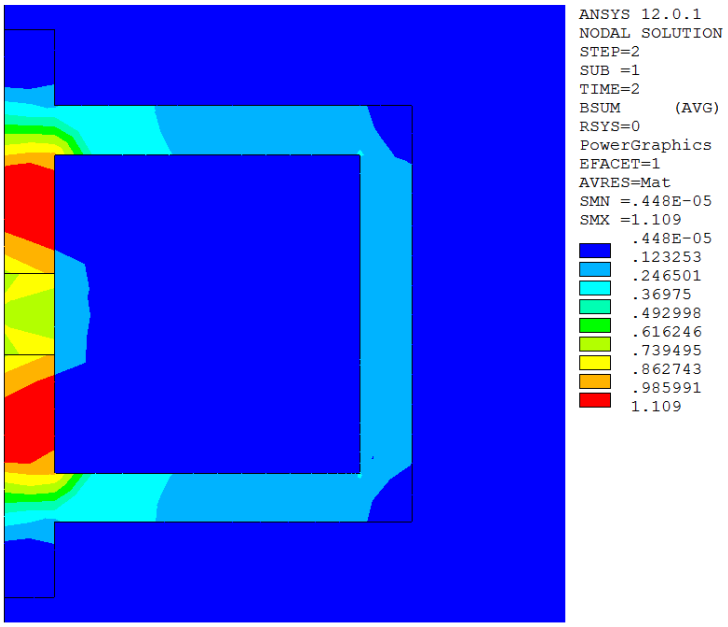

Figure 4.2: Magnetic flux density vector sum of the testing apparatus as presented by the FEM program.

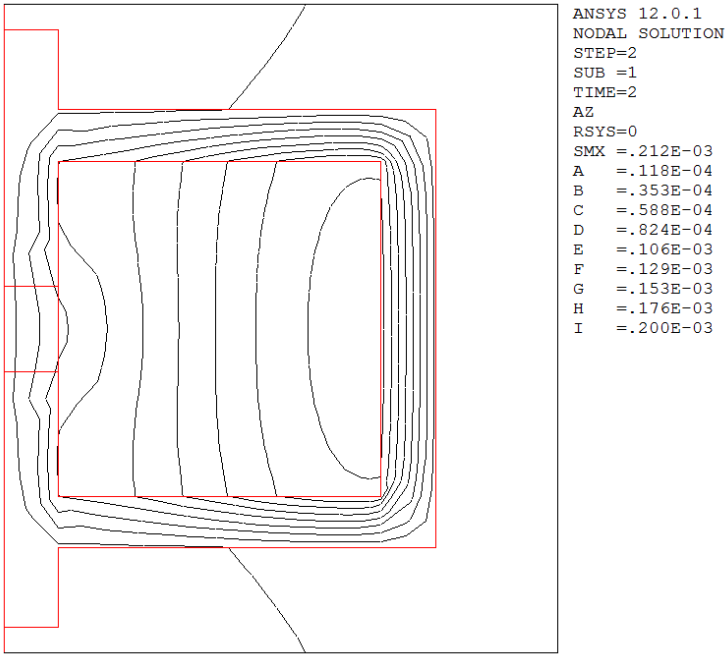

Figure 4.3: Flux lines through the testing apparatus and MRE sample as presented by the FEM program.

This testing apparatus was attached to an MTS QTest axial materials testing machine with aluminum grips to minimize magnetic interactions with the testing machine. A Hall probe was placed below the MRE sample to measure the flux density with a Tel Atomic Smart Magnetic Sensor. Figure 4.4 shows a photo of the testing rig.

Figure 4.4: Testing rig

4.2 Testing Results

For all compression testing of the samples, the maximum strain applied was 15%. Initial sample testing at maximum strain 30% showed samples getting damaged, see for example Figure 4.5. For the purpose of getting stable results and keeping samples undamaged it was decided that the maximum strain measured would be 15%.

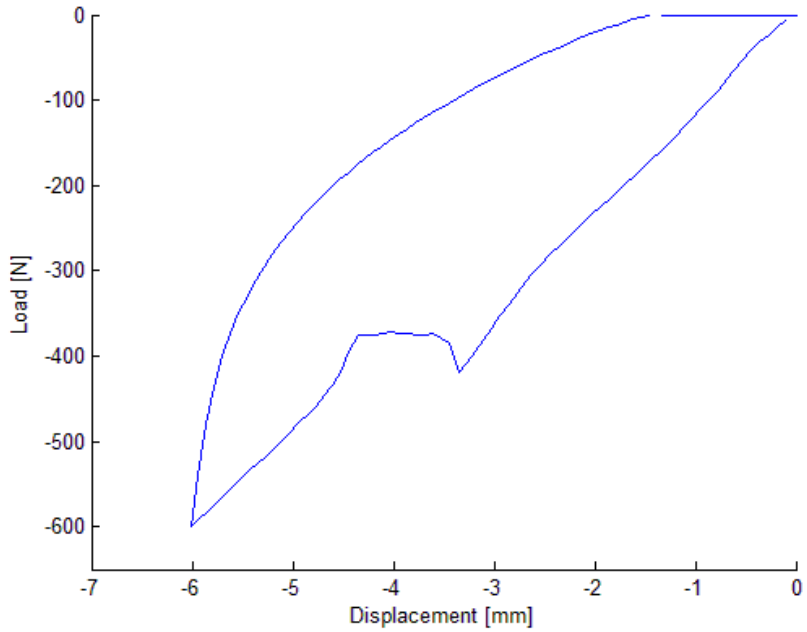

Figure 4.5: Fracture at high strain

Table 4.1 and Figure 4.6 show an overview of the 17 samples on which the testing was performed. All specimens were cylindrical with height of 20 mm and diameter of 25 mm and had a particle concentration of 27% vol./vol.. The table shows the off-state load measured at 15% strain (3 mm dislacement), as well as the on-state load measured at the same 15 % strain. Spring rate, k, is calculated accordingly. The figure shows the off-state and on-state spring rates at 15% strain. The Magnetic flux density through the samples measured 0,56 T.

Table 4.1: MRE samples and measuring results at 15 % strain.

Sample No.	Matrix Material	CIP Type	Particle Distribution	F_{off} [N]	F_{on} [N]	ΔF [N]	k_{off} [N/mm]	k_{on} [N/mm]	Δk [N/mm]	Δk/ k_{off}
1	Silicone	CM	Aligned	375	414	39	125	138	13	10 %
2	Silicone	CM	Aligned	372	434	62	124	145	21	17 %
3	Silicone	CM	Aligned	365	408	43	122	136	14	12 %
4	Silicone	CM	Aligned	334	370	36	111	123	12	11 %
5	Silicone	CM	Aligned	249	295	46	83	98	15	19 %
6	Silicone	CM	Isotropic	179	200	21	60	67	7	12 %
7	Silicone	CM	Isotropic	201	203	2	67	68	1	0 %
8	Silicone	CC	Aligned	209	248	39	70	83	13	19 %
9	PU	CM	Aligned	636	695	59	212	232	20	9 %
10	PU	CM	Aligned	335	373	38	112	124	12	11 %
11	PU	CM	Aligned	416	448	32	139	149	10	8 %
12	PU	CM	Aligned	553	606	53	184	202	18	10 %
13	PU	CC	Aligned	491	591	100	164	197	33	20 %
14	PU	CC	Aligned	437	548	111	146	183	37	25 %
15	PU	CC	Aligned	293	318	25	98	106	8	9 %
16	PU	CC	Aligned	363	442	79	121	147	26	22 %
17	PU	CC	Isotropic	354	412	58	118	137	19	16 %

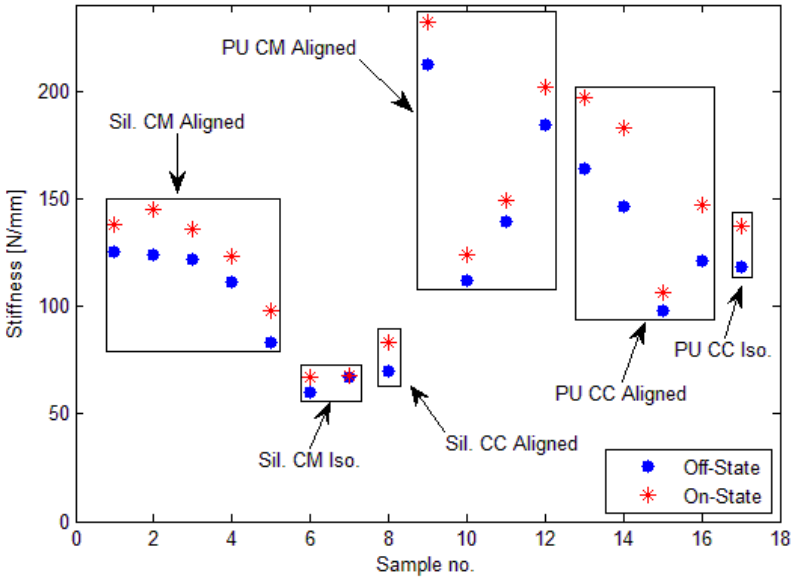

Figure 4.6: Off-State and on-state stiffness of the samples at 15% strain

Considerable unstability is seen in the off-state stiffness between samples of same type. Although isotropic samples and samples with smaller particles tend to have lower off-state stiffness, no concrete conclusions can be drawn on the difference in off-state stiffness between types of samples without further research and proper statistical methods.

A particularily large difference in off-state stiffness is found between the polyurethane-based samples. In Figure 4.7 a probable explanation of this difference can be seen. The photo is taken through the lense of an optical microscope and shows the cross-section of

two polyurethane-based samples. The upper one, referred to as sample no. 14 in Table 4.1 has considerably higher off-state stiffness than the one below it, referred to as sample no. 15. Figure 4.7 shows that the stiffer sample also has much less airgaps in it. It may be that the air in the samples are causing instable results, demanding further degassing during the fabrication of polyurethane-based samples.

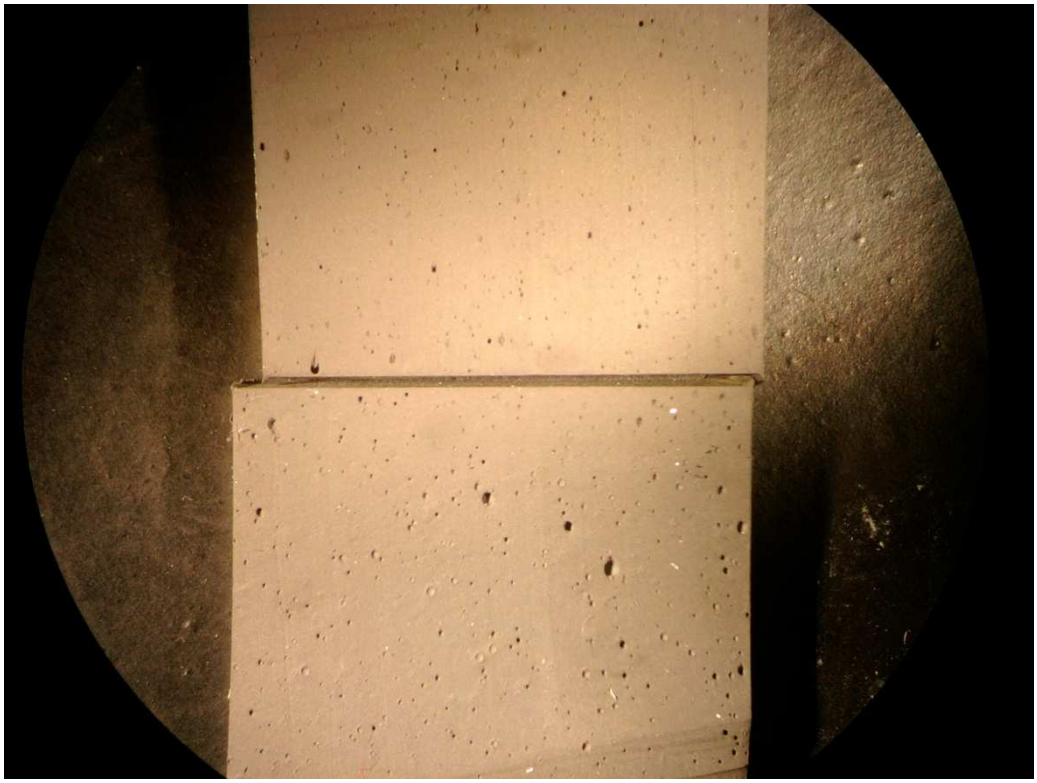

Figure 4.7: Photo of two polyurethane samples (upper no. 14, lower no. 15), taken through an optical microscope.

This problem of trapped air was not as significant in the silicone-based samples. If sample no. 5 is disregarded, the off-state stiffness is relatively constant between aligned silicone-based samples with CM particles. Possible causes for inconsistency are the formation of agglomerates and improper mixing, due to the rapid curing of the silicone material as well as possible inconsistency in the alignment of particles.

The most impressive absolute MR effect is found in samples no. 13 and 14, which are polyurethane-based. The reason for the elevated effect may be that these samples were properly mixed, showing less agglomeration than the silicone-based samples, and they have less air content than the other polyurethane samples. Whether the low uncured viscosity of the PU had effect on the particle alignment is left unsaid since a good assessment of the alignment has not been done. Interestingly, sample no. 17, which is an isotropic sample, has a larger absolute change in spring rate than most other aligned samples. Still the change is much lower than for samples of same material and fabrication method.

No magnetostriction was apparent in the samples. Possibly, the nominal stiffnesses of the materials are too stiff for such an effect

Figure 4.8 is an example of load-displacement curves from the compression testing. The blue and red curves show off- and on-state measurements of an isotropic sample (sample no. 6) and the green and black curve show off- and on-state measurements of an aligned sample (sample no. 2). The figure represents well the general behaviour observed and it shows how samples with isotropic particle distribution have lower off-state and on-state stiffness, less absolute MR effect and less energy loss than samples with aligned particle distribution. It furthermore shows that the difference in the derivatives of the on-state and off-state curves is mainly found where the displacement is well below 1 mm, or 5% strain, which means that the MR effect is mainly found at low strains.

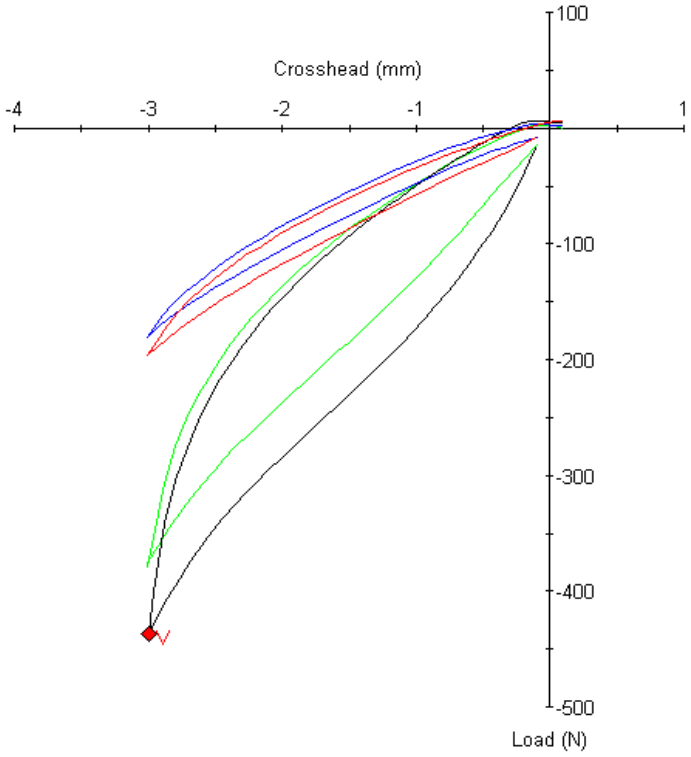

Figure 4.8: Compression testing results for an isotropic sample (blue: off-state, red: on-state) and an aligned sample (green: off-state, black: on-state)

Figure 4.9 to Figure 4.14 further describe how the MR effect depends on strain amplitude, comparing the off-state and on-state elastic moduli as well as the off-state and on-state spring rates. These are the results for sample no.2 which is a good representative. The difference between the moduli is highest for the lowest strain but drops down to practically zero at 3 % strain. The off-state modulus never surpasses the on-state modulus and, due to the high difference at low strains, a 17% difference in total spring rate is still seen at 15% strain.

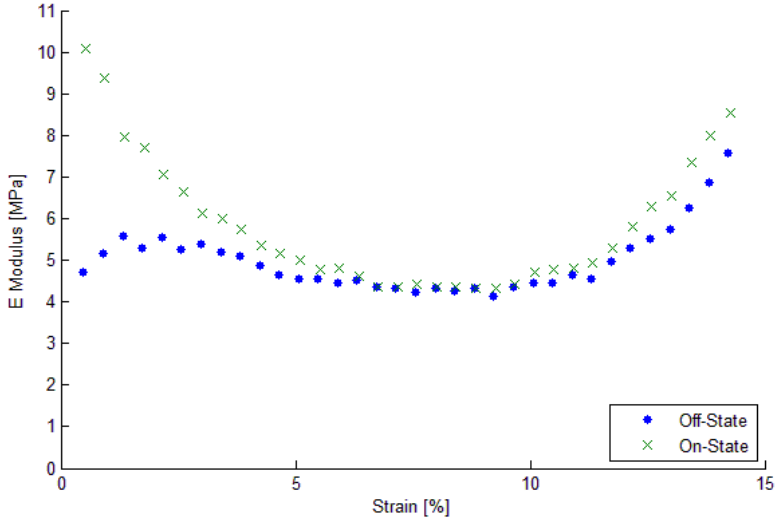

Figure 4.9: Comparison of the off-state and on-state elastic modulus vs. strain of sample no.2.

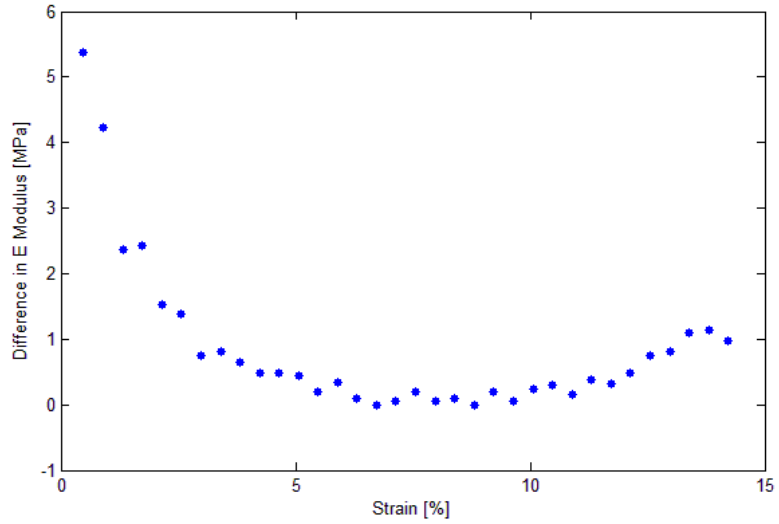

Figure 4.10: Absolute MR effect - The difference between off-state and on-state elastic modulus vs. strain.

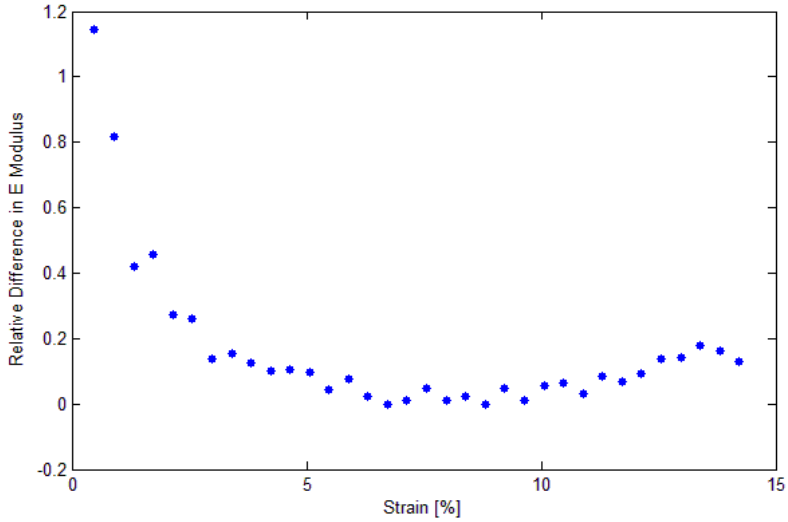

Figure 4.11: Relative MR effect - The relative difference between off-state and on-state elastic modulus vs. strain

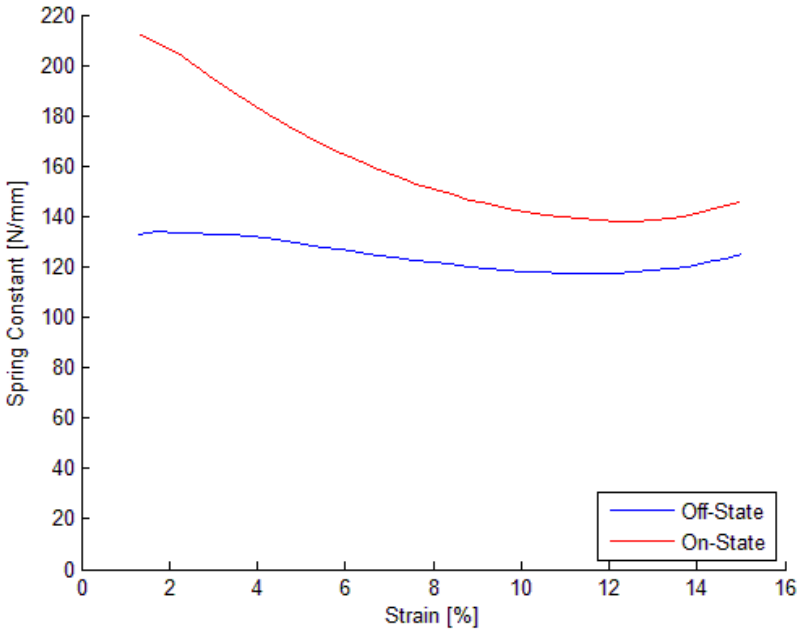

Figure 4.12: Comparison of the off-state and on-state spring rate vs. strain of sample no. 2.

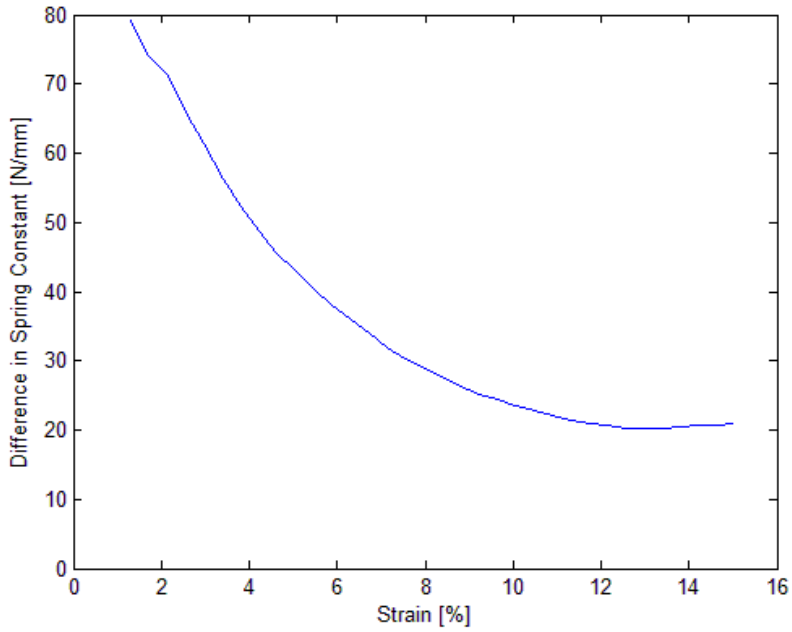

Figure 4.13: The difference between off-state and on-state spring rate vs. strain

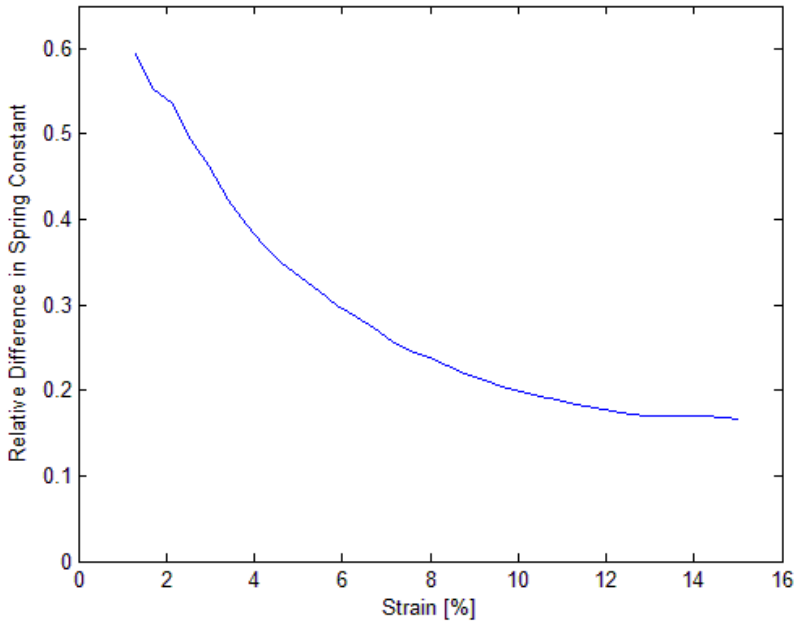

Figure 4.14: The relative difference between off-state and on-state spring rate vs. strain

The change in stiffness experienced when subjecting the MRE samples to a magnetic field is in accordance with the results of other research groups, as discussed above in chapter 2. The results demonstrate that to fully utilize the change in elastic modulus, the MRE should be applied where low strains are to be expected. MREs should however provide a considerable change in total spring rate at higher strains. The maximum change in spring rate at 15% strain seen in the present study was 25%. Larger relative

effect could probably be attained using a matrix material that has even lower stiffness than those used in the present study.

5 Prototyping

The motivation for this study was to see if MREs could be utilized to provide variable structural stiffness in prosthetics. Specifically, a lower-limb, below-knee, prosthetic foot was considered.

The design of prosthetic feet aims for different goals, depending on the users' activity levels and what qualities they prefer in their feet. High activity, such as running, jumping or carrying weight requires more stiffness while low stiffness is preferred at low activity to provide more comfort and less strain to the residual limb. Many users call for more robust feet for use in everyday life to be able to switch between low activity and high activity and retain both comfort and performance. This calls for feet that have real-time variable stiffness.

Following the fabrication and basic characterization described in the previous chapters, an attempt was made to make a working prototype MRE spring that could meet the requirements for use in a prosthetic foot. This means designing a unit with a suitable magnetic circuit that involves an MRE section and a way to allow relative movement of two structural members with the MRE providing elasticity.

5.1 Design

A popular prosthetic foot design is the carbon-fiber design, where the foot is made of a layered carbon-fiber composite that extends from the amputees residual limb and aims to provide natural progression through the stages of normal gait. The stiffness of the foot and its response to load may be controlled via the thickness profile of the foot as well as its shape. Additionally, a spring may be introduced to the structure to provide further shock absorption. One such design can be seen in Figure 5.1 which shows the Re-Flex Rotate™ prosthetic foot, produced by Össur. The Re-Flex Rotate is based on a conventional carbon-fiber foot design but has a vertical shock absorbtion member connecting the foot and the limb. While, from a wide perspective, many ways of applying shock absorption members to prosthetics may exist, this is one that is relatively simple and has already been used with success. From there, it was considered obvious to try and make an MRE based spring unit that could replace that shock absorbtion member to provide variable stiffness.

According to an informal technical study done by Össur, one stiffness category of the foot has the following specifications:

- Weight of user: 69 kg – 77 kg
- Spring rate of shock absorption member at low activity level: k_{low} 112 N/mm
- Spring rate of shock absorption member at high activity level: k_{high} 122 N/mm
- Deflection at walking: d = 6mm

Figure 5.1: The Re-Flex Rotate™ prosthetic foot.

The goal is to have a foot that can dynamically alter its stiffness from the low activity to the high activity level. The spring rates presented conveniently lie on a similar order of magnitude as the spring rates seen in the MRE sample testing of the present study (see chapter 4.2). To simplify calculations, the strain at the maximum deflection is assumed to be 15% and the stress-strain curves of MREs are assumed to be independent of the cross-section and length (intensive property). Further simplifying, linear elasticity and constant cross-sectional area are assumed so the off-state and on-state elastic moduli, E_{off} and E_{on}, can be derived from equation (2):

$$E = \frac{kL}{A} \qquad (2)$$

The considered mechanical properties of MREs are taken from sample no. 14 in Table 4.1, since that sample showed the strongest MR effect. Inserting the values for spring rates k_{off} and k_{on} of sample no. 14 at 15% strain into equation (2), along with the sample geometry values, L and A, on-state and off-state moduli are found to be

E_{off} = 5,9 MPa

E_{on} = 7,5 MPa

Thus, the required geometry of the spring made out of MRE material can be derived. For the material to be at 15 % strain at 6 mm displacement, it has to have total length

L = 40mm

With off-state modulus E_{off} 5,9 MPa and length 40 mm, to obtain off-state spring rate of k_{off} = 112 N/mm, the cross-sectional area must be

$A = 759\ mm^2$

Given the on-state modulus of the material E_{on} = 7,5 MPa, an MRE spring material with the above geometry should give an on state spring rate k_{on} = 142 N/mm. This already exceeds the change in stiffness specified in the study on the Re-Flex Rotate™.

The next step in designing the prototype MRE spring unit was to choose a suitable electromagnetic circuit that would involve an MRE section and provide it with magnetic flux density of at least 0,6 T. It was considered convenient to use an already existing magnetic circuit, used in an MR fluid device, namely the Rheo Knee®, a prosthetic knee product by Össur. The magnetic circuit in the Rheo Knee is schematically described in Figure 5.2, which is an axisymmetric section view. A copper coil is wound around a highly magnetizable core, made of Vacoflux, which is press-fit at its ends into Vacoflux discs. The discs direct the magnetic flux through a cylindrical MR fluid section, where MR fluid is dispersed between thin steel blades. The coil is made of 352 turns of 28 AWG copper wire and its total length is 19mm.

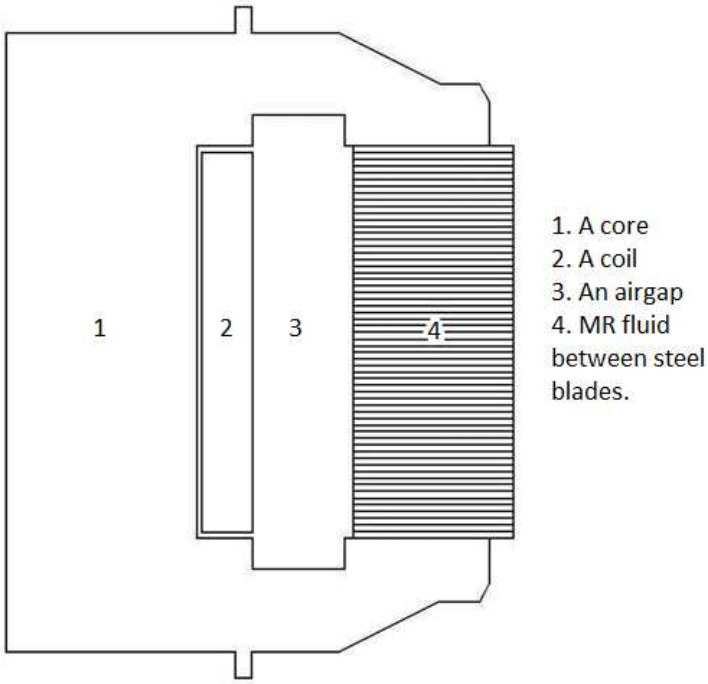

Figure 5.2: Axisymmetric cross-section schematic of the magnetic circuit in the Rheo Knee.

A finite element model has been made by Jonsdottir et al. [20] to evaluate the magnetic flux in the Rheo Knee's magnetic circuit. The results in magnetic flux density can be seen in Figure 5.3. The MFD through the MR fluid section was found to be approximately 0,6 T at an electric current of 1,4 A through the coil.

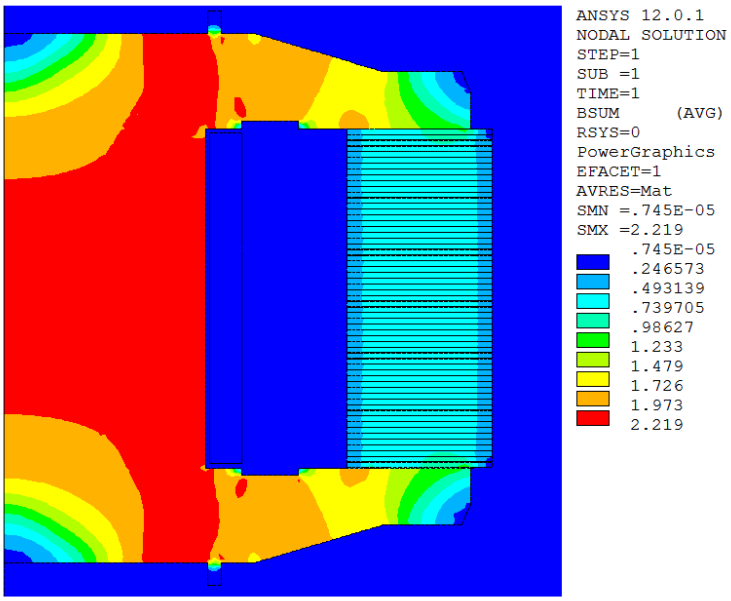

Figure 5.3: Magnetic flux density in the RheoKnee® [20]

A prototype MRE spring unit was built and its isometric section view can be seen in Figure 5.4. Some parts are used from the Rheo Knee. The same coil and upper- and lower discs are used but the upper disc, instead of being press-fit on the core, has a loose fit to allow movement relative to the core. The MR fluid section was replaced by a hollow cylinder made of polyurethane-based MRE. The MRE cylinder had inner diameter 33 mm and outer diameter 48 mm to correctly fit it between the Vacoflux discs, making the cross-sectional area equal to 954 mm^2. The length of the MRE cylinder is 40 mm so, accordingly, the core is made longer than in the Rheo Knee. Above the magnetic circuit is a structure, made of a non-magnetizable material, such as aluminum. This structure's purpose is to take on horizontal loads and direct the spring along the vertical axis. All in all, the aluminum housing, linear bearing and upper disc are fixed together and move vertically relative to the aluminum rod, core and lower disc which are fixed together.

It was assumed that the magnetic circuit of the RheoKnee would provide the appropriate flux density of 0,6 T through an MRE with similar cross section as the MR fluid chamber of the RheoKnee. This was based on the assumption that no flux leakage would be present since the relative magnetic permeability of the MRE would be high enough. This magnetic circuit design would furthermore be relatively lightweight.

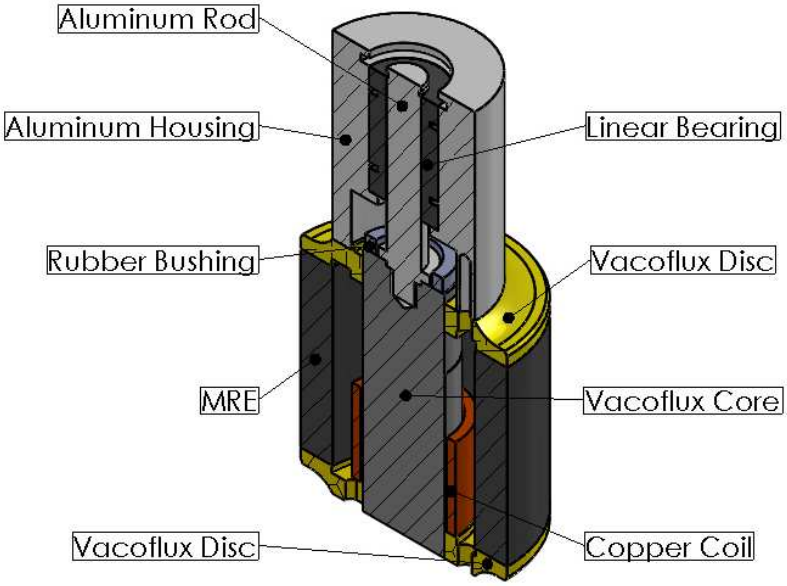

Figure 5.4: Isometric cross section of an MRE spring

The method to produce the MRE was similar to the one described in chapter 3 for polyurethane samples. Thus, the material properties were assumed to come close to the properties of the polyurethane-samples. Given the properties of sample no. 14, and the length and cross-sectional area of the MRE, the prototype spring was expected to have spring rates of

k_{off} = 140 N/mm

k_{on} = 178 N/mm

This is slightly higher than the spring rates specified in the study of Re-Flex Rotate™ and the difference is due to a larger cross-sectional area. This would correspond to a foot intended for a slightly heavier user.

A visualization of how the MRE spring could fit on a prosthetic foot is shown in Figure 5.5.

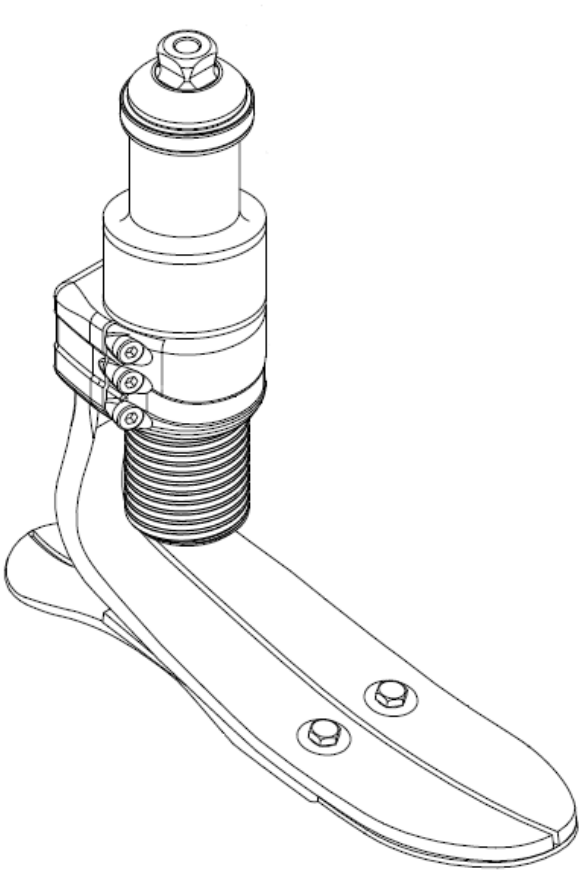

Figure 5.5: A prosthetic foot with an MRE spring used on the vertical axis.

5.2 Testing and improvement

Compression testing was conducted on the MRE spring prototype, both in off-state and on-state modes. An MTS QTest materials testing machine was used.

The load-displacement curves obtained in off-state were similar in terms of shape and energy loss to those obtained from the cylindrical samples with aligned particles in chapter 4. The maximum load at 6 mm displacement was 450 N, meaning a spring rate k_{off} = 75 N/mm. This is considerably lower than the expected 140 N/mm. This difference is probably due to air bubble cavities in the MRE.

The load-displacement curves obtained in on-state, when 1,4 Ampere current was applied to the coil, were identical to the off-state curves, meaning that no MR effect was found during testing of the prototype MRE spring. The magnetic flux density was measured with a Tel Atomic Smart Magnetic Sensor, showing only 30 mT magnetic flux between the MRE and the upper disc. It was concluded that the magnetic circuit could not supply the MRE with enough MFD.

To investigate the causes of low MFD, finite element modeling was used.

The first hypothesis was that the effect of steel blades in the RheoKnee's magnetic circuit of the Rheo Knee® had been underestimated.

Figure 5.6 and Figure 5.7 show flux lines and MFD vector sum of the magnetic circuit in the RheoKnee respectively. The magnetic flux properly goes through the MR fluid chamber and very little flux leakage is seen, resulting in an MFD of 0,6 T through the MR fluid.

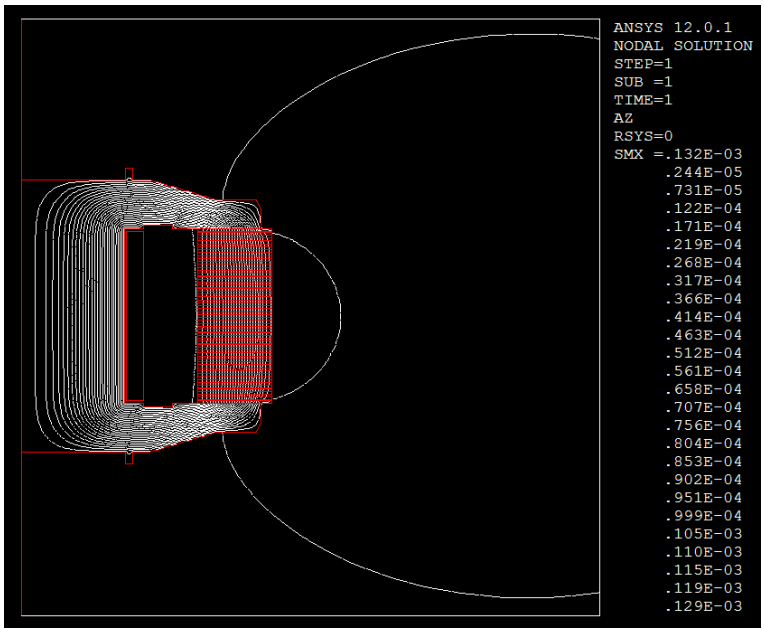

Figure 5.6: Flux lines of the magnetic circuit in the RheoKnee

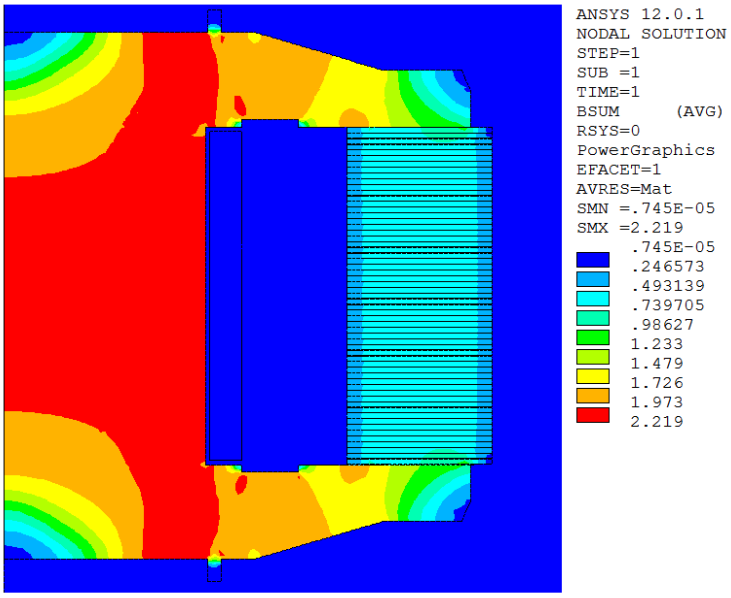

Figure 5.7: Magnetic flux density in the RheoKnee

Figure 5.8 and Figure 5.9 show the flux lines and MFD vector sum of the magnetic circuit when the material properties of the steel blades have been changed to MR Fluid, making the MR Fluid section undivided. It can be seen that flux leakage is greatly affected by omitting the steel blades, resulting in much less MFD through the whole magnetic circuit. Flux lines are seen exiting the intended flux path and the MFD through the MR fluid section is found to be about 0.15 T. It is concluded that the effect of the steel blades on the total magnetic permeability of the MR fluid section has been greatly underestimated.

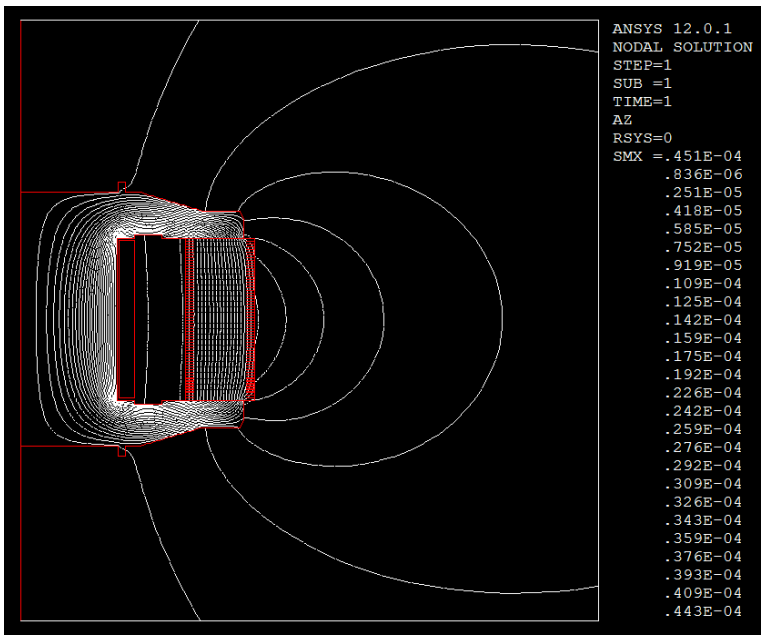

Figure 5.8: Flux lines in the RheoKnee® when steel blades are replaced by MR fluid.

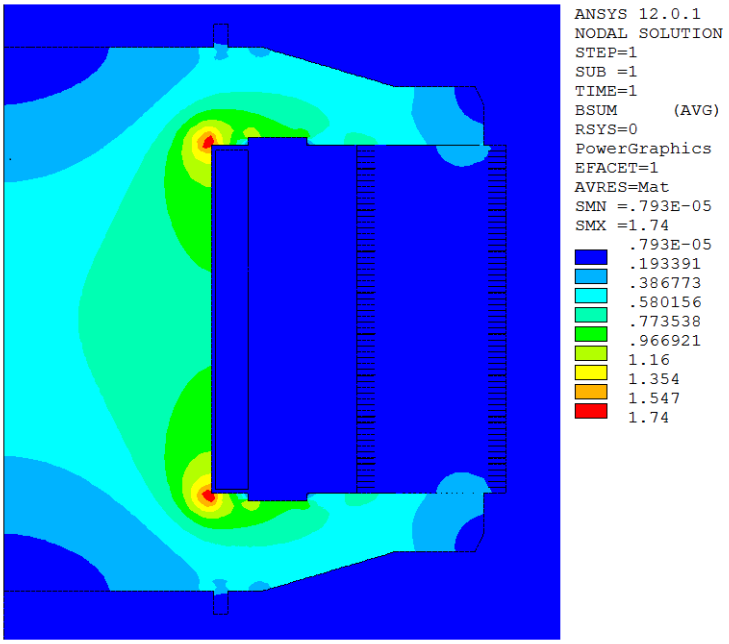

Figure 5.9: Magnetic flux density in the RheoKnee when steel blades are replaced by MR fluid.

The second hypothesis was that the efficiency of the magnetic circuit was reduced by the gap between the core and upper disc or by the threaded hole in the core. Figure 5.10, Figure 5.11 and Figure 5.12 show the vector sum of the magnetic flux density in the MRE spring's magnetic circuit, for the prototype unchanged, the prototype when the gap between core and upper disc were eliminated and the prototype when the hole depth was reduced from 10 mm to 6 mm. It can be seen that these changes only affect the MFD by about 5 %. It is therefore concluded that airgaps are not the causes for low MFD in the prototype at present.

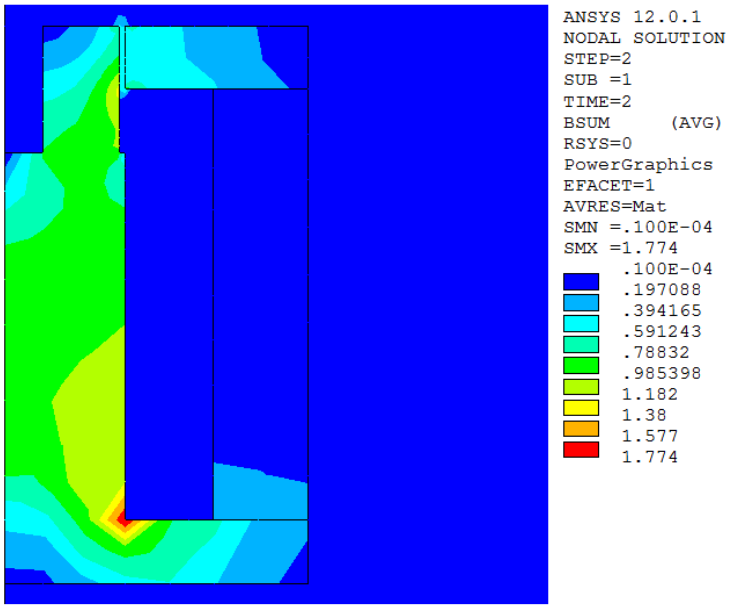

Figure 5.10: Magnetic flux density of the MRE spring.

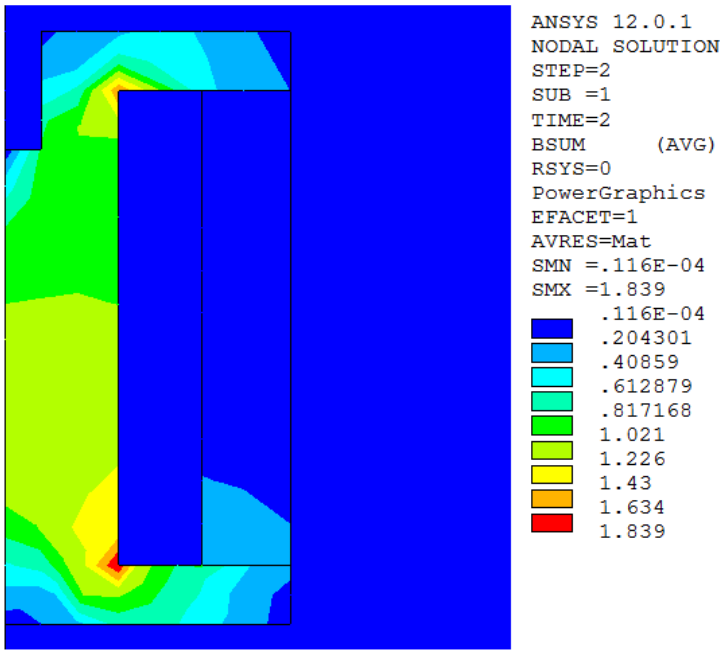

Figure 5.11: Magnetic flux density of the MRE spring with no gap.

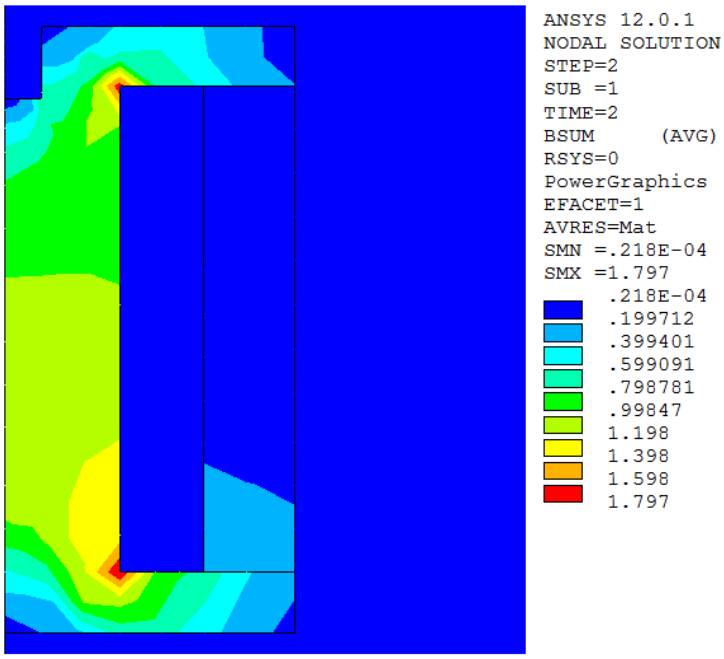

Figure 5.12: Magnetic flux density of the MRE spring with smaller hole.

To initialize the search for a solution to the non-functionality of the MRE spring, an attempt was made to see if increased MFD would be obtainable by using a larger coil and by applying more current. Figure 5.13 shows an FEM model of a magnetic circuit with a coil of length 28 mm, width 5 mm and current of 2.8 A. The core is near its saturation and the MFD in the MRE is substantially higher, between 0.3 and 0.4 T, but rather heterogenous. A larger, more powerful coil will therefore increase the MFD

substantially, however, if the device should be improved to obtain 0,6 T through the MRE, more work and optimization of the magnetic circuit and coil is necessary.

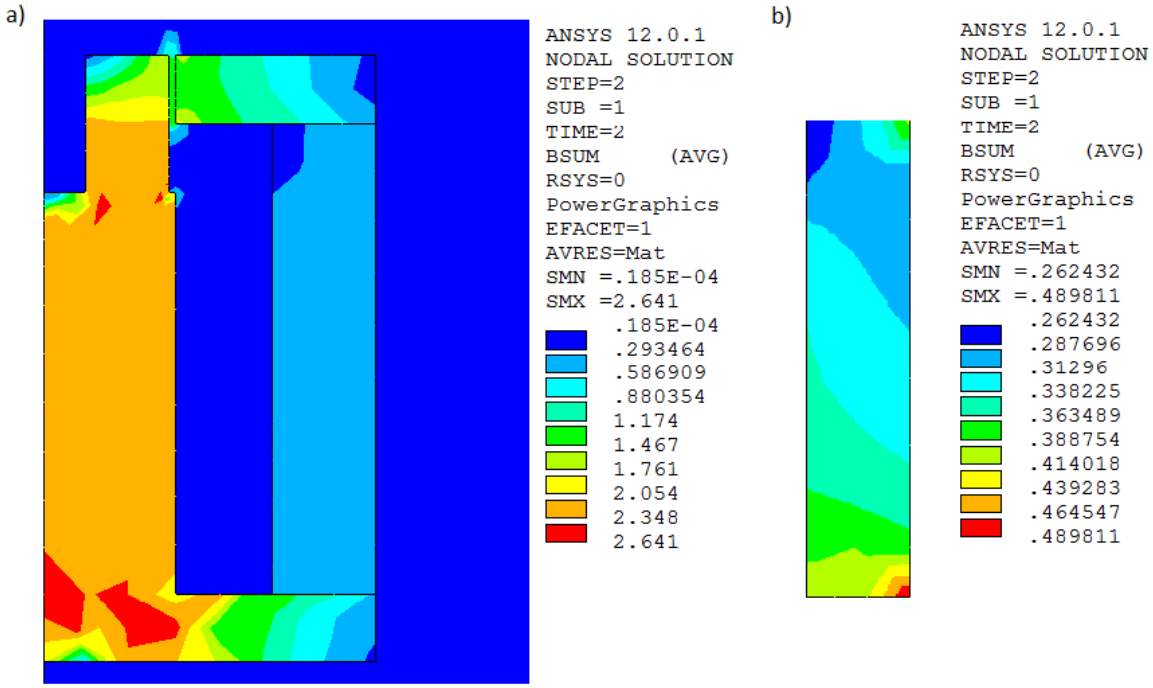

Figure 5.13: Magnetic flux density with a larger coil and higher current . a) The whole MRE Spring unit. b) A closer look of the MRE section

5.3 Further design proposals

Figure 5.14 shows schematic presentations of using MREs to provide variable stiffness in prosthetics. It demonstrates various placements for MRE spring. Figure 5.14a) shows the method already described in the section here above, with one vertical spring. Figures b) through f) describe additional placements, where the MRE spring could be positioned between wedged structures. Figure g) shows how one or several MRE springs (two are shown in the figure) could be embedded within an elastic structure, such as a polyurethane foam.

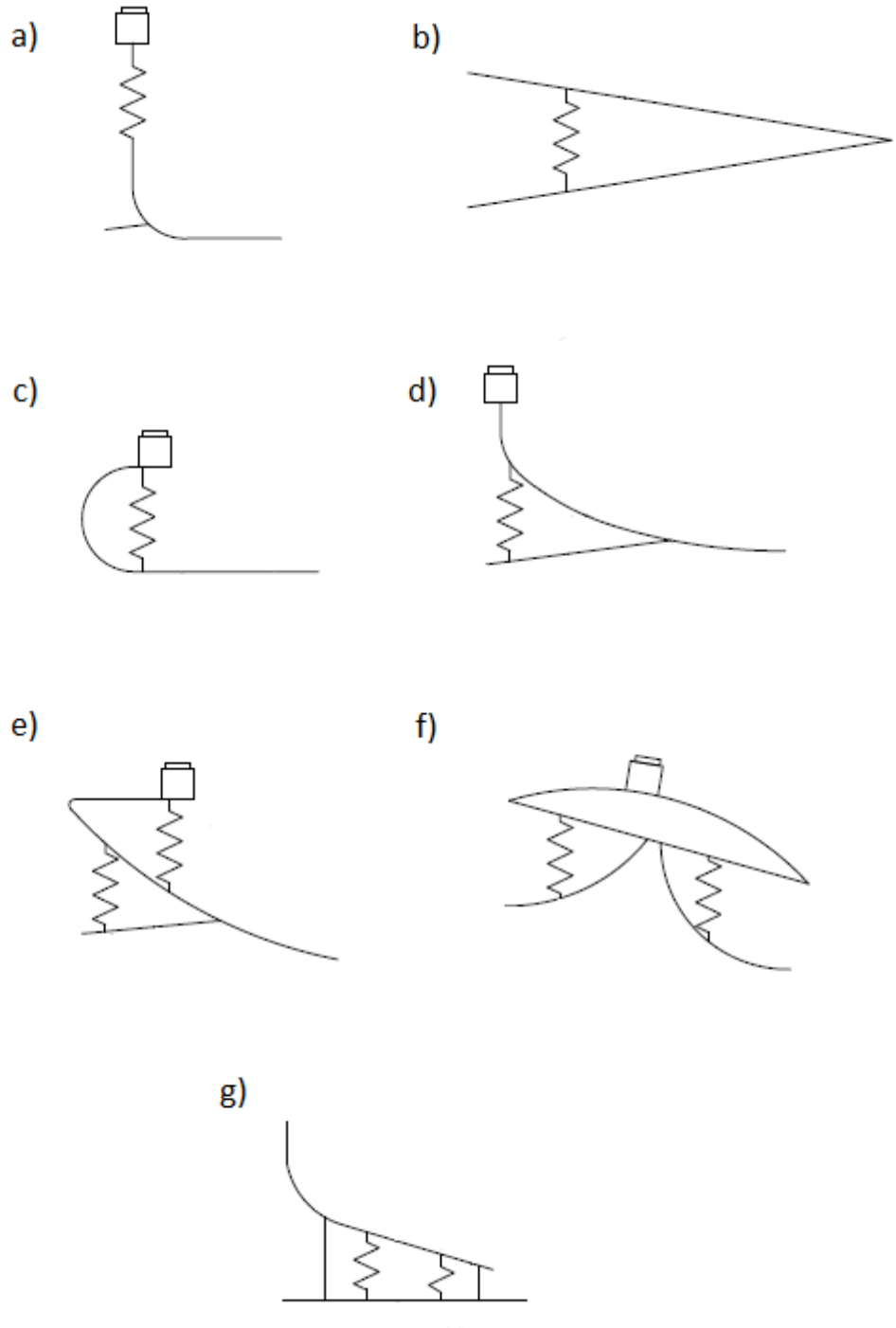

Figure 5.14: Various placements of MRE springs within prosthetic feet. a) Vertical axis b) Basic wedging idea c) Vertical wedge d) Heel wedge e)Vertical/Heel wedge f) Heel/toe wedge g) MRE springs within an inert elastic medium

Furthermore, various designs exist or can be visualized for the MRE spring itself. Good examples can be found in Figure 5.15, which is taken from a paper by Albanese-Lerner [18]. The MR Elastomer can be used in compression, tension or shear or a combination of all.The magnetic field can be applied on the MRE in various ways, for example with a C- or U-shaped magnetic core, as shown in Figure 5.15, or with a magnetic circuit

such as found in the Rheo Knee®. If used in prosthetics, what is called absorber mass in Figure 5.15 would be attached to one structural member of the prosthetic device and the base mass would be attached to the other structural member.

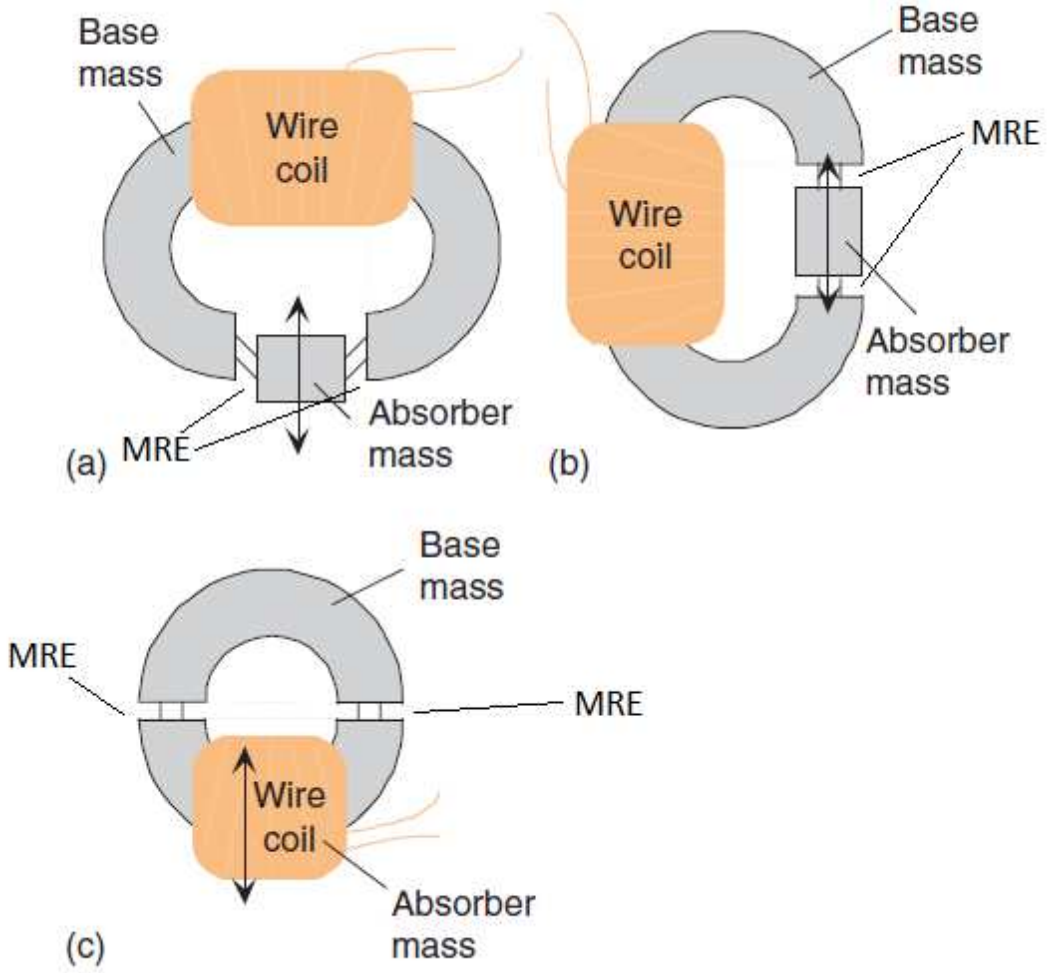

Figure 5.15: Various designs for MRE springs [18]. a) MRE with shear strain applied b) MRE in tension/compression c) MRE in compression.

Following the present study, a provisional patent application, named *Prosthetic and Orthotic Devices Having a Magnetorheological Elastomer Spring with Controllable Stiffness,* was filed by Össur. The specifications and drawings enclosed in the application can be found in the appendix to this thesis. These specifications thoroughly describe the above application proposals of MRE springs in prosthetics. The claims in the patent application furthermore include all use of MRE spring units to provide variable stiffness in prosthetic and orthotic structures.

6 Conclusions

6.1 Discussion

In this study, samples of MRE materials were produced from two different matrix materials and two types of magnetizable particles. The samples were tested in compression loading, both with and without magnetic field They showed considerable change in stiffness although the results were unstable due to manufacturing challenges. The change in stiffness is most impressive at low strains of about 1-2% while a change in total spring constant of up to 25% was exhibited at 15% strain. The highest stiffness change was exhibited by polyurethane samples that were specially treated to ensure low agglomeration of particles.

A prototype MRE spring unit was built, having a magnetic circuit based on the magnetic circuit of an MR fluid device. This prototype showed no change in stiffness between on- and off-states. This non-functionality was explained with insufficient magnetic flux through its MRE section. For a fully functional MRE spring, more work is needed on the design of the magnetic circuit.

Following the study, a patent application was filed by Össur, claiming the use of MRE spring units to provide variable stiffness in prosthetic and orthotic devices

6.2 Proposals for future work

A number of questions have risen from the present study. For a clearer vision of the potentials of MREs in prosthetics, further study should be made on the magnetic circuit of the MRE spring unit. Finite element analysis is an essential tool for such studies, making it possible to foresee the effect of flux leakage and optimize the design. Making a proper B-H curve for the MRE material could yield more accurate results but for the purpose of an initial design study the use of an MR fluid B-H curve may suffice.

While designing an MRE spring unit a number of factors should be considered. The objective is to maximize the change in stiffness of the structure while keeping its weight and size at minimum. The variables involved include the mode of loading (compression, shear, tension), the geometry of the MRE section, the composition of the MRE composite, the core and magnetic flux path and the coil design. Choosing a softer matrix material would mean lower off-state stiffness and should, according to previous studies, result in a larger relative MR effect since the absolute MR effect would remain the same [11]. Thus, an MRE spring with larger cross-section could exhibit a larger stiffness change but would also need to be supported by a larger magnetic circuit.

Along with the design improvements of the MRE spring unit, the MRE material itself should be studied more thoroughly. Its durability should be investigated, both in terms of static and cyclic loading. The present study only considers static stiffness of the material but dynamic stiffness should also be investigated. The fabrication methods and choice of materials could be improved, one aspect being the alignment of particles. An assessment of the alignment could possibly be executed with the aid of image analysis.

When possessed with a decent MRE spring unit, various control methods could be visualized. In addition to switching between an off-state mode and an on-state mode with the turn of a knob or push of a button, the stiffness could be controlled via a computer processor. The stiffness of the MRE spring could then be controlled based on input signals from sensors related to the current activity of the user. This could also be used to improve battery life and minimize heating in the coil as the MRE spring could be switched to on-state only at the time of impact.

In addition to having potential as structural spring units in prosthetics, the impressive MR effect seen at low strains could suggest that the ideal application of MREs in prosthetics be to semi-actively absorb vibrations in the structure. This calls for a further investigation.

References

1. Jolly, M.R., J.D. Carlson, and B.C. Munoz. 1996. *A model of the behaviour of magnetorheological materials.* Smart Materials & Structures, **5**(5): p. 607-614.
2. Davis, L.C. 1999. *Model of magnetorheological elastomers.* Journal of Applied Physics, **85**(6): p. 3348-3351.
3. Watson, J.R. 1997. *U.S. Patent 5609353A.* Ford Motor Company.
4. Xu, Z.B., et al. 2010. *An Active-damping-compensated Magnetorheological Elastomer Adaptive Tuned Vibration Absorber.* Journal of Intelligent Material Systems and Structures, **21**(10): p. 1039-1047.
5. Farshad, M. and M. Le Roux. 2004. *A new active noise abatement barrier system.* Polymer Testing, **23**(7): p. 855-860.
6. Bose, H. 2007. *Viscoelastic properties of silicone-based magnetorheological elastomers.* International Journal of Modern Physics B, **21**(28-29): p. 4790-4797.
7. Chen, L., et al. 2007. *Investigation on magnetorheological elastomers based on natural rubber.* Journal of Materials Science, **42**(14): p. 5483-5489.
8. Diguet, G., E. Beaugnon, and J.Y. Cavaillé. 2010. *Shape effect in the magnetostriction of ferromagnetic composite.* Journal of Magnetism and Magnetic Materials, **322**(21): p. 3337-3341.
9. Jiang, W.-q., et al. 2008. *Enhancement in Magnetorheological Effect of Magnetorheological Elastomers by Surface Modification of Iron Particles.* Chinese Journal of Chemical Physics, **21**(1): p. 87-92.
10. Kallio, M. 2005. *The elastic and damping properties of magnetorheological elastomers*. Department of Materials Science, Tampere University of Technology, Tampere.
11. Lokander, M. 2003. *Improving the magnetorheological effect in isotropic magnetorheological rubber materials.* Polymer Testing, **22**(6): p. 677-680.
12. Demchuk, S.A. 2002. *Viscoelastic properties of magnetorheological elastomers in the regime of dynamic deformation.* Journal of Engineering Physics and Thermophysics, **75**(2): p. 396-400.
13. Zhang, W., et al. 2010. *Effect of Cyclic Deformation on Magnetorheological Elastomers.* Chinese Journal of Chemical Physics, **23**(2): p. 226-230.
14. BASF SE. 2009. *Product specification. Carbonyl Iron Powder CM. CAS-CEPCM-E. Revision 8.*
15. Carlson, J.D. and M.R. Jolly. 2000. *MR fluid, foam and elastomer devices.* Mechatronics, **10**(4-5): p. 555-569.
16. BASF SE. *Carbonyl Iron Powder for Metal Injection Molding.* From the web: http://www.inorganics.basf.com/ca/internet/en/content/Produkte/Metallsysteme/CIP/Technology. Accessed january 2011.
17. Boczkowska, A., et al. 2009. *Image analysis of the microstructure of magnetorheological elastomers.* Journal of Materials Science, **44**(12): p. 3135-3140.
18. Lerner, A.A. and K.A. Cunefare. 2007. *Performance of MRE-based Vibration Absorbers.* Journal of Intelligent Material Systems and Structures, **19**(5): p. 551-563.
19. Woods, B.K.S., et al. 2007. *Manufacture of bulk magnetorheological elastomers using vacuum assisted resin transfer molding.* International Journal of Modern Physics B, **21**(28-29): p. 5010-5017.

20. Jonsdottir, F., et al. 2008. *Influence of Parameter Variations on the Braking Torque of a Magnetorheological Prosthetic Knee.* Journal of Intelligent Material Systems and Structures, **20**(6): p. 659-667.

Appendix

PROSTHETIC AND ORTHOTIC DEVICES HAVING MAGNETORHEOLOGICAL ELASTOMER SPRING WITH CONTROLLABLE STIFFNESS

BACKGROUND

Field

[0001] The present application relates in certain embodiments to prosthetic and orthotic devices. In particular, the present application in certain embodiments relates to prosthetic and orthotic device with one or more magnetorheological (MR) elastomer springs having a controllable stiffness.

Description of the Related Art

[0002] Conventional prosthetic and orthotic devices seek to approximate the feel and fluid range of motion of a human limb's natural movement, such as the natural stride of a human foot. Additionally, prosthetic and orthotic devices seek to provide the appropriate level of stiffness for the user, based on the activity level of the user. High stiffness is required in more demanding tasks (e.g., running, jumping), while low stiffness is required for comfort while at rest or moving casually (e.g., walking). However, the components in conventional orthotic and prosthetic devices (e.g., prosthetic foot plates and heel plates) generally have a set stiffness, regardless of the activity level of the user.

[0003] Accordingly, there is a need for orthotic and prosthetic devices where the stiffness of the device is controllable and adaptable to the user's current activity level, and capable of being controlled either manually or automatically by responding to signals that represent the current activity level of the user, where the operating characteristics of the device can be changed in real-time.

SUMMARY OF SOME EXEMPLIFYING EMBODIMENTS

[0004] In accordance with one embodiment, orthotic and prosthetic devices are provided where the stiffness of the device is controllable and adaptable to the user's current activity level, and capable of changing the stiffness characteristics of the device in real time. In one embodiment, the stiffness of the device is controlled manually by the user. In another embodiment, the stiffness of the device is controlled automatically (e.g. via a computer processor) by responding to signals that represent the current activity level of the user.

[0005] In accordance with one embodiment, a prosthetic or orthotic device is provided comprising a body configured to support a human limb of a user wearing the prosthetic or orthotic device. The device further comprises a shock absorption member coupled to the body. The shock absorption member comprises one or more magnetorheological elastomer (MRE) springs disposed between a first portion of the body and a second portion of the body. The one or more MRE springs are selectively actuatable to vary a stiffness of the shock absorption member via the application of a magnetic flux, thereby adjusting a stiffness of the body of the prosthetic or orthotic device to a level corresponding to an activity level of the user.

[0006] In accordance with another embodiment, a prosthetic foot is provided. The prosthetic foot comprises a foot plate extending from a generally vertical proximal portion to a generally horizontal distal portion, the foot plate curving generally downwardly and forwardly between the proximal and distal portions. The prosthetic foot also comprises an adapter coupled to the proximal portion of the foot plate. The prosthetic foot further comprises a shock absorbing member removably coupled to the adapter. The shock absorbing member comprises a cylindrical core extending along a generally vertical axis and an electrically conducting coil disposed about the cylindrical core. The shock absorbing member further comprises a spring surrounding the core and the coil, the spring comprising a magnetorheological elastomer (MRE) material. The MRE spring can be actuated to vary the stiffness of the shock absorbing member via the application of a magnetic flux to the spring.

BRIEF DESCRIPTION OF THE DRAWINGS

[0007] FIGURE 1A is a schematic perspective view of one embodiment of a prosthetic foot with a magnetorheological elastomer (MRE) spring.

[0008] FIGURE 1B is a schematic side view of the prosthetic foot of FIG. 1A disposed in a cosmesis foot cover (shown in cross-section).

[0009] FIGURE 2 is a schematic cross-sectional side view of one embodiment of a shock absorber having a MRE spring.

[0010] FIGURE 3 is a representation of the magnetic flux density in the resulting magnetic circuit of one embodiment of a MRE spring, as computed by an axis-symmetric finite element model of the magnetic circuit.

[0011] FIGURE 4 is a graph showing testing results, showing the spring constant k of a material test sample with a solid cross-section with and without the magnetic flux. The x-axis shows the displacement (in mm) and the y axis shows the force (in N), from which the spring constant can be derived.

[0012] FIGURE 5A-G are schematic side views of several embodiments of prosthetic foot designs with one or more MRE springs.

[0013] FIGURES 6A-C re schematic views of several embodiments of a MRE spring element.

DETAILED DESCRIPTION OF SOME EXEMPLIFYING EMBODIMENTS

[0014] Described below are embodiments of prosthetic and orthotic devices having a magnetorheological elastomer spring with controllable stiffness (hereinafter "MRE spring"). The stiffness and related mechanical properties of the MRE spring can be changed rapidly and reversibly by inducing a magnetic flux through the MRE spring. The magnetic flux required to change the stiffness of the spring is generated by other structures within the device that are magnetized in response to an externally applied electrical current through a coil.

[0015] In some embodiments, the prosthetic or orthotic device can operate at more than one level of stiffness and other related mechanical properties so that it adapts to the user's activity level. For example, a high stiffness may be desired in more demanding tasks (e.g., running, jumping) while low stiffness is desired for comfort while at rest or moving casually (e.g., walking). In some embodiments, the user may control the stiffness of the MRE spring manually (e.g., by pressing a button, actuating a lever) to apply an electrical current or voltage in response to changing intensity of the activity level. In another embodiment, the user can control the stiffness of the MRE spring remotely, for example via a hand held remote control that communicates wirelessly with a receiver in the prosthetic or orthotic device (e.g., via an Rf communication system). In another embodiment, the stiffness of the MRE spring can be controlled automatically (e.g., via a computer processor) in response to some input signal based on the user's activity. For example, one or more sensors (e.g., as a force sensor) can be provided in the prosthetic or orthotic device to sense one or more parameter (e.g., the amount of force being applied by the user) during ambulation, and based on the sensed

parameter(s), a controller can determine (e.g., using one or more control algorithms) whether the user is in a low activity level or a high activity level, and apply an electrical current or voltage to the MRE spring to provide a corresponding level of stiffness.

[0016] In one embodiment, the disclosed magnetorheological elastomers (MREs) comprise ferromagnetic particles interspersed within an elastomer matrix, whose resulting properties such as stiffness changes in response to a magnetic flux. For example, in one embodiment a MRE may comprise magnetizable carbonyl iron particles embedded in silicone. MREs may be produced by mixing magnetizable particles with an uncured elastomer, and subsequently curing the compound in a mold under the presence of a magnetic flux. The presence of the magnetic flux induces the ferromagnetic particles having magnetic dipoles to form columnar chains of ferromagnetic particles. The degree of the chain formation and the particle density are proportional to the magnitude of the change in stiffness the resulting MRE can display. For example, having a high density of ferromagnetic particles and a high level of chain formation results in a higher stiffness of the MRE under a magnetic flux compared to the stiffness without the magnetic flux

[0017] Figures 1A-1B show one embodiment of a prosthetic foot 100 with a MRE spring. The prosthetic foot 100 can have a foot member 10 that extends from a proximal section 12 to a distal section 14. In the illustrated embodiment, the proximal section 12 can be generally vertically oriented, and the distal section 14 be generally horizontally oriented with the foot member 10 curving downward from the proximal section 12 to the distal section 14. The proximal section 12 can extend to a proximal end 12a and be generally at a location of a natural human ankle. In one embodiment, the distal section 14 can extend to a distal end 14a generally at a location of natural human toes.

[0018] With continued reference to FIGS. 1A-1B, the foot member 10 can have multiple elongate segments that can flex independently relative to each other. In the illustrated embodiment, the foot member 10 has two elongate segments 16a, 16b that are separated from each other by a slot 17 that extends along a length between the distal end 14a and the proximal end 12a of the foot member 10. In one embodiment, the slot extends along the entire length of the foot member 10. In another embodiment, the slot 17 extends along a length that is shorter than the entire length of the foot member 10. In one embodiment, the

slot 17 extends linearly along its length, so that the width of all the elongate segments 16a, 16b is generally the same. In another embodiment, the slot 17 can have a curved section, such that one of the elongate segments has a different width than another of the elongate segments over at least a portion of their lengths.

[0019] The prosthetic foot 100 can also have a heel member 20 that extends between a proximal end 22 and a distal end 24 and is disposed below at least a portion of the foot member 10. In one embodiment, the heel member 20 can be coupled to the foot member 10 via one or more fasteners 30 (e.g., bolts) at a location between the proximal and distal ends 12a, 14a of the foot member 10 such that the heel member is cantilevered relative to the foot member 10 and extends to a free rear end at the distal end 24. The heel member 20 can have a curvilinear profile along its length that defines an arch 28 between the proximal and distal ends 22, 24. As best seen in FIG. 1B, the foot and heel members 10, 20 can define a slot 32 in the fore-aft direction at a rear portion of the prosthetic foot 100. In one embodiment, the slot 32 can taper toward a front end of the prosthetic foot 100. A resilient member 40 can be interposed between the heel member 20 and the foot member 10 within the slot 32. In one embodiment, the resilient member 40 can separate at least a portion of the foot member 10 from the heel member 20. In another embodiment, the resilient member 40 can completely separate the foot member 10 from the heel member 20.

[0020] In one embodiment, the foot and heel members 10, 20 are plate-like members with generally planar top and bottom surfaces. The foot and heel members 10, 20 can be made of lightweight resilient materials, such as graphite, fiberglass, carbon fiber and the like. In some embodiments, the foot and heel members 10, 20 can formed of multiple layers of material that define a monolithic piece.

[0021] The prosthetic foot 100 can also have a connector 50 that attaches to the proximal section 12 of the foot member 10. In one embodiment, the connector 50 can have a recess at a rear portion 52 thereof that fits over the proximal section 12 of the foot member 10. In one embodiment, the connector 50 can be attached to the foot member 10 by an adhesive (e.g., delivered into the recesses to bond the connector 50 to the proximal section 12 of the foot member 10). In another embodiment, the connector 50 can be coupled to the foot member 10 with one or more fasteners (e.g., threaded fasteners).

[0022] With continued reference to Figures 1A-1B, the prosthetic foot 100 can have a shock absorbing module 60 that couples to a front portion 54 of the connector 50. In one embodiment, the shock absorbing module 60 can have a threaded distal section 62 that threadably couples to an inner threaded surface (not shown) of the front portion 54 to couple the module 60 to the connector 50, and one or more fasteners 56 can be adjusted to lock the shock module 60 relative to the connector 50 to fix the axial position of the module 60. The shock module 60 can also have a proximal portion 64 that extends above the connector 50, and an adapter 66 at its proximal end. In the illustrated embodiment, the adapter 66 is a male pyramid adapter. However, in other embodiments, the adapter 66 can be a tube connector. The shock absorbing module 60 can also include a spring module 70 between the adapter 66 and the connector 50 that includes a MRE spring, and is further described below.

[0023] As shown in FIG. 1B, the prosthetic foot 100 can be coupled (e.g., removably coupled) to a cosmesis foot cover 80 that has an upper portion 82 and a sole portion 84. In one embodiment, the sole portion 84 can have an insole portion 86 with a convex surface 86a that corresponds to the curvature of a concave bottom surface 28a of the arch 28 of the heel member 20, such that the insole portion 86 maintains contact with the bottom surface 28a of the heel member 20 during ambulation of the prosthetic foot 100 from heel strike to toe-off.

[0024] Further details on prosthetic feet can be found in U.S. Publication 2005/0038524, US Patent 7,846,213, US Application No. 13/034,474, filed February 24, 2011 and titled "Prosthetic Foot with a Curved Split," and U.S. Application No. 13/149,118, filed 5/31/2011 and titled "Height-adjustable Threaded Shock Absorbing Module and Associated Coupling Member," the entire contents of all of which are hereby incorporated by reference and should be considered a part of this specification. Further details of foot covers and insole portions can be found in US Publication 2010/0004757 titled "Smooth Rollover Insole for Prosthetic Foot" and US Publication 2006/0015192 titled "Functional Foot Cover," the entire contents of all of which are hereby incorporated by reference and should be considered a part of this specification.

[0025] Figure 2 shows a cross sectional structural view of one embodiment of the spring module 70 of the shock absorbing module 60. Disposed along a vertical axis Y on the

lower portion of the spring module 70 is a cylindrical core 71 (hereinafter "core") comprising a magnetizable material. An example of a magnetizable material is Vacoflux™, which is an Fe-Co alloy. However, other suitable magnetizable materials can be used. The core 71 is connected to a magnetizable lower disc 72 (e.g., made of Vacoflux™) on the bottom end 71a, and a non-magnetizable rod 73 on the upper end 71b. The rod 73 can be made, for example, out of aluminum. However, the rod 73 can be made of other suitable non-magnetizable materials. The core 71 can also be connected on the bottom to a structural member, such as the threaded distal section 62 of the shock absorbing module 60 (see FIG. 1). In another embodiment, the core 71 can be connected at its bottom end 71a to an adapter, such as a pyramid adapter of a prosthetic device.

[0026] Disposed around the vertical axis Y and surrounding the core 71 can be a coil 74 that can be actuated to induce a magnetic flux having a magnitude sufficient to magnetize surrounding magnetizable structures, including the core 71, in response to an applied current. In one embodiment, said current can be applied by a power source, such as a battery, that can be external to the shock absorbing module 60. In another embodiment, the power source can be coupled to, or housed in the shock absorbing module assembly.

[0027] With continued reference to the embodiment in FIG. 2, an MRE spring 75 can be disposed around, and housing, both the core 71 and the coil 74. In the illustrated embodiment, the MRE spring 75 is a hollow cylinder (e.g., cylinder with an annulus) made of a MRE material. In another embodiment, the MRE spring 75 can be a solid piece (e.g., not annular) that is disposed generally parallel to the core 71. The MRE spring 75 can be disposed between a magnetizable upper disc 76 (e.g., made of Vacoflux™) and the magnetizable lower disc 72, and can provide variable elasticity to the spring module 70 depending on whether or not a magnetic flux is directed through the MRE.

[0028] The upper disc 76 can be attached to a top end 75b of the MRE spring 75 about the top end 71b of the core 71, and the lower disc 72 can be attached to a bottom end 75a of the MRE spring 75, for example with a suitable adhesive. The upper disc 76 can also be attached to a non-magnetizable housing 77 (e.g., a cylindrical housing) that surrounds the non-magnetizable rod 73. In one embodiment, the housing 77 can be made of aluminum. In another embodiment, the housing 77 can be made of titanium. However, the housing 77 can

be made of other suitable non-magnetizable materials. A linear ball bearing 78 can be interposed between the rod 73 and the non-magnetizable housing 77 and attached to the housing 77. The ball bearing 78 advantageously allows and directs the motion of the upper disc 76 relative to the lower disc 76, while keeping the upper disc 76 sufficiently separated (e.g., radially separated) from the core 71 to minimize friction between the core 71 and the upper disc 76. The spacing 79 (e.g. radial gap) between the core 71 and upper disc 76 is kept at minimum to avoid losses in the magnetic circuit. In one embodiment, the spacing 79 is between about 0.1 mm and about 2 mm. In another embodiment, the spacing 79 can be between about 0.1 mm and about 0.2 mm. In still another embodiment, the spacing 79 can be less than about 0.1 mm.

[0029] With continued reference to FIGS 1A-2, during operation of the prosthetic foot 100, an electrical current can be applied to the coil 74 of the spring module 70, thereby inducing a magnetic flux through the core 71, the upper disc 76, and the lower disc 72. The flux magnetizes the core 71, the upper disc 76, and the lower disc 72, which in turn induces a magnetic flux through the MRE spring 75 that effects a change in the stiffness of the MRE spring 75 to a level that is different from the stiffness without the magnetic flux. Upon removal of the applied current, the stiffness of the MRE spring 75 reverts back to the stiffness value that the MRE spring 75 has when the magnetic flux is not present. In one example, the magnetic flux results in a higher level of stiffness of the MRE spring 75 compared to the stiffness without the flux.

[0030] Figure 3 shows a representation of the magnetic flux density in the resulting magnetic circuit of one embodiment of a MRE spring module 70′, as computed by an axis-symmetric finite element model of the magnetic circuit. In one embodiment, the MRE spring 75 has a magnetic flux density of about 0.6 Tesla. In another embodiment, the MRE spring 75 can have a magnetic flux density greater than 0.6 Tesla. In still another embodiment, the MRE spring 75 can have a magnetic flux density less than 0.6 Tesla. In still another embodiment, the MRE spring 75 has a magnetic flux density such that substantial magnetic saturation of the ferromagnetic particles in the MRE composite is achieved. For example, where the MRE spring 75 includes a MRE composite with about 27% iron particles, near complete magnetic saturation of the particles is achieved with a magnetic flux density of

about 2.2 Tesla through the iron particles, or a magnetic flux density of about 0.6 Tesla through the MRE spring 75.

[0031] Figure 4 shows testing results, showing a force-displacement curve for a material test sample, with and without a magnetic flux applied to it. The x-axis shows the displacement (in mm) and the y axis shows the force (in N), from which the spring constant can be derived. Figure 4 shows, for example, that a force of about 170 N is needed to effect a displacement of about 3 mm when no magnetic flux is present (curve N), whereas a force of about 210 N is needed to effect the same 3 mm displacement when a magnetic flux is present (curve F). A MRE spring can have a similar force/displacement performance. Accordingly, the spring constant of the MRE spring can change from about 56,666 N/m to about 70,000 N/m, or an increase of about 23.5%, with and without a magnetic flux density of 0.6 Teslas. In another embodiment, the spring constant of the MRE spring, such as the MRE spring 75, can change from about 100,000 N/m, without a magnetic field present, to about 120,000 N/m with a magnetic field present, or an increase of about 20%. However, in other embodiments, the spring constant of the MRE spring can be lower or higher than the values above and can be achieved, for example, by varying the size and shape of the MRE spring module. Advantageously, such an increase in the stiffness of the MRE spring 75, when incorporated into a prosthetic device, such as the prosthetic foot 100, provides the variable stiffness that allows a user to transition between low activity and high activity levels, with the MRE spring 75 providing the corresponding level of stiffness.

[0032] Figures 5A-G show additional embodiments of prosthetic devices that incorporate a spring module, such as the spring module 70 with the MRE spring 75 described above. FIG. 5A is a schematic side view of the prosthetic foot 100 described above.

[0033] FIG. 5B is a schematic side view of another embodiment of a prosthetic foot 200. The prosthetic foot 200 has a generally planar upper member 210 and a generally planar lower member 220 disposed below the upper member 210. In the illustrated embodiment, the front ends 212, 222 of the upper and lower members 210, 220 can be attached to each other, and the rear ends 214, 224 of the upper and lower members 210, 220 can be spaced apart from each other, such that the members 210, 220 define a lengthwise slot 230 in the fore-aft direction between the members 210, 220. With continued reference to

FIG. 5B, the slot 230 can taper toward the front ends 212, 222. In one embodiment, an adapter (not shown) can be coupled to the upper member 210 proximate its rear end 214 to allow the prosthetic foot 200 to be operatively attached to a socket.

[0034] In one embodiment, the lower member 220 can be a sole portion of the prosthetic foot 200 that contacts the ground during ambulation, and the upper member 201 can include an ankle section of the prosthetic foot 200. A MRE spring module 270 can be disposed between the upper member 210 and the lower member 220 (e.g., at a rear portion of the prosthetic foot 200), where the MRE spring module 270 can be selectively actuated to vary its stiffness, thereby varying the amount that the upper member 210 displaces toward the lower member 220 during ambulation of the prosthetic foot 200.

[0035] FIG. 5C shows a schematic side view of another embodiment of a prosthetic foot 300. The prosthetic foot 300 has as foot member 310 with a proximal portion 312, a distal portion 314 and an intermediate portion 316. In the illustrated embodiment, the proximal portion 312 and distal portion 314 extend generally horizontally, with the proximal portion 312 disposed above the distal portion 314. In one embodiment, the proximal and/or distal portions 312, 314 can be generally planar. The intermediate portion 316 can be curved and interconnect the proximal portion 312 and the distal portion 314. In the illustrated embodiment, the intermediate portion 316 can be C-shaped. In another embodiment, the intermediate portion 316 can be U-shaped. However, the intermediate embodiments can have other suitable shapes. In one embodiment, the foot member 310 can be monolithic, so that the proximal, distal and intermediate portions 312, 314, 316 form part of a single piece. In another embodiment, the proximal, distal and intermediate portions 312 314, 316 can be separate pieces that attach to each other to define the foot member 310. The intermediate portion 316 can operate like a spring and allow the deflection of the proximal portion 312 relative to the distal portion 314. An adapter 330 can be attached to the proximal portion 312 of the foot member 310, to allow the prosthetic foot 300 to be operatively coupled to a socket (e.g., via a pylon member).

[0036] A MRE spring module 370 can be disposed between the proximal portion 312 and he distal portion 314 (e.g., at a rear portion of the prosthetic foot 200). In one embodiment, the MRE spring module 370 is aligned with the adapter 330. The MRE spring

module 370 can be selectively actuated to vary its stiffness, and as a result the amount that the proximal portion 312 deflects toward the distal portion 314 during ambulation of the prosthetic foot 300 (e.g., when transitioning from mid-stance to toe-off) can be varied.

[0037] FIG. 5D shows a schematic side view of another embodiment of a prosthetic foot 400. The prosthetic foot 400 can have a first foot member 410 that extends from a generally vertical proximal portion 412 to a generally horizontal distal portion 414, with an intermediate portion 416 that curves downwardly and forwardly from the proximal portion 412 toward the distal portion 414. The prosthetic foot 400 can also have a second foot member 420 disposed below the first foot member 410 at a rear portion of the foot 400, where the second foot member 420 extends from a proximal end 422 at a rear most end of the foot 400 to a distal end 424. In one embodiment, the distal end 424 of the second foot member 420 is adjacent and attached to the first foot member 410 at a location between the proximal and distal portions 412, 414 of the first foot member. In one embodiment, the second foot member 420 can be generally planar or flat along its length. In the illustrated embodiment, the first and second foot members 410, 420 define a slot 428 therebetween in the fore-aft direction. The prosthetic foot can also have an adapter 430 attached to the proximal portion 412.

[0038] A MRE spring module 470 can be disposed in the slot 428 between the first and second foot members 410, 420 at a rear portion of the prosthetic foot 400. In the illustrated embodiment, the MRE spring module 470 is disposed axially between the intermediate portion 416 of the first foot member 410 and a location proximate the distal end 422 of the second foot member 420. In one embodiment, the MRE spring module 470 is aligned with the adapter 430. The MRE spring module 470 can be selectively actuated to vary its stiffness, and as a result the amount that the second foot member 420 deflects toward the first foot member 410, for example at heel strike of the prosthetic foot 400 during ambulation, can be varied.

[0039] FIG. 5E shows a schematic side view of another embodiment of a prosthetic foot 500. The prosthetic foot 500 can have a first foot member 510 that includes a generally horizontal upper portion 512 and a lower portion 514. The upper portion 512 extends from a distal end 512a to a transition 516 with the lower portion 514. The lower

portion 514 curves downwardly and forwardly from the transition 516 to a distal end 514a. In another embodiment, the lower portion 514 can have a curved portion near the transition 516 and a generally horizontal portion near the distal end 514a. In one embodiment, the transition 516 can be v-shaped. In another embodiment, the transition 516 can be U-shaped. The prosthetic foot 500 can also have a second foot member 520 disposed below the first foot member 510 at a rear portion of the foot 500, where the second foot member 520 extends from a proximal end 522 at a rear most end of the foot 500 to a distal end 524. In one embodiment, the distal end 524 of the second foot member 520 is adjacent and attached to the first foot member 510 at a location between the transition 516 and the distal end 514a of the lower portion 514. In one embodiment, the second foot member 520 can be generally planar or flat along its length. In the illustrated embodiment, the first and second foot members 510, 520 define a slot 528 therebetween in the fore-aft direction at a rear portion of the prosthetic foot 500. The prosthetic foot 500 can also have an adapter 530 attached to the upper portion 512 near its distal end 512a.

[0040] A first MRE spring module 570 can be disposed generally vertically between the upper portion 512 and the lower portion 514 of the first foot member 510. In one embodiment, the first MRE spring module 570 can be axially aligned with the adapter 530. In the illustrated embodiment, a second MRE spring module 580 can be disposed generally vertically in the slot 528 between the first and second foot members 510, 520 at a rear portion of the prosthetic foot 500. As shown in FIG. 5E, the first MRE spring module 570 contacts the lower portion 514 of the first foot member 510 at a location distal of the location at which the second MRE spring module 580 contacts the first foot member 510. Accordingly, the first and second MRE spring modules 570, 580 act as parallel springs or shock modules. The second MRE spring module 580 can be selectively actuated to vary its stiffness, and as a result the amount that the second foot member 520 deflects toward the first foot member 510, for example at heel strike of the prosthetic foot 500 during ambulation, can be varied. Similarly, the first spring module 570 can be selectively actuated to vary its stiffness, and as a result the amount that the upper portion 512 deflects toward the lower portion 514, for example at mid-stance and toe-off of the prosthetic foot 500 during ambulation, can be varied.

[0041] FIG. 5F shows a schematic side view of another embodiment of a prosthetic foot 600. The prosthetic foot 600 includes a foot member 610 that extends between a proximal end 612 and a distal end 614. An adapter 630 can be coupled to an upper surface of the foot member 610 at a location between the proximal and distal ends 612, 614. The prosthetic foot 600 can also have a first lower member 620a and a second lower member 620b disposed below the foot member 610. The first lower member 620a can extend forwardly from a proximal end 622a attached to the foot member 610 to a distal end 624, so as to define a slot 628a in the fore-aft direction between the foot member 610 and the first lower member 620a at a front portion of the prosthetic foot 600. The second lower member 620b can extend rearwardly from a distal end 622b attached to the foot member 610 to a proximal end 626, so as to define a slot 628b in the fore-aft direction between the foot member 610 and the second lower member 620b at a rear portion of the prosthetic foot 600. As shown in FIG. 5F, the first and second lower members 620a, 620b attach to the foot member 610 generally midway between the proximal and distal ends 612, 614 of the foot member 610. In the illustrated embodiment, the first and second lower members 620a, 620b have a generally curved profile. However, the first and second lower members 620a, 620b can have other suitable profiles, such as planar or generally flat.

[0042] A first MRE spring module 670 can be disposed generally vertically between the foot member 610 and the first lower member 620a at a front portion of the prosthetic foot 600. A second MRE spring module 680 can be disposed generally vertically between the foot member 610 and the second lower member 620b at a rear portion of the prosthetic foot 600. In one embodiment, one of the MRE spring modules 670, 680 can be axially aligned with the adapter 630. In the illustrated embodiment, the second MRE spring module 680 can be disposed generally vertically in the slot 628b between the foot member 610 and the second lower member 620b at a rear portion of the prosthetic foot 600. As shown in FIG. 5F, the second MRE spring module 680 contacts the foot member 610 at a location distal of the location at which the first MRE spring module 670 contacts the foot member 610. Accordingly, the first and second MRE spring modules 670, 680 act as parallel springs or shock modules. The second MRE spring module 680 can be selectively actuated to vary its stiffness, and as a result the amount that the second lower member 620b deflects toward the

foot member 610, for example at heel strike of the prosthetic foot 600 during ambulation, can be varied. Similarly, the first spring module 670 can be selectively actuated to vary its stiffness, and as a result the amount that the first lower member 620a deflects toward the foot member 610, for example at toe-off of the prosthetic foot 600 during ambulation, can be varied.

[0043] FIG. 5G shows a schematic side view of another embodiment of a prosthetic foot 700. The prosthetic foot 700 can have an upper foot member 710 and a lower foot member 720 disposed below the upper foot member 710. The upper foot member 710 can extend from a proximal portion 712 to a distal portion 714, with an intermediate portion 716 between the proximal and distal portions 712, 714. In the illustrated embodiment, the proximal portion 712 is generally vertical and extends to a proximal end 712a, and the distal portion 714 is generally planar and extends to a distal end 714a. In the illustrated embodiment, the intermediate portion 716 can be curved so that the upper foot member 710 curves downwardly and forwardly from the proximal portion 712 to the distal portion 714. The upper foot member 710 can be a single monolithic piece. In another embodiment, the upper foot member 710 can be modular, with the proximal, intermediate and distal portions 712, 716, 714 being separate pieces that attach to each other. An adapter (not shown) can be attached to the proximal portion 712 of the upper foot member 710.

[0044] The lower foot member 720 can extend between a proximal end 722 and a distal end 724. In one embodiment, the lower foot member 720 can extend along a length generally corresponding to the length between the heel and toes of a natural human foot. As shown in FIG. 5G, the distal end 724 of the lower foot member 720 can be disposed forwardly of the distal end 714a of the upper foot member 710, and the proximal end 722 of the lower foot member 720 can be generally aligned with the proximal end 712a of the upper foot member 710. However, in other embodiments, the distal end 724 of the lower foot member 720 can be aligned with the distal end 714a of the upper foot member and/or the proximal end 722 of the lower foot member 720 can be disposed rearwardly of the location of the proximal end 712a of the upper foot member 710. In still another embodiment, the proximal and distal ends 722, 724 of the lower foot member 720 can extend rearwardly and forwardly, respectively, of the proximal and distal ends 712a, 714a of the upper foot member

710. In the illustrated embodiment, the lower foot member 720 is generally planar or flat between the proximal and distal ends 722, 724. In another embodiment, at least a portion of the lower foot member 720 can be curved. For example, the lower foot member 720 can have an arch portion, such as the arch 28 described above in connection with the prosthetic foot 100.

[0045] The prosthetic foot 700 can also have an ankle block 740 interposed between and completely separating the upper foot member 710 and lower foot member 720. In one embodiment, the ankle block 740 can be made of an inert elastic material and/or resilient material (e.g., urethane, natural or synthetic rubber, compressible foam such as expanded polyurethane foam or cellular foam) having desired compliance and energy return characteristics. Further information on prosthetic foot designs with ankle blocks can be found in US Patent Nos. 6,206,934; 6,280,479; and 6,899,737, the entire contents of all of which are hereby incorporated by reference and should be considered a part of this specification.

[0046] The prosthetic foot 700 can also include a first MRE spring module 770 and a second MRE spring module 780 disposed between and in contact with the upper foot member 710 and lower foot member 720. In the illustrated embodiment, the first MRE spring module 770 can be disposed between the lower foot member 720 and the distal portion 714 of the upper foot member 710 at a front portion of the prosthetic foot 700. The second MRE spring module 780 can be disposed generally between the lower foot member 720 and the intermediate portion 716 of the upper foot member 710 at a mid-portion of the prosthetic foot 700. In one embodiment, the second MRE spring module 780 can be disposed so that it aligns with the proximal portion 712 of the upper foot member 710. With continued reference to FIG. 5G, the first and second MRE spring modules 770, 780 can be disposed in the ankle block 740. In one embodiment, the MRE spring modules 770, 780 can be embedded in the ankle block 740. In another embodiment, the MRE spring modules 770, 780 can be disposed in openings or cavities within the ankle block 740. Accordingly, the first and second MRE spring modules 770, 780 act as parallel springs or shock modules. The second MRE spring module 780 can be selectively actuated to vary its stiffness, and as a result the amount that the lower foot member deflects toward the upper foot member 710, for example at heel strike or mid-stance of the prosthetic foot 700 during ambulation, can be varied. Similarly, the first

MRE spring module 770 can be selectively actuated to vary its stiffness, and as a result the amount that the lower foot member 720 deflects toward the upper foot member 710, for example at toe-off of the prosthetic foot 700 during ambulation, can be varied.

[0047] The prosthetic foot embodiments discussed above in connection with FIGS. 5A-G include various foot members (e.g., upper/lower foot members, heel member). In one embodiment, the foot members can have a substantially rectangular transverse cross-section with a generally linear (e.g., not curved) upper edge and lower edge. In another embodiment, the foot members can include two or more longitudinal members separated along at least a portion of their length by a longitudinal slot, such as the members 16a 16b and slot 17 described above in connection with the prosthetic foot 100. Where the prosthetic foot device includes multiple MRE spring modules, actuation of the multiple spring modules can be controlled together (e.g., via one controller) so as to provide a smooth rollover to the prosthetic foot during ambulation.

[0048] FIGS. 6A shows a schematic view of one embodiment of a MRE spring module 800. The MRE spring module 800 can have a first component 810 coupled to a second component 820 by MR elastomer portions 840. In the illustrated embodiment, the first component 810 is c-shaped and has spaced apart ends 812, 814 that define an opening 815 therebetween. In another embodiment, the first components can be u-shaped. The first component 810 can be a magnetic core. The second component 820 can be shaped like a block and movably extend in the opening between the spaced apart ends 812, 814. The MR elastomer portions 840 are disposed on either side of the second component 820 between the second component 820 and the ends 812, 814 of the first component. As shown in FIG. 6A, a wire coil is disposed about a central portion 816 of the first component 810 at a location aligned with the second component 820.

[0049] As discussed above, a current can be applied to the MRE spring module 800, which generates a magnetic flux. The MR elastomer portions 840 can have ferromagnetic particles interspersed within an elastomeric matrix in a manner whereby the MRE spring module 800 operates in shear when the magnetic flux is applied. For example the properties (e.g., stiffness) of the MR elastomer portions 840 can change in the presence of the magnetic flux so that the second component 820 moves into and out of the opening 815

between the ends 812, 814 of the first component 810. In one embodiment, the MRE spring module 800 can be incorporated into a prosthetic device, such as a prosthetic foot, where the first component 810 is coupled to one member of the prosthetic device and the second component 820 is coupled to another member of the prosthetic device. Accordingly, actuation of the MRE spring module 800 can vary the relative movement of the members of the prosthetic device.

[0050] FIG. 6B is a schematic view of another embodiment of a MRE spring module 800′. The MRE spring module 800′ is similar to the MRE spring module 800, except as noted below. Thus, the reference numerals used to designate the various components of the MRE spring module 800′ are identical to those used for identifying the corresponding components of the MRE spring module 800 in FIG. 6A, except that a "′" has been added to the reference numerals.

[0051] The MRE spring module 800′ can have a first component 810′ and a second component 820′ that are interconnected by MR elastomer portions 840′. The first component 810′ can be c-shaped and have a wire coil 830′ disposed about an intermediate portion 816′ of the first component 810′ at a location generally aligned with the second component 820′. However, the first component 810′ can have other suitable shapes, such as a u-shape. The first component 810′ can function as a magnetic core. The second component 820′ can be shaped like a block and movably extend in an opening 815′ between spaced apart ends 812′, 814′ of the first component 810′. The MR elastomer portions 840′ are disposed on either side of the second component 820′ between the second component 820′ and the ends 812′, 814′ of the first component.

[0052] With continued reference to FIG. 6B, the MR elastomer portions 840′ can have ferromagnetic particles interspersed within an elastomeric matrix in a manner whereby the MRE spring module 800′ operates in tension and compression when a magnetic flux is applied to the spring module 800′. For example the properties (e.g., stiffness) of the MR elastomer portions 840′ can change in the presence of the magnetic flux so that the ends 812′, 814′ of the first component 810′ move toward or away from the second component 820′. In one embodiment, the MRE spring module 800′ can be incorporated into a prosthetic device, such as a prosthetic foot, where the first component 810′ is coupled to one member of the

prosthetic device and the second component 820′ is coupled to another member of the prosthetic device. Accordingly, actuation of the MRE spring module 800′ can vary the relative movement of the members of the prosthetic device, and the stiffness of the prosthetic device.

[0053] FIG. 6C is a schematic view of another embodiment of a MRE spring module 800′′. The MRE spring module 800′′ is similar to the MRE spring module 800, except as noted below. Thus, the reference numerals used to designate the various components of the MRE spring module 800′′ are identical to those used for identifying the corresponding components of the MRE spring module 800 in FIG. 6C, except that a "′′" has been added to the reference numerals.

[0054] The MRE spring module 800′′ can have a first component 810′′ and a second component 820′′ that are interconnected by MR elastomer portions 840′′. The first component 810′′ can be c-shaped. However, the first component 810′′ can have other suitable shapes, such as a u-shape. The first component 810′′ can function as a magnetic core. The second component 820′′ can be c-shaped with ends 822′′, 824′′ that are disposed opposite ends 812′′, 814′′ of the first component 810′′ so that the first and second components 810′′, 820′′ face each other. A wire coil 830′′ can be disposed about an intermediate portion 826′′ of the second component 820′. In another embodiment, the second component 820′′can be u-shaped. The MR elastomer portions 840′′ are disposed between the ends 812′′, 814′′ of the first component 810′′ and the ends 822′′, 824′′ of the second component 820′′.

[0055] With continued reference to FIG. 6C, the MR elastomer portions 840′′ can have ferromagnetic particles interspersed within an elastomeric matrix in a manner whereby the MRE spring module 800′′ operates only in compression when a magnetic flux is applied to the spring module 800′′. For example the properties (e.g., stiffness) of the MR elastomer portions 840′′ can change in the presence of the magnetic flux so that the ends 812′′, 814′′ of the first component 810′′ move toward the ends 822′′, 824′′ of the second component 820′′. In one embodiment, the MRE spring module 800′′ can be incorporated into a prosthetic device, such as a prosthetic foot, where the first component 810′′ is coupled to one member of the prosthetic device and the second component 820′′ is coupled to another member of the

prosthetic device. Accordingly, actuation of the MRE spring module 800′′ can vary the stiffness of the members of the prosthetic device.

[0056] As described in the embodiments above, a magnetorheological elastomer (MRE) spring element can be placed in various locations of any variation of a prosthetic or orthotic device. By choosing the location of one or more MRE spring elements, relative to the device's structure, the spring elements could, for example, provide variable stiffness for heel-strike, toe-off, or in general shock absorption for the prosthetic or orthotic device. Additionally, the design and structure of the MRE spring element can vary, with MR elastomers that can be used in one or more of compression, tension and shear. Further examples of MRE spring element designs can be found in the Lerner-Cunefare publication[1], which is attached hereto as Appendix A, the entire contents of which are hereby incorporated by reference and should be considered a part of this specification.

[0057] Accordingly, the embodiments above disclose orthotic and prosthetic devices where the stiffness of the device is controllable and adaptable to the user's current activity level. The device can be controlled either manually or automatically by responding to signals that represent the current activity level of the user, and be able to change its operating characteristics (e.g., stiffness) in real-time.

[0058] Of course, the foregoing description is that of certain features, aspects and advantages of the present invention, to which various changes and modifications can be made without departing from the spirit and scope of the present invention. Moreover, the prosthetic or orthotic device with the MRE spring need not feature all of the objects, advantages, features and aspects discussed above. Thus, for example, those skill in the art will recognize that the invention can be embodied or carried out in a manner that achieves or optimizes one advantage or a group of advantages as taught herein without necessarily achieving other objects or advantages as may be taught or suggested herein. In addition, while a number of variations of the invention have been shown and described in detail, other modifications and methods of use, which are within the scope of this invention, will be readily apparent to those of skill in the art based upon this disclosure. It is contemplated that various combinations or

---

[1] Lerner, A.A. and K.A. Cunefare. 2007. *Performance of MRE-based Vibration Absorbers.* Journal of Intelligent Material Systems and Structures, Vol. **19**(5): p. 551-563, 2008.

subcombinations of the specific features and aspects between and among the different embodiments may be made and still fall within the scope of the invention. Accordingly, it should be understood that various features and aspects of the disclosed embodiments can be combined with or substituted for one another in order to form varying modes of the discussed prosthetic or orthotic device having MRE springs.

WHAT IS CLAIMED IS:

1. A prosthetic or orthotic device, comprising:

a body configured to support a human limb of a user wearing the prosthetic or orthotic device; and

a shock absorption member coupled to the body, the shock absorption member comprising one or more magnetorheological elastomer (MRE) springs disposed between a first portion of the body and a second portion of the body,

wherein the one or more MRE springs are selectively actuatable to vary a stiffness of the shock absorption member via the application of a magnetic flux to thereby adjust a stiffness of the body of the prosthetic or orthotic device to a level corresponding to an activity level of the user.

2. The device of claim 1, wherein the one or more MRE springs operate in one or more of compression, tension and shear when the magnetic flux is applied to the MRE spring.

3. The device of claim 1, wherein a spring constant of the one or more MRE springs increases by about 24% when the magnetic flux is applied so that the MRE spring increases in stiffness in the presence of the magnetic flux.

4. The device of claim 1, wherein the prosthetic or orthotic device is a prosthetic foot.

5. The device of claim 4, wherein the first portion is an upper foot member and the second portion is a lower foot member of the prosthetic foot.

6. The device of claim 5, wherein the one or more MRE springs comprise two MRE springs disposed between the upper and lower foot members, wherein a first of the two MRE springs is disposed at a front portion of the prosthetic foot and a second of the two MRE springs is disposed at a rear portion of the prosthetic foot, the second MRE spring actuatable to vary the stiffness of the prosthetic foot during heel-strike and the first MRE spring actautable to vary the stiffness of the prosthetic foot during toe-off of the prosthetic foot.

7. The device of claim 1, wherein the one or more MRE springs are actuated by a user of the prosthetic or orthotic device.

8. The device of claim 7, wherein the one or more MRE springs are actuated manually by the user.

9. The device of claim 7, wherein the one or more MRE springs are actuated remotely by the user with a hand held remote control.

10. The device of claim 1, further comprising an electronic controller that controls the actuation of the one or more MRE springs.

11. The device of claim 10, further comprising one or more sensors disposed on the body and configured to sense one or more parameters during ambulation, the one or more sensors configured to communicate with the controller, the controller determining an activity level of the user based at least in part on the sensed parameters.

12. A prosthetic foot, comprising:

a foot plate extending from a generally vertical proximal portion to a generally horizontal distal portion, the foot plate curving generally downwardly and forwardly between the proximal and distal portions;

an adapter coupled to the proximal portion of the foot plate; and

a shock absorbing member removably coupled to the adapter, the shock absorbing member comprising:

a cylindrical core extending along a generally vertical axis,

an electrically conducting coil disposed about the cylindrical core, and

a spring surrounding the core and the coil, the spring comprising a magnetorheological elastomer (MRE) material, wherein the MRE spring can be actuated to vary the stiffness of the shock absorbing member via the application of a magnetic flux to the spring.

13. The prosthetic foot of claim 12, wherein the MRE spring operates in one or more of compression, tension and shear when the magnetic flux is applied thereto.

14. The prosthetic foot of claim 12, wherein a spring constant of the MRE spring increases by about 24% when the magnetic flux is applied so that the MRE spring increases in stiffness in the presence of the magnetic flux.

15. The prosthetic foot of claim 12, wherein the MRE spring is disposed at a rear portion of the prosthetic foot, the MRE spring actuatable to vary the stiffness of the prosthetic foot during heel-strike of the prosthetic foot.

16. The prosthetic foot of claim 12, wherein the MRE spring is actuated by a user of the prosthetic foot.

17. The prosthetic foot of claim 16, wherein the MRE spring is actuated manually by the user.

18. The prosthetic foot of claim 16, wherein the MRE spring is actuated remotely by the user with a hand held remote control.

19. The prosthetic foot of claim 12, further comprising an electronic controller that controls the actuation of the MRE spring.

20. The prosthetic foot of claim 19, further comprising one or more sensors disposed on the prosthetic foot and configured to sense one or more parameters during ambulation, the one or more sensors configured to communicate with the controller, the controller determining an activity level of the user based at least in part on the sensed parameters.

PROSTHETIC AND ORTHOTIC DEVICES HAVING MAGNETORHEOLOGICAL ELASTOMER SPRING WITH CONTROLLABLE STIFFNESS

ABSTRACT OF THE DISCLOSURE

A prosthetic or orthotic device includes a body configured to support a human limb of a user wearing the prosthetic or orthotic device. The device can also include a shock absorption member coupled to the body. The shock absorption member includes one or more magnetorheological elastomer (MRE) springs disposed between a first portion of the body and a second portion of the body. The one or more MRE springs are selectively actuatable to vary a stiffness of the shock absorption member via the application of a magnetic flux, thereby adjusting a stiffness of the body of the prosthetic or orthotic device to a level corresponding to an activity level of the user.

11764778_1
082411

APPENDIX A

Performance of MRE-based Vibration Absorbers

A. Albanese Lerner and K.A. Cunefare

Journal of Intelligent Material Systems and Structures 2008 19: 551 originally published online 30 May 2007
DOI: 10.1177/1045389X07077850

Performance of MRE-based Vibration Absorbers

A. ALBANESE LERNER AND K. A. CUNEFARE*

Georgia Institute of Technology, 350159 Georgia Tech Station, Atlanta, GA 30332, USA

ABSTRACT: The purpose of this work is to use magnetorheological elastomers (MREs) as field-dependent springs within three vibration absorber configurations, and to determine their vibration absorption characteristics. Magnetorheological elastomers are fabricated from silicone gel and iron microparticles, and implemented as tunable springs in three vibration absorber configurations, which excited the MREs in shear, squeeze mode, and compression. Each vibration absorber configuration exploits different magneto-mechanical properties, achieving very different results. The MRE iron concentration is varied to find the largest natural frequency shift for the squeeze-mode absorber due to an applied magnetic field. Absorbers with MREs containing 35% iron by volume exhibits the largest natural frequency shift, 507%. MREs containing 35% iron are placed into shear and longitudinal mode vibration absorber devices, which exhibit 470% and 180% frequency increases, respectively.

Key Words: magnetorheological elastomer, adaptive vibration absorber, variable stiffness, controllable spring.

INTRODUCTION AND BACKGROUND

TUNED vibration absorbers (TVAs) are spring–mass–damper devices used to suppress vibration in mechanical systems. TVAs are prevalent in mechanical systems because they are inexpensive to produce and have well-defined vibration characteristics (Meirovitch, 1986), but a TVA's design must be compromised when controlling complex vibration patterns, including variable, broadband, or unknown excitation frequencies. If instead, a spring, mass, or damper element within an absorber is able to adaptively change to 'retune' the vibration absorber, complex vibration patterns can be more easily controlled without the design compromises. This work investigates the effects of different vibration absorber configurations on frequency changes due to the presence of magnetorheological elastomers (MREs), particularly to be used in the future with a state-switched absorber (SSA) control schema (Cunefare et al., 2000). The design of the absorbers in this work were chosen to emulate the performance of vibration absorbers found on ATR 42 and 74 aircraft fuselages.

An adaptive spring, whose stiffness can be modified in a controllable manner, may be implemented as a variable stiffness spring according to active vibration absorber (AVA), hybrid vibration absorber (HVA), or semiactive absorber (SA) control algorithms. AVAs, HVAs, and SAs possess superior vibration suppression capabilities for controlling complex vibration patterns, such as variable, broadband, and unknown excitation frequencies (Sun et al., 1995). AVAs, HVAs, and SAs are more effective than TVAs in these situations because they all contain at least one changeable element that can 'retune' the device's operational frequency, which increases the effective operational bandwidth. While AVAs, HVAs, and SAs suppress complex vibration patterns more effectively than TVAs, not every control algorithm suppresses vibration equally. Each algorithm, its strengths and weaknesses, will be briefly discussed to understand the choice of an SSA for this particular application of ATR 42/74 fuselage control.

Active vibration absorbers are vibration suppression devices that contain at least one dynamic element that continuously changes. Although AVAs are effective vibration suppression tools, they carry the risk of inducing instability if controlled improperly (Abe and Igusa, 1996). Additionally, AVA control algorithms are complex and expensive, and thus normally reserved for only the most critical vibration suppression cases. AVAs are best suited for applications where TVA devices cannot prevent instability (Karnopp, 1973), such as to helicopter rotors, flexible aerospace vehicle bending vibration, or when TVAs cannot control vibration within acceptable limits, such as fighter pilot motion within aircraft (Karnopp et al., 1974).

*Author to whom correspondence should be addressed.
E-mail: ken.cunefare@me.gatech.edu
Figures 1, 4 and 5 appear in color online: http://jim.sagepub.com

1045-389X/08/05 0551–13 $10.00/0 DOI: 10.1177/1045389X07077850

While AVAs continuously change and thus require a continuous power source, SAs feature active and passive components that operate concurrently. They have been shown to be useful in vibration damping applications with buildings while conserving power requirements (Hrovat et al., 1983). SAs can also be used to control transient disturbances. An SA is fundamentally an AVA, but the algorithm controlling the active component dictates that the device may only change at specific, discrete instances (Sun et al., 1995). This means that in between these instances, SAs behave as passive devices. SAs are used in applications that do not require AVAs, but where TVA's performance cannot achieve the desired specifications (Abe and Igusa, 1996).

An SSA is a particular class of SA that allows switching to occur only at discrete instances. This type of absorber has been found to equal or improve upon optimal TVA performance for multitone vibration excitation (Cunefare, 2000; Cunefare et al., 2000). The objective of the research at hand was to develop a tunable spring useful in SSA applications. Since AVAs, HVAs, and SAs all possess changeable elements, tunable springs developed here could feasibly also be implemented in a variety of active and semiactive control schema. The work at hand was concerned with developing a changeable spring element and optimizing the spring's properties to generate a vibration absorber capable of a maximum frequency increase; once an optimal spring was found, absorber performance was compared and transient properties were analyzed.

Depending upon the application, any number of different changeable elements may be employed. Several materials, including piezoceramics, magnetorheological (MR) fluids and elastomers, and electrorheological (ER) fluids and elastomers, can be used as a changeable element in an AVA, HVA, or SA. An MRE was used as a changeable element in this research for two reasons. MREs have magnetic field-dependent spring rates, and their stiffness in absence of any magnetic field, or 'baseline stiffness', is easy to vary according to the vibration control situation, because elastomer foams, gels, and rubbers are available in a wide variety of stiffness moduli.

An MRE contains ferromagnetic particles embedded within an elastomer matrix. The ferromagnetic particles cause the MRE stiffness to change at a rate dependent upon the applied magnetic field. MREs consisting of silicone gel and iron microparticles are presented here as changeable stiffness elements in three types of vibration absorber devices, discussed in the 'Absorber designs' section.

MRE stiffness is typically modeled as a spring with complex stiffness, such that

$$K' = Ke^{i\delta}, \tag{1}$$

where δ is a loss factor (Payne and Whittaker, 1971). MRE stiffness in the absence of a magnetic field, or baseline stiffness, is determined not only by the host elastomer stiffness, but also by the amount of particulate matter present in an elastomer. The Young's modulus of a filled elastomer is (Guth, 1945)

$$E = E_0\left(1 + 2.5\phi + 14.1\phi^2\right), \tag{2}$$

where E_0 is the host elastomer's unfilled Young's modulus and ϕ is the volume fraction of particles in the elastomer, by volume. Although Equation (2) was derived assuming random dispersion of spherical particles, it has been determined experimentally to hold also for aligned particles (Meinecke and Taftaf, 1988). The Young's modulus, as calculated in Equation (2), can be used to find baseline stiffness, which is defined as an elastomer's stiffness in the absence of a magnetic field. Spring baseline stiffness can be found such that

$$K = \frac{EA}{L}, \tag{3}$$

where A is the area of the elastomer, L is the elastomer length, and E is the Young's modulus as determined by Equation (2).

The amount of particulate matter in an elastomer affects not only the baseline stiffness, but the quantity and the particulate matter's orientation within an MRE also affects the MRE's ability to change its stiffness when subjected to a magnetic field. Ferromagnetic particles aligned in chains can yield a 20% larger stiffness increase in the presence of a magnetic field than unaligned particles (Bossis et al., 1999). When particles were aligned in chains, MREs excited in shear with 27% iron particles by volume were found to increase in stiffness by about 50% (Davis, 1999). Furthermore, the magneto-mechanical properties of an MRE is substantially different from those of similar elastomers cured in the absence of a field, known as an elastomers–ferromagnet composite. For details about these differences (Zhou and Jiang, 2004).

MRE particles are aligned in chains by applying a magnetic field during MRE cure. Iron particles within the MRE will align in the direction of the magnetic field lines. Because the particles are aligned in chains, MREs are anisotropic materials, meaning their material properties are orientation-dependent. This orientation dependency will be a critical factor in terms of how an MRE spring will perform in a given device, dependent upon the loading axis relative to the particle chain alignment axis. In fact, the magneto-mechanical forces cause radically different responses in each configuration.

For the purposes of the work presented here, a shear-mode configuration implies that the excitation direction is perpendicular to the particle chains, whereas longitudinal and squeeze mode excitations feature excitation parallel to the direction of particle chains. The primary

difference between a longitudinal and a squeeze mode configuration is that the static equilibrium of a longitudinal configuration is determined by geometric conditions, whereas a squeeze-mode configuration has a static equilibrium determined by a force balance. In other words, the MREs in longitudinal devices were placed in between gaps of set and known lengths, whereas MREs in squeeze mode were placed in between two masses, and the weight of the absorber mass determined the static displacement. While research has been conducted on MREs in shear mode (Shiga et al., 1995; Jolly et al., 1996; Davis, 1999; Ginder et al., 1999), published work has not been found in the area of longitudinal or squeeze mode excitation. Furthermore, no mechanism has been presented that would explain a stiffness increase when a device is excited in parallel with the magnetic force, which would be the case for both longitudinal and squeeze mode devices.

Three devices were designed to examine the relative effect of magnetic field on MREs in shear, longitudinal, and squeeze mode absorber configurations. Each device was designed to operate in a frequency range below 100 Hz, weigh <100 g, and be no longer than 6 cm in any dimension. To achieve these performance goals, six design variables were selected and isolated to generate three absorber devices.

ABSORBER DESIGNS

The absorbers considered in this research were designed to be analogs to the TVAs aboard ATR42 and ATR72 aircraft fuselages. In order to be similar to these TVAs, the three vibration absorber configurations were designed to operate below 100 Hz, have a total mass <100 g, and be no longer than 6 cm in any dimension. State-switched absorber design research has also demonstrated that damping values ranging between 0.27 and 0.42 yield optimal performance results (Holdhusen and Cunefare, 2003), which translate to Q-values ranging between 0.84 and 1.86. It should be noted that this application is significantly different from other previous applications of MREs. The MREs in this work are nonload bearing, and therefore can be substantially softer than those used in previous applications.

Each device, shown in Figure 1 consisted of five components: two masses, a wire coil, and two MRE springs. Since the devices were designed to eventually be AVAs, SAs, or HVAs, one mass was considered to be a base mass, and the other mass was referred to as an absorber mass. Wire coils generate magnetic fields when current runs through them; a wire coil was wound around either an absorber or base mass for each device to provide a source of magnetic field. Two MREs were placed between the base and absorber masses in each device, acting as a spring.

Figure 1 shows the three devices designed to excite MREs in different configurations. The shear and longitudinal mode devices, Figure 1(a) and 1(b) respectively, were in fact the same device but excited in different directions. The shear device was excited perpendicular to the direction of magnetic field, whereas the longitudinal device was excited in parallel to the direction of magnetic field. The squeeze mode device, shown in Figure 1(c), also was excited parallel to the direction of magnetic field, but its geometry allowed the MRE's static displacement to be determined by a force balance rather than by geometric constraints. This means that rather than the static displacement being the set length as in the longitudinal configuration, the static displacement was determined by the static equation of motion, $kx_{st} = M_{abs}g$, where k is the stiffness, x_{st} is the static displacement, M_{abs} is the absorber mass, and g is gravitational acceleration.

The devices needed to satisfy the geometric and mass constraints as well as have a wire coil capable of delivering 2 T magnetic flux density through the iron particles in the MREs, in order to magnetically saturate the particles. The flux density through the iron particles in the MRE was not measurable, but assuming that flux density would travel exclusively through the iron particles and a particle volume fraction of $\phi = 0.3$, the overall flux density would be $B_{MRE} = 0.6$T. The flux density through the steel core was found to be

$$B_{st} = \frac{B_{MRE} \cdot A'_{MRE}}{A_{st}}, \tag{4}$$

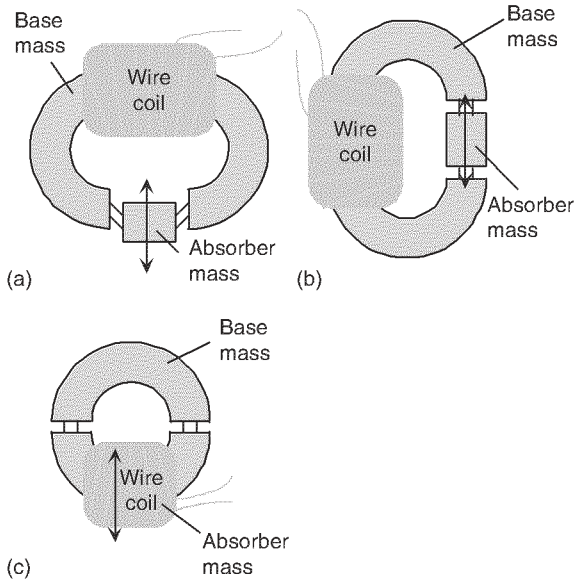

Figure 1. *(a) Shear device; (b) longitudinal device; and (c) squeeze mode device with direction of excitation.*

where A_{st} was the steel mass face area and A'_{MRE} was the effective pole area, which accounted for fringing effects (Lord M Solutions, 2001). A'_{MRE} was found by

$$A'_{MRE} = \pi\left(r_{MRE} + \frac{1}{2}L\right)^2, \quad (5)$$

where r_{MRE} is the radius of the MRE and L is the MRE length. Using Equation 5 and substituting $B_{MRE} = 0.6$T into Equation4, the required saturation flux density through the steel mass was found to be

$$B_{st} = \frac{6\pi(r_{MRE} + (1/2)L)^2}{10000s^2}, \quad (6)$$

in T, where s is the length and width of the base and absorber mass cross-sectional areas.

The flux densities, B_{MRE} and B_{st}, describe the concentration or dispersion through MREs and steel as the result of an applied magnetic field. The applied magnetic field is created by a wire coil, where the number of turns and amount of current flowing through the solenoid can be described as

$$NI = \oint H \cdot dl, \quad (7)$$

where H is the magnetic field intensity, and dl is a differential length along the magnetic circuit. For the specific application of an absorber, Ampere's circuit law can be applied as

$$NI = 2(LH_{MRE} + \pi r_{st}H_{st}), \quad (8)$$

where L is the length of an MRE, H_{MRE} is the magnetic field in the MREs, r_{st} is the mean radius of the absorber and base masses, as depicted in Figure 2 for the squeeze mode device, and H_{st} is the magnetic field present in the masses. The relationship between B_{st} and H_{st}, or that between B_{MRE} and H_{MRE}, is described as $B = \mu H$, where μ is the relative permeativity, which is nonlinear and a function of both material properties and magnetic field. Because μ has nonlinear traits, it is common to determine the relationship between B and H through B–H curves. B–H curves are readily available for low-carbon steel, but there have been none published for the particular MRE that was investigated in this research. However, a B–H curve was found for MR fluids (Lord M Solutions, 2001). While MR fluids behave differently from elastomers, they were assumed to exhibit similar flux-field properties for design purposes. Using the B–H curve for an MR fluid, a flux density of $B_{MRE} = 0.6$T was found to correspond to a magnetic field of $H_{MRE} = 150$ kA/m (Lord M Solutions, 2001).

Since magnetic fields affect MRE stiffness, a low reluctance path was created by constructing the base and absorber masses out of low-carbon steel. Since the face area of the MRE is different from the steel loop, fringing was taken into account when calculating the flux density through the MRE. The natural frequency is then

$$\omega_n = \sqrt{\frac{2E'A_{MRE}}{lM_{abs}}}, \quad (9)$$

where E' was determined from Equation (2), A_{MRE} was the cross-sectional area of the MRE, and M_{abs} was the absorber mass.

Figure 2 shows the basic design parameters that were manipulated for the squeeze mode device design. The devices were assumed to have an optimal iron content of about 30%, which would be consistent with another research (Davis 1999). If iron particles were magnetically saturated in a 30% MRE, a flux density of $B_{MRE} = 0.6$ T through the MRE would be required. The base and absorber masses were described by the mean radius r_{st} and the length of the side, s. The MRE's geometry was determined by its radius, r_{MRE}, and its elastomer length, L. The wire coil was defined by the wire size and the number of turns, N. These six parameters were manipulated until the design specifications were met and Equations (8) and (9) were satisfied.

Figure 3 shows the final designs and their geometries. Cylindrical MREs were created having 0.1 cm radii and 0.5 cm lengths, and were sliced in half lengthwise before

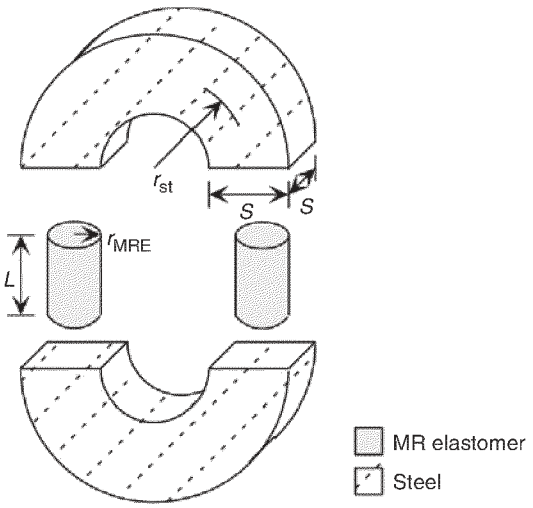

Figure 2. *An exploded view of the device and its design variables.*

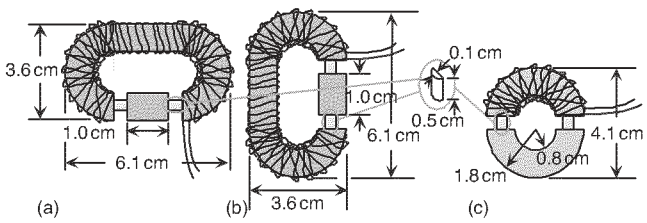

Figure 3. *Dimensions of a fully assembled (a) shear mode absorber device, (b) longitudinal mode absorber device, and (c) squeeze mode absorber device.*

being attached to the devices. The shear mode device and the longitudinal mode device both had longest length scales of 6.1 cm. The overall squeeze mode height was 4.1 cm, the width was 3.6 cm, and the depth, not shown in Figure 3, was 1.0 cm. All three devices had cross-sectional areas of 1.0 cm × 1.0 cm.

The devices were designed so that identically shaped MREs could be placed in each configuration. MREs were cured in a special mold and placed into these devices. These processes are presented in the Experimental Setup section.

EXPERIMENTAL SETUP

The experimental objective was to determine the effective stiffness of the MR elastomer in longitudinal, shear, and squeeze vibration modes. This section describes the procedure used for mixing and curing MREs, as well as the method used to incorporate MREs into vibration absorbers. A description of the experimental setup is also included.

MREs consisted of a two-part silicone, GE Silicone's RTV 6186, and an iron micropowder, ISP grade R-1430. The iron micropowder had an average particle diameter of 6–9 μm, and contained a minimum of 99.5% iron by mass. The iron micropowder consisted a maximum of 0.3% carbon, 0.4% oxygen, and 0.1% nitrogen. MREs containing <30% iron by volume broke under the stress of the absorber mass. This is consistent with the findings that filled elastomers have increased ultimate strengths with increased amounts of filler particles, provided that the filler particle diameter is small (Drozdov and Dorfmann, 2001). Therefore, MREs containing <30% iron by volume were additionally filled with talc powder to produce an MRE with a total particle volume of 30%. This procedure increased the strength of the MRE, and allowed the MREs to be tested without breaking.

MREs were compounded by measuring one part of silicone, then adding the appropriate amount of the iron micropowder and talc powder as necessary to achieve the desired volume fraction. Once the silicone part and the powder had been mixed thoroughly, the second silicone part was added. This was mixed over moderate heat for 5 min, and then transferred to a mold specially designed to cure elastomers in the presence of a magnetic field.

MREs were compounded with different amounts of iron micropowder. The iron micropowder was added so that it comprised a certain percentage of the total MRE volume. Hence, a '35% MRE' refers to an MRE that contains 35% iron by volume.

Figure 4 depicts a cross-sectional view of the mold and its different material components. Flux density lines were generated by applying 4.5 A current through ~900 turns of magnet wire. The flux path was promoted through the mold using low-carbon steel. The flux density through the thinnest section of steel was estimated to be 1 T, and caused the iron micropowder to align in chains inside the curing elastomer. The mold and MRE was heated to an average temperature of 150°C for 30 min.

Figure 5 shows a thin slice of 35% MRE cured in the mold with a magnetic field. The MRE was embedded in methyl methacrylate, and sliced along the direction of the magnetic field to a thickness of 210 μm. The slice was then placed on a slide and polished. The MRE was backlit and magnified by a factor of 10. The black dots are in fact iron particles; Figure 5 shows that the iron particles did in fact line up in chains when they were cured in the presence of a magnetic field, as described.

Once an MRE had cooled, it was removed from the mold. The cured MRE was sliced in half parallel to the direction of aligned iron chains, as indicated in Figure 3, such that the cross-sectional area was 'D'-shaped. Each MRE half was placed on either side of the base mass.

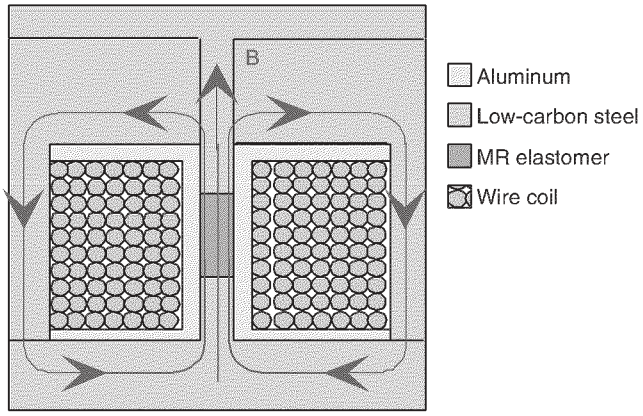

Figure 4. *The mold promotes magnetic field concentration through curing MREs.*

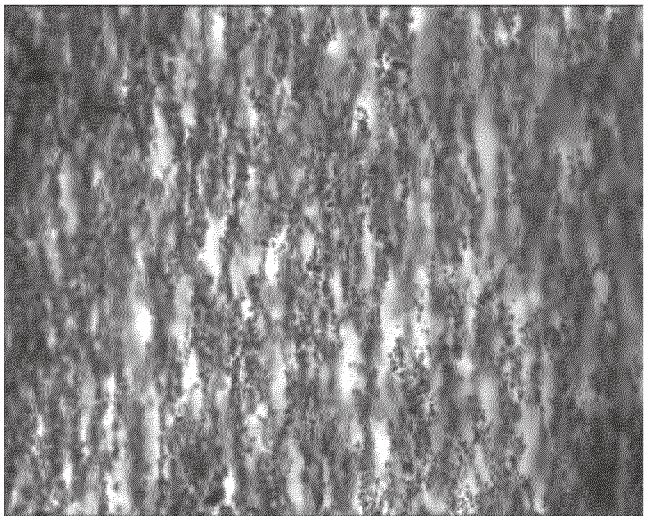

Figure 5. *A 35% MRE magnified 10 times.*

The MRE pieces were secured to the base mass using a Loctite 454 epoxy. The MRE pieces were held in place during epoxy cure, for a minimum of 1 h but typically for 12 h to ensure a complete cure. The MRE pieces were then epoxied to the absorber mass, and the setup was held in place during the epoxy cure.

The fully assembled device was placed into the experimental setup depicted in Figure 6. A white noise signal, low-pass filtered to 1000 Hz, was amplified by a LDS PA25E power amplifier and delivered to the base mass via an LDS V205 shaker. A PCB 288A11 accelerometer was attached to the base mass, while the absorber mass was instrumented with a PCB 303A02 accelerometer. The accelerometer signals were band-limited by a Siglab model 50-21 data acquisition system to 500 Hz, and transferred to a PC. Flux density data from each test was recorded manually from a Lakeshore model 480 fluxmeter.

The devices were placed in the experimental setup shown in Figure 6 and subjected to three types of tests. One test measured the ratio of flux density through the MRE to the flux density through the base mass iron, another test evaluated the devices' natural frequencies and loss factors, and a third test measured the static displacement in the squeeze mode device for different current levels. The flux density ratio was conducted in the absence of an excitation force to ensure accurate results, and the static displacement tests were conducted with step current inputs. Both the flux density ratio and static displacement tests were conducted while mounted into the experimental setup to duplicate as much of the natural frequency test environment as possible. The details of each of these tests, their results and implications are presented in the 'Results and discussion' section.

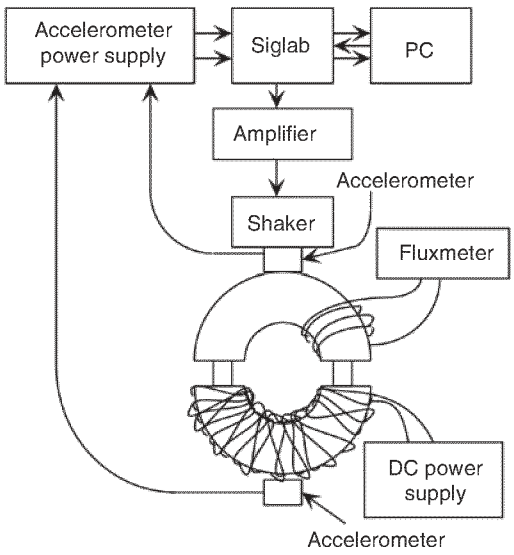

Figure 6. Experimental setup with squeeze mode device.

RESULTS AND DISCUSSION

Performance of the absorber designs was determined experimentally as a function of iron content and as a function of absorber geometry. The extent to which flux–field lines concentrated through MREs of varying concentrations, or recipes, is presented in the sub section 'Flux density tests'. Absorber performance was tested as a function of iron to silicone ratio, with the results presented in the Section 'Natural frequency response versus MRE content in a squeeze-mode device' The elastomer-iron mixture that yielded the largest frequency change was placed in three different vibration absorbers to examine the effect of different absorber configurations on natural frequency change, with the results presented in the subSection 'Natural frequency response in longitudinal, shear, and squeeze mode devices'.

Flux Density Tests

Flux density between identical materials of two different cross-sectional areas A_1 and A_2 can be found to be

$$B_2 = \frac{B_1 A_1}{A_2} \tag{10}$$

where B_1 and B_2 are flux densities through cross-sectional areas A_1 and A_2, respectively. However, this relationship does not hold true if the materials are not identical. Furthermore, if one of these materials is heterogeneous, as is the case for MREs, there are no known equations to define the relationship between B_2 and B_1.

Figure 7 illustrates flux lines travelling through an MRE sample. Some flux lines condense to travel through the MRE, and others fringe around the MRE. Because MREs have heterogeneous magnetic properties, Equation (10) does not predict the flux density that will travel through the MRE. Since Equation (10) exists, it was known that the ratio of flux density through the MRE to the flux density through the base mass would be constant for a given MRE composition. The flux

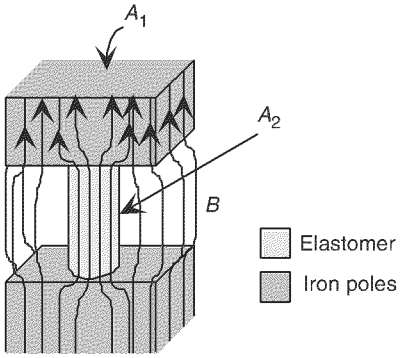

Figure 7. Flux density through two unlike areas.

density ratio tests were conducted to determine the relationship between B_2 and B_1.

Six MRE compositions, or recipes, were cured and placed into the experimental setup. Prior to the second MRE epoxy stage, a 125-turn wire coil was fitted around one MRE piece. This wire coil was connected to the fluxmeter, and flux density was measured through the MRE piece at field intensity values between 0 and 18.3 kA/m, with intervals of 2.3 kA/m. The flux density through the base mass was measured at the same current values. Each measurement was conducted three times. The results displayed in Figures 8 and 9 reflect the average value for these measurements. The results were extremely consistent, and variance between measurements was observed to be <0.0065 T.

Flux density was measured through MREs as a function of magnetic field intensity, as can be seen in Figure 8(a). The relationship between field intensity and flux density was found to fit a linear relationship such that $R^2 > 0.99$ for each MRE recipe. The corresponding slope of flux density to field intensity is shown in Figure 8(b) as it relates to MRE iron content. The slope of flux density to field intensity was determined via a least-squared error method. Figure 8(a) and (b) demonstrates that larger iron content in an MRE generally results in a larger flux density to field intensity ratio, although the 40% MRE showed the highest flux density to field intensity ratio.

The flux density recorded in Figure 8 was measured by placing a 125-turn coil around one MRE. The coil fit very snugly around undeformed MREs in order to minimize the effects of fringing as much as possible; however, this meant that the MRE was constrained by the presence of the coil. This constraint was unacceptable for further testing. In order to measure the magnetic flux in the device while allowing the MRE to behave unencumbered by coil, magnetic flux needed to be measured somewhere else on the device, where the flux density through this other location would have a known relationship to the flux density through the MRE.

It turns out that a coil around the steel base mass did not interfere with device motion, so flux density was measured through the steel masses as well. The flux density–field intensity level relationship through the steel also fit a linear relationship. As a consequence, MRE flux density was found to fit a linear relationship to the steel flux density, which was predicted by Equation 10. Figure 9 shows the ratios of flux density through MREs to flux density through the base mass, or flux density ratio = $B_{\mathrm{MRE}}/B_{\mathrm{base\ mass}}$, for a squeeze mode device containing MREs of different iron content. The 0% MRE was the only MRE to have a flux density ratio of <1, which indicates that fringing effects occurred. Although only moderate flux density concentration was observed for MREs containing iron microparticles, it can be presumed that because there was concentration,

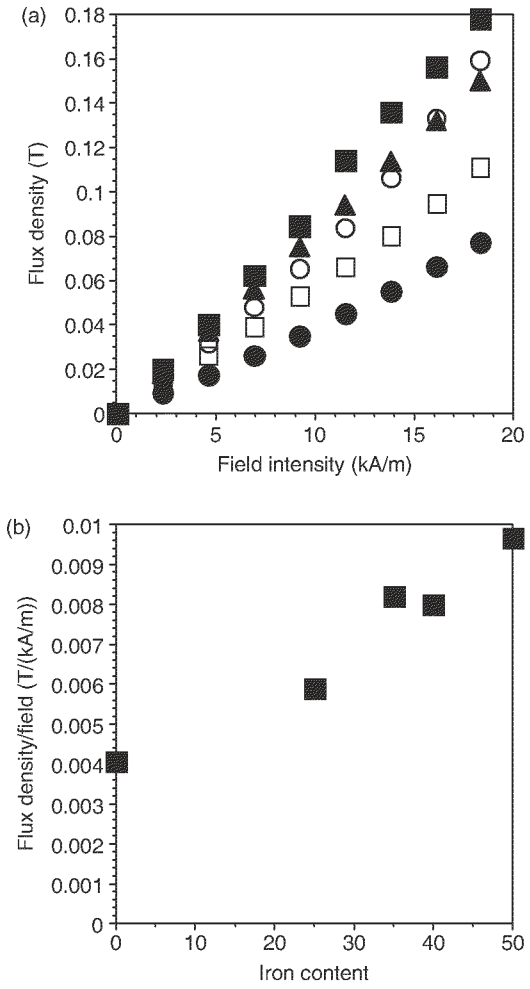

Figure 8. *(a) Flux density through an MRE at different field intensity levels, ■ 50%, ○ 40%, ▲ 35%, □ 30%, • 25%, △ 0% and (b) the magnetic flux density/field slope for MREs of different iron content, by volume.*

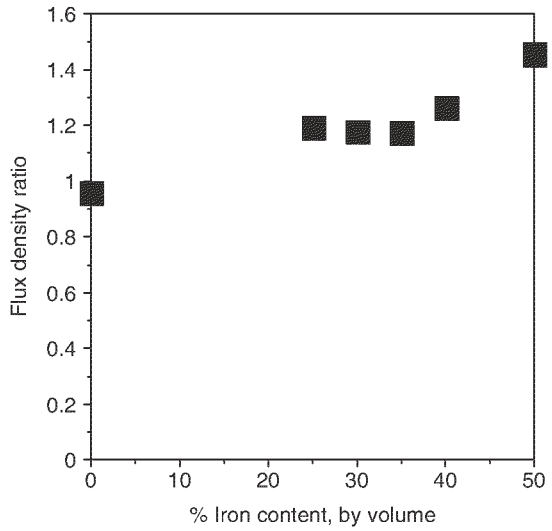

Figure 9. *Flux density ratios for MREs of different iron concentrations.*

the flux density was inclined to travel through the iron paths within the MRE.

Figure 8 indicates that for the field intensity values implemented here, the highest flux density value through the MRE would be no more than 0.2 T. This would lead to a maximum iron flux density of 0.67 T, well short of the 2 T necessary to saturate the iron particles inside an MRE. However, these values were found when a wire coil was wrapped around the MRE. This coil limited the motion and geometry that the MRE was able to be in; in fact, steel flux density values were found to be significantly higher when the absorbers were excited, and no coil was placed around the MREs. It is safe to assume that the absence of the coil allowed the flux density values to increase through the MRE as well.

Natural Frequency Response versus MRE Content in a Squeeze-Mode Device

The wire coil used for finding flux density through the MRE was not present during natural frequency and loss factor identification tests, as it limited the MRE motion. MREs of different iron composition were set up according to Figure 6. Each MRE was subjected to a white noise vibratory source, band-limited to 1000 Hz. The vibratory source's amplitude was set such that the vibration amplitude was small with respect to the size of the MRE, and left constant from test to test within the same elastomer. While it was not possible to ensure that amplitude levels were kept the same between elastomer compositions, they were constrained to the same order of magnitude, such that $\varepsilon \approx 0.001 \pm 0.0005$. This is below the threshold for which strain levels become a factor in either the Young's modulus (Bellan and Bossis, 2002) or the shear modulus (Jolly et al., 1996).

The natural frequency and loss factor information was found by applying a broadband signal through the shaker, band-limited to 1000 Hz. Time data from the accelerometers was collected, and FFTs of the data were taken. The absorber mass and MREs were modeled in the same manner as Ginder et al. did, as a single degree of freedom system described as (Ginder et al., 2002)

$$M_{\text{abs}}\ddot{x}_{\text{abs}} + K' x_{\text{abs}} = K' x_{\text{base}} \tag{11}$$

where x_{abs} is the displacement of the absorber mass, x_{base} is the displacement of the base mass, M_{abs} is the absorber mass and $K\prime$ is a complex stiffness such that $K\prime = Ke^{i\delta}$, and δ is the loss factor (Ginder et al., 2002). The natural frequency of this system was defined as $\omega_{\text{n}} = K/M_{\text{abs}}$. Equation (11) could then be rewritten as

$$\ddot{x}_{\text{abs}} + \omega_n^2 e^{i\delta} x_{\text{abs}} = \omega_n^2 e^{i\delta} x_{\text{base}}. \tag{12}$$

Assuming a harmonic excitation, the transfer function between the absorber mass and base mass can be found to be

$$H(\omega) = \frac{X_{\text{abs}}}{X_{\text{base}}} = \frac{\omega_{\text{n}}^2\left(\omega_{\text{n}}^2 - \omega^2 e^{i\delta}\right)}{\omega_{\text{n}}^4 - 2\omega_{\text{n}}^2\omega^2\cos(\delta) + \omega^4} \tag{13}$$

Using Equation 13, it can be found that the phase angle between x_{abs} and x_{base} will be equal to -90° when

$$\omega^2 = \omega_d^2 = \omega_n^2[\cos(\delta)]^{-1} \tag{14}$$

where ω_d is referred to the as the damped natural frequency, and will be defined as the frequency at which the phase angle equals -90° for the purposes of this article. Substituting Equation (14) into Equation (13) and solving for the magnitude of H yields

$$\left|H(\omega)\right| = \frac{\omega_d^2\cos(\delta)}{\left[\left(\omega_{\text{d}}^2 - 2\omega^2\right)\omega_{\text{d}}^2\cos^2(\delta) + \omega^4\right]^{1/2}}. \tag{15}$$

Equations (14) and (15) were used as analytical curves to fit to the experimental data, and to empirically determine two variables, ω_{n} and δ. The damped natural frequency, ω_d, was determined to be the frequency at which the phase angle of the transfer function crossed -90°. The error was defined as the difference between the amplitude of the frequency response of the data less the amplitude of the frequency response of the transfer function, or $e = \left|y(\omega)\right| - \left|H(\omega_{\text{p}},\delta_m)\right|$. The loss factor was found by using a least squares fit. This entails finding where the derivative of the squared error,

$$\frac{\partial(e^2)}{\partial\delta} = -2\sum_{m=1}^{20}\sum_{p=1}^{N}\left\{\left[y(\omega_p) - \left|H(\omega_p,\delta_m)\right|\right]\frac{\partial\left(\left|H(\omega_p,\delta_m)\right|\right)}{\partial\delta_m}\right\}, \tag{16}$$

equaled zero, where N is the number of data sampled, and $\delta_m = m\pi/40$. When Equation 16 was zero, the squared error was minimized. Once the loss factor had been found, the natural frequency was calculated using Equation (14). Figure 10 depicts data from a 35% MRE exposed to a magnetic field intensity of 18.3 kA/m, and fitted to a curve such that $\omega_n = 377$ Hz and $\delta = 0.43$ radians, by using Equations (14) and (15).

Using this data fitting technique, natural frequency data for absorbers were recorded at 2.3 kA/m field intensity level intervals from 0 to 18.3 kA/m. Figure 11 shows a plot of average natural frequencies for each MRE at 0 kA/m, with error bars indicating the SD in the samples. The 0 kA/m natural frequency increases as a function of iron content for MREs containing at least 30% iron. As mentioned in the section 'Experimental setup', MREs containing <30% iron by volume had talc powder added so that 30% of the overall MRE volume consisted of particulate matter. The increase in 0 kA/m natural frequency above iron contents of 30% is expected, then, as increasing iron content above 30%

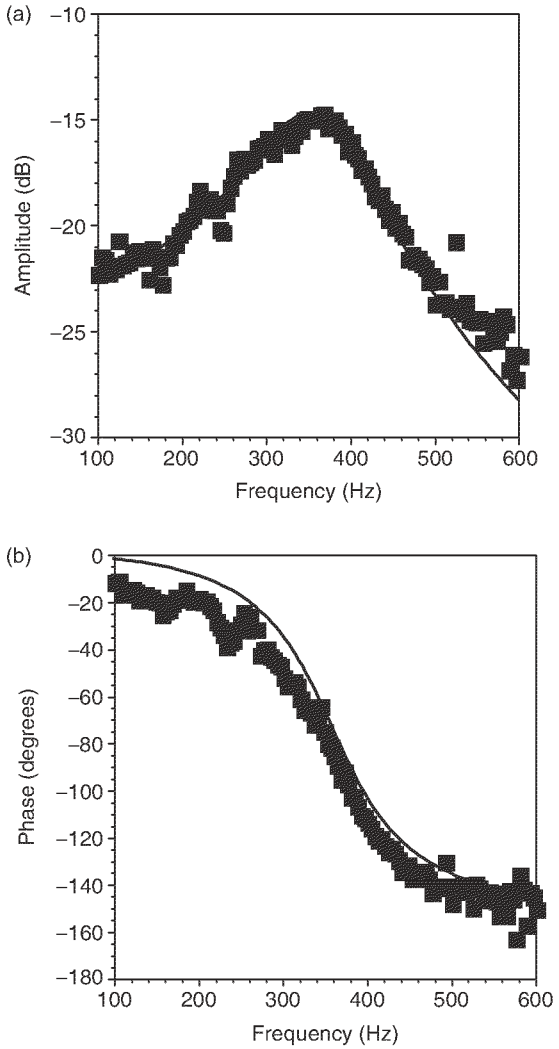

Figure 10. *(a) Experimental amplitude data and (b) phase angle data, fitted to a single-degree-of-freedom curve. ■ Experimental data, – calculated curve.*

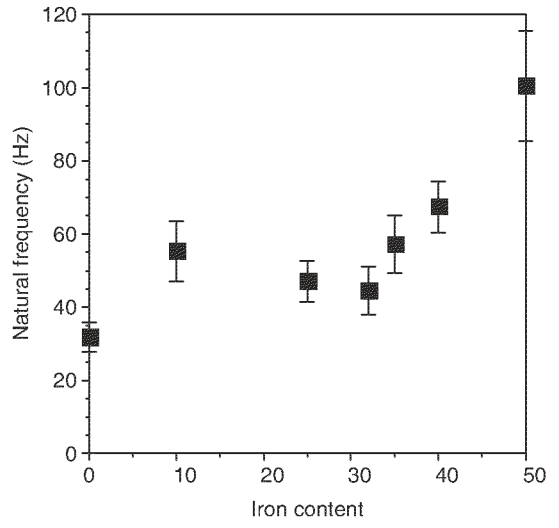

Figure 11. *Natural frequencies for squeeze mode absorbers containing different MREs at 0 kA/m field intensity. Error shows ± 1SD.*

increases the base natural frequency. The natural frequencies below 30% would be expected to be constant, and while that is roughly the case between 10 and 25%, the 0% iron is clearly significantly lower in natural frequency than any other MRE. While the precise reason for this is unknown, one reason for this discrepancy between expectation and outcome could be explained by the difference between the talc powder and the iron powder; while a concerted effort was made to find an inert powder close in size to the iron, the talc powder particles were smaller than the iron particles. This means that to make up the same volume, the elastomeric matrix must spread around more particulate surface area, which could change the results. It has also been found that particulate matter composition within an elastomer does in fact affect the composite material's moduli (Guth, 1945). However, the fact that the particles are aligned in chains have been empirically shown not to significantly affect the composite's moduli (Davis, 1999).

Figure 12(a) shows the absorber's average natural frequency, calculated using Equations (14) and (15), for each MRE recipe at each current level, normalized by the average natural frequency at 0 kA/m, or 'baseline frequency'. Each MRE recipe, with the exception of the 35% iron recipe, exhibited baseline natural frequencies for all current levels below about 16.1 kA/m, at which point the natural frequency increased. The 35% iron recipe showed increased natural frequencies beginning at 6.7 kA/m. Figure 12(b) shows the relative natural frequency increase between the frequency at 18.3 kA/m, to the zero-field frequency for each MRE recipe. The 35% iron MRE exhibited the largest relative natural frequency increase, with an ~510% increase in terms of relative change.

The natural frequency and loss factor characteristics for a 35% MRE in squeeze mode are shown against field intensity input in Figure 13. The loss factors were found to vary between 0.4 and 0.8. The baseline frequency was found to be 57 Hz and the maximum natural frequency was found to be 347 Hz. Since this device is operable between 57 and 100 Hz, and can be further tunable into higher frequency ranges, the use of MREs would yield an acceptable design in terms of operational frequency range.

Figure 13 also indicates that 35% MREs had loss factors that ranged between 0.4 and 0.8. Figure 14(a) shows average Q-values for MREs of different iron content, and Figure 14(b) shows 35% MREs in longitudinal, shear, and squeeze mode absorbers. Research into SSA performance has determined that damping ratio values of 0.27–0.42 yield optimal performance characteristics (Holdhusen and Cunefare, 2003). This translates to Q-values of 0.84–1.68. Figure 14(a) shows that most of the MRE recipes had average Q-values ranging between 0.8 and 2.5. Notable exceptions include

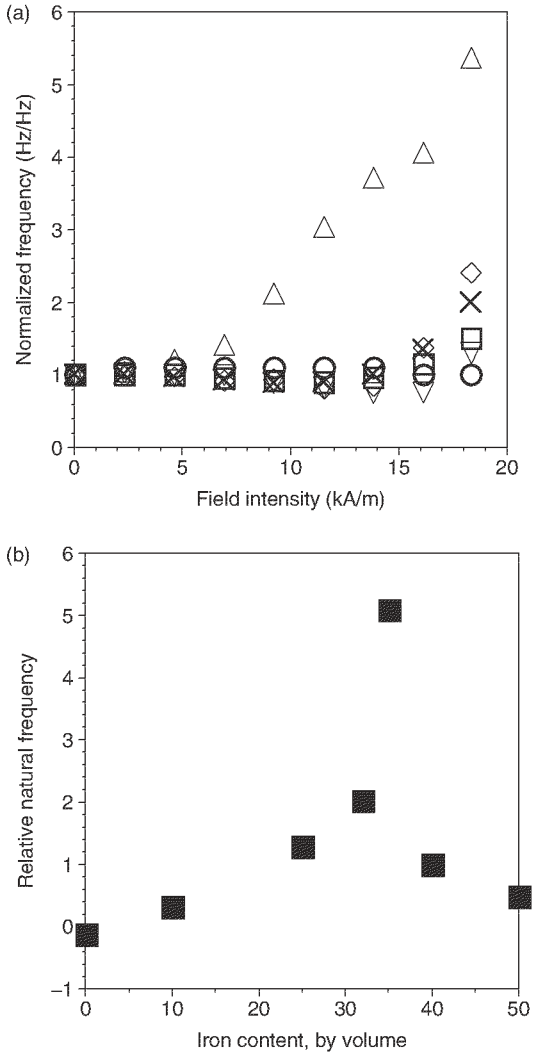

Figure 12. (a) Frequency normalized by the natural frequency at $H = 0$ kA/m vs field intensity for each iron content level. □ 50%, ×40%, △ 35%, ◇25%, ▽ 10%, ○ 0% and (b) Maximum frequency ratio vs iron content.

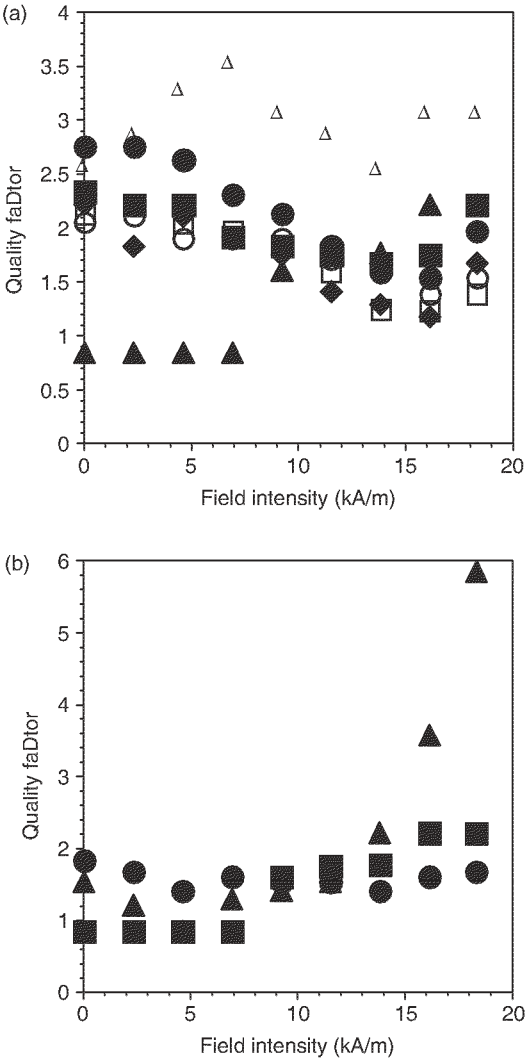

Figure 14. Quality factors for MREs at different field intensity levels: (a) different MREs in squeeze mode configuration: ■ 50%, • 40%, ▲ 35%, ◆ 32%, □ 25%, ○ 10%, △ 0% .and (b) 35% MREs in different absorber configurations: ■ longitudinal mode, ▲ shear mode, △ squeeze mode.

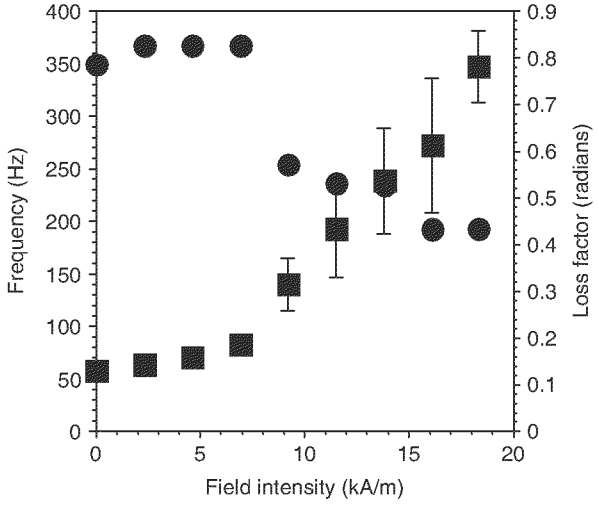

Figure 13. Natural frequency and loss factor vs field intensity for a 35% iron MRE placed in squeeze mode. ■ Frequency, • loss factor.

the 0% MRE, which has Q-values ranging between 2.6 and 3.6. Figure 14(b) also shows that the 35% longitudinal MRE also displays Q-values that are high for field intensity levels of 16.1 and 18.3 kA/m. Although the devices developed in this research would not be suitable for many TVA applications, the Q-values are in the range found by Holdhusen and Cunefare to be beneficial for SSA applications.

Natural Frequency Response in Longitudinal, Shear, and Squeeze-Mode Devices

Since 35% MREs place in squeeze mode absorbers were found to exhibit the larger frequency increases than any other MRE recipe tested, 35% MREs were then placed in three different absorber configurations to

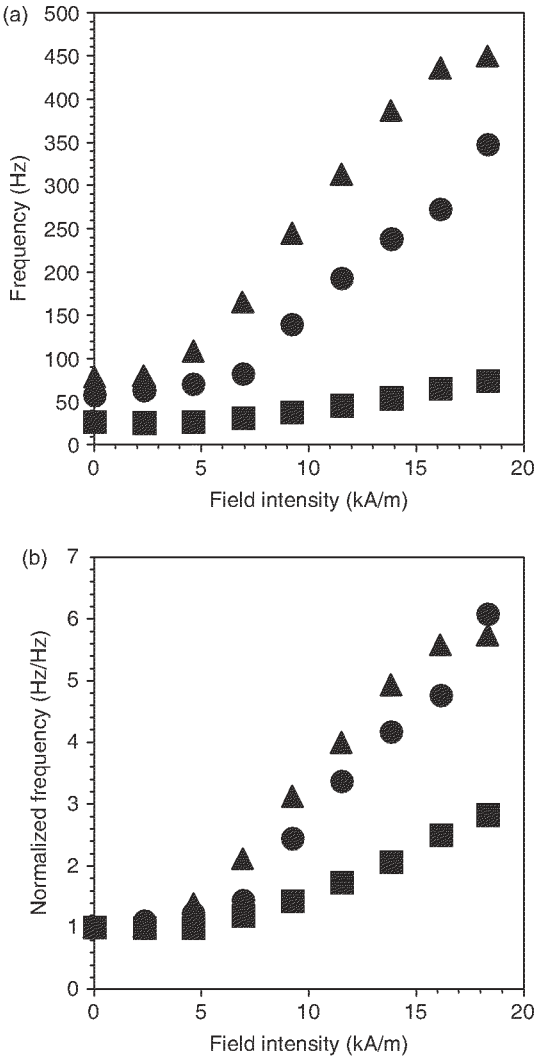

Figure 15. *(a) Natural frequencies for 35% MREs in shear, squeeze, and longitudinal modes, and (b) natural frequencies normalized to $H = 0$ kA/m natural frequency for 35% MREs in shear, squeeze, and longitudinal mode devices. ■ Longitudinal device, • squeeze device, ▲ shear device.*

determine how absorber configuration affects frequency changes. MREs containing 35% iron were placed into squeeze, shear, and longitudinal mode devices. Figure 15(a) shows natural frequencies of each device for field intensity inputs, and Figure 15(b) shows frequencies normalized by the natural frequency at $H = 0$ kA/m for different field intensity inputs. From the normalized plot, it can be seen that the squeeze mode device exhibited the largest frequency change, with a natural frequency increase of 507%, with a tunable frequency range of 57–347 Hz. The longitudinal mode device, operating in a frequency range of 78–449 Hz, exhibited a 473% frequency increase. However, the longitudinal mode device was magnetically saturated, as the 16.1 and 18.3 kA/m values are not different in a statistically significant manner. The shear mode device exhibited the smallest increase at 183%, with a frequency range of 26–74 Hz. While the longitudinal mode device appears to have saturated, the shear mode device has not. This could be due to the difference in how gravity affects the device in the different orientations. Gravity pulls the iron chains in a direction perpendicular to the line of magnetic field for the shear device; therefore, the magnetic field would have to become larger in order for the effects of gravity to be overcome.

The shear device exhibited a 183% increase in natural frequency, which corresponds to a 698% increase in stiffness. Note that Davis' (Davis, 1999) analysis of shear stiffening yielded

$$\frac{\Delta G_{\max}}{G(0)} = \frac{1.913\varphi \text{ MPa}}{G_0}, \tag{17}$$

which predicts a stiffness change of only 171%, much lower than what was found here. However, the elastomer used here was significantly softer than that used by Davis, and therefore any deviations between analytical predictions and experimental results would be accentuated for soft springs.

It is important to remember the difference between the intended application of this work, which is as a small vibration absorber, and the applications cited in works by Davis, Ginder, and other researchers in this area (Rigbi and Jilken, 1983; Davis, 1999; Ginder et al., 1999, 2001a, 2001b), which is primarily in load-bearing damping applications. While this work finds significant natural frequency increases that were not found in other research, the type of MRE employed for this work would also not be suitable for load-bearing applications.

The squeeze mode device exhibited the largest natural frequency change ratio, but the longitudinal mode device had a natural frequency change ratio that was comparable. The longitudinal mode device had a fixed gap of 1 cm, which held the iron particles close together. The squeeze mode device instead allowed the device to have a total gap of 1.3 cm, which meant that the iron particles were stretched apart. This means that a magnetic field would need to be applied to cause the squeeze mode device gap to decrease to 1 cm. However, the squeeze mode device has the capability to decrease the total gap to <1 cm, which means that the squeeze mode device should be able to exhibit a larger frequency change. It is apparent from Figure 15 that the longitudinal device has magnetically saturated, and will not exhibit a natural frequency increase with larger current values, but the squeeze mode device has not saturated, and could potentially exhibit an even larger frequency shift for larger current inputs.

Static Displacement in Squeeze Mode

One of the largest geometric differences between the longitudinal and squeeze mode devices was that the

MREs in the squeeze mode device were able to contract in response to magnetic fields. This contraction, or static displacement, was measured in response to different input magnetic field intensities to evaluate what the relationship between static displacement change and the frequency increase resulting from magnetic fields. Figure 16 shows the change in static displacement for a 35% MRE in a squeeze mode device against input magnetic field intensity. The displacement in Figure 16 was measured such that

$$\delta = \delta_0 - \delta_i, \tag{18}$$

where δ_0 is the static displacement when there is no magnetic field, and δ_i is the static displacement at the i^{th} field intensity level. This measures a net increase in static displacement; the overall distance between the base mass and absorber mass decreased with increasing magnetic field. The static displacement changed by 0.006 mm between 0 and 18.3 kA/m, but did not measurably change between 0 and 5 kA/m. The average natural frequency changed at lower field intensity levels than the static displacement. Although Figure 16 indicates that the static displacement decreases slightly with increasing field intensity, actual static displacement changes between 0 and 18.3 kA/m during natural frequency tests were large enough to be visible to the naked eye. One possible explanation for this discrepancy is that the wire coil heated after prolonged exposure to field intensity levels above 9 kA/m. However, the step current input test used to generate Figure 16 allowed only high current levels to travel through the wire coil for 2 s at a time, which was not sufficient to allow the coil to heat.

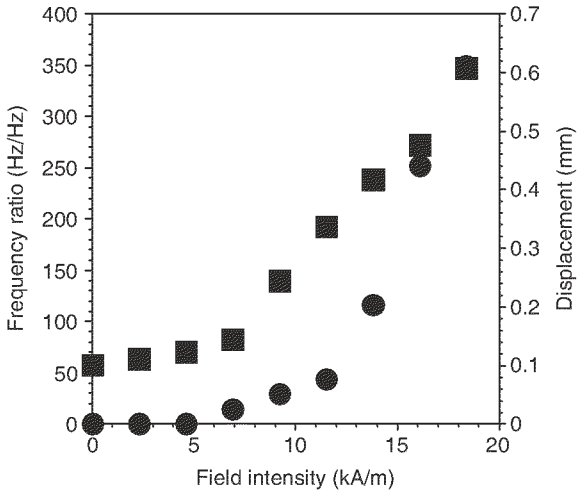

Figure 16. *Static displacement and natural frequency vs field intensity for a squeeze mode device with a 35% iron MRE. • Displacement, (mm), ■ average natural frequency (Hz).*

CONCLUSIONS

This work examined MREs placed in three different absorber configurations for use in an anticipated alternative to TVAs currently present on ATR 42 and 74 aircraft fuselages. MREs were cured and placed into three vibration absorber configurations; shear, longitudinal, and squeeze modes. The effect of the MRE's iron concentration on natural frequency shift was tested in the shear mode device. MREs that were composed of 35% iron by volume yielded the largest natural frequency shift between 0 and 18.3 kA/m field intensity increase, an increase of 507%. MREs containing 35% iron were placed into shear and longitudinal mode devices, and their natural frequencies increased by 183 and 473%, respectively. MREs placed into all three devices exhibited Q-values between 0.8 and 2, for the most part. While this is low for traditional TVA values, it is an appropriate Q-value range for semiactive applications such as SSAs MREs are therefore concluded to be an appropriate material for use in semiactive vibration absorber applications.

The squeeze mode device exhibited the largest frequency shift of 507%, although the longitudinal mode device exhibited a frequency shift in the same range. While the longitudinal mode device exhibited signs of magnetic saturation, the squeeze mode had not yet saturated and could possibly exhibit even larger natural frequency changes at higher magnetic fields. The squeeze mode device's ability to allow static displacement decreases in the presence of a magnetic field may lead to a larger frequency shift at even higher field intensity levels.

The primary difference between the longitudinal mode device and the squeeze mode device was that the absorber mass in the latter had a static displacement that was dependent upon applied forces, as opposed to being constrained by geometric conditions. To measure the effect of magnetic forces on static displacement, the squeeze mode device's static displacement was tested as a function of input field intensity. The spring's length (static displacement) decreased as the input field intensity increased, particularly when the magnetic field intensity was above 5 kA/m.

This work demonstrates that if a vibration absorber has flexible design constraints, a squeeze mode device will yield the largest frequency shift for active, semiactive, and hybrid vibration absorber design configurations. MREs comprised of 35% iron content by volume yielded the largest frequency shifts when incorporated in squeeze mode device.

REFERENCES

Lord MR Solutions (2001). "Magnetic Circuit Design," Engineering Notes.

Abe, M. and Igusa, T. 1996. "Semi-active Dynamic Vibration Absorbers for Controlling Transient Response," *Journal of Sound and Vibration*, 198(5):547–569.

Bellan, C. and Bossis, G. 2002. "Field Dependence of Viscoelastic Properties of MR Elastomers," *International Journal of Modern Physics B*, 16(17–18):2447–2453.

Bossis, G., Abbo, C., Cutillas, S., Lalis, S. and Metayer, C. 1999. "Electroactive and Electrostructured Elastomers," *International Journal of Modern Physics B*, 15(6–7):564–573.

Cunefare, K.A. 2000. "State-switched Absorber for Vibration Control of Point-excited Beams," *Journal of Intelligent Material Systems and Structures*, 13(2–3):97–105.

Cunefare, K.A., DeRosa, S., Sadegh, N. and Larson, G. 2000. "State-switched Absorber for Semi-active Structural Control," *Journal of Intelligent Material Systems and Structures*, 11(4):300–310.

Davis, L.C. 1999. "Model of Magnetorheological Elastomers," *Journal of Applied Physics*, 85(6):3348–3351.

Drozdov, A.D. and Dorfmann, A. 2001. "The Stress-strain Response and Ultimate Strength of Filled Elastomers," *Computational Materials Science*, 21(3):395–417.

Ginder, J.M., Clark, S.M., Schlotter, W.F. and Nichols, M.E. 2002. "Magnetostrictive Phenomena in Magnetorheological Elastomers," *International Journal of Modern Physics B*, 16(17–18): 2412–2418.

Ginder, J.M., Schlotter, W.F., Elie, L.D. and Clark, S.M. 2001a. "Magnetorheological Elastomers in Tunable Vibration Absorbers," *SPIE Smart Structures 2001*, Newport Beach, CA.

Ginder, J.M., Nichols, M.E., Elie, L.D. and Tardiff, J.D. 1999. "Magnetorheological Elastomers: Properties and Applications," *SPIE Conference on Smart Materials Technologies*, Newport Beach, CA.

Ginder, J.M., Schlotter, W.F. and Nichols, M.E. 2001b. "Controllable-stiffness Components Based on Magnetorheological Elastomers," *Smart Structures and Materials 2000 – Smart Structures and Integrated Systems*, Newport Beach, CA.

Guth, E. 1945. "Theory of Filler Reinforcement," *Journal of Applied Physics*, 16(20):20–25.

Holdhusen, M. and Cunefare, K.A. 2003. "Damping Effects on the State-switched Absorber Used for Vibration Suppression," *Journal of Intelligent Material Systems and Structures*, 14(9):551–561.

Hrovat, D., Baral, P. and Rabins, M. 1983. "Semi-active Versus Passive or Active Tuned Mass Dampers for Structural Control," *ASCE Journal of Engineering Mechanics*, 109(3): 691–705.

Jolly, M.R., Carlson, J.D., Munoz, B.C. and Bullions, T.A. 1996. "The Magnetoviscoelastic Response of Elastomer Composites Consisting of Ferrous Particles Embedded in a Polymer Matrix," *Journal of Intelligent Material Systems and Structures*, 7(November):613–622.

Karnopp, D., Crosby, M.J. and Harwood, R.A. 1974. "Vibration Control Using Semi-active Force Generators," *Journal of Engineering for Industry*, 96(Series B, no. 2):619–626.

Karnopp, D.C. 1973. "Active and Passive Isolation of Random Vibration, In: Snowdon, J.C. (ed.), *Isolation of Mechanical Vibration, Impact, and Noise*, Vol. 1, pp. 64–86, ASME. New York, NY.

Meinecke, E.A. and Taftaf, M.I. 1988. "Effect of Carbon Black on the Mechanical Properties of Elastomers," *Rubber Chemistry and Technology*, 61(3):534–547.

Meirovitch, L. 1986. *Elements of Vibration Analysis*, McGraw Hill, New York.

Payne, A.R. and Whittaker, R.E. 1971. "Low Strain Dynamic Properties of Filled Rubber," *Rubber Chemistry Technology*, 44: 440–478.

Rigbi, Z. and Jilken, L. 1983. "The Response of an Elastomer Filled with Soft Ferrite to Mechanical and Magnetic Influences." *Journal of Magnetism and Magnetic Materials*, 37:267–276.

Shiga, T., Okada, A. and Kurauchi, T. 1995. "Magnetroviscoelastic Behavior of Composite Gels," *Journal of Applied Polymer Science*, 58(4):787–792.

Sun, J.Q., Jolly, M. and Norris, M. 1995. "Passive, Adaptive, and Active Tuned Vibration Absorbers – A Survey," *Journal of Vibration and Acoustics*, 177(3B):234–242.

Zhou, G.Y. and Jiang, Z.Y. 2004. "Deformation in Magnetorheological Elastomer and Elastomer-Ferromagnet Composite Driven by a Magnetic Field," *Smart Materials and Structures*, 13(2):309–316.

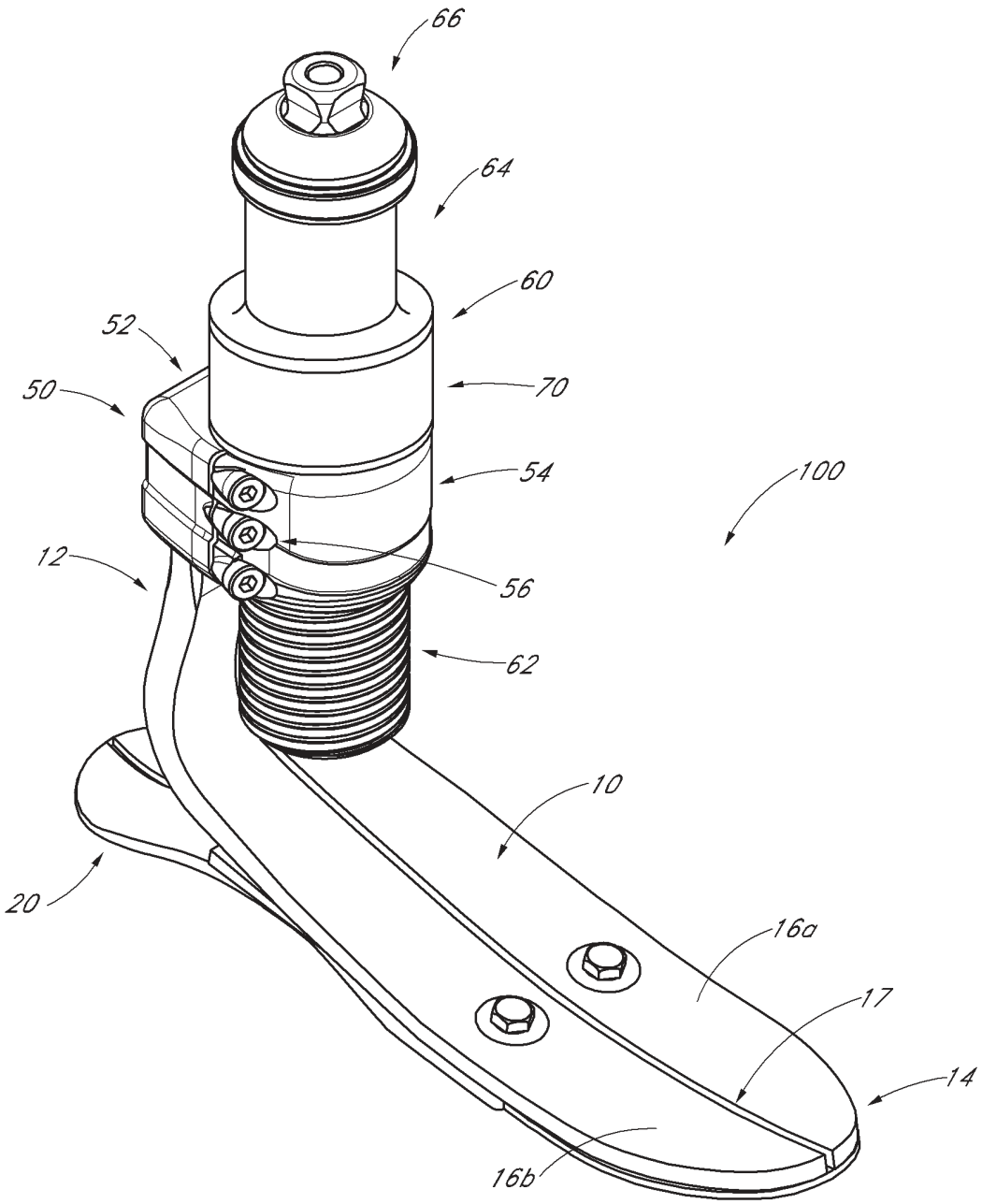

FIG. 1A

FIG. 1B

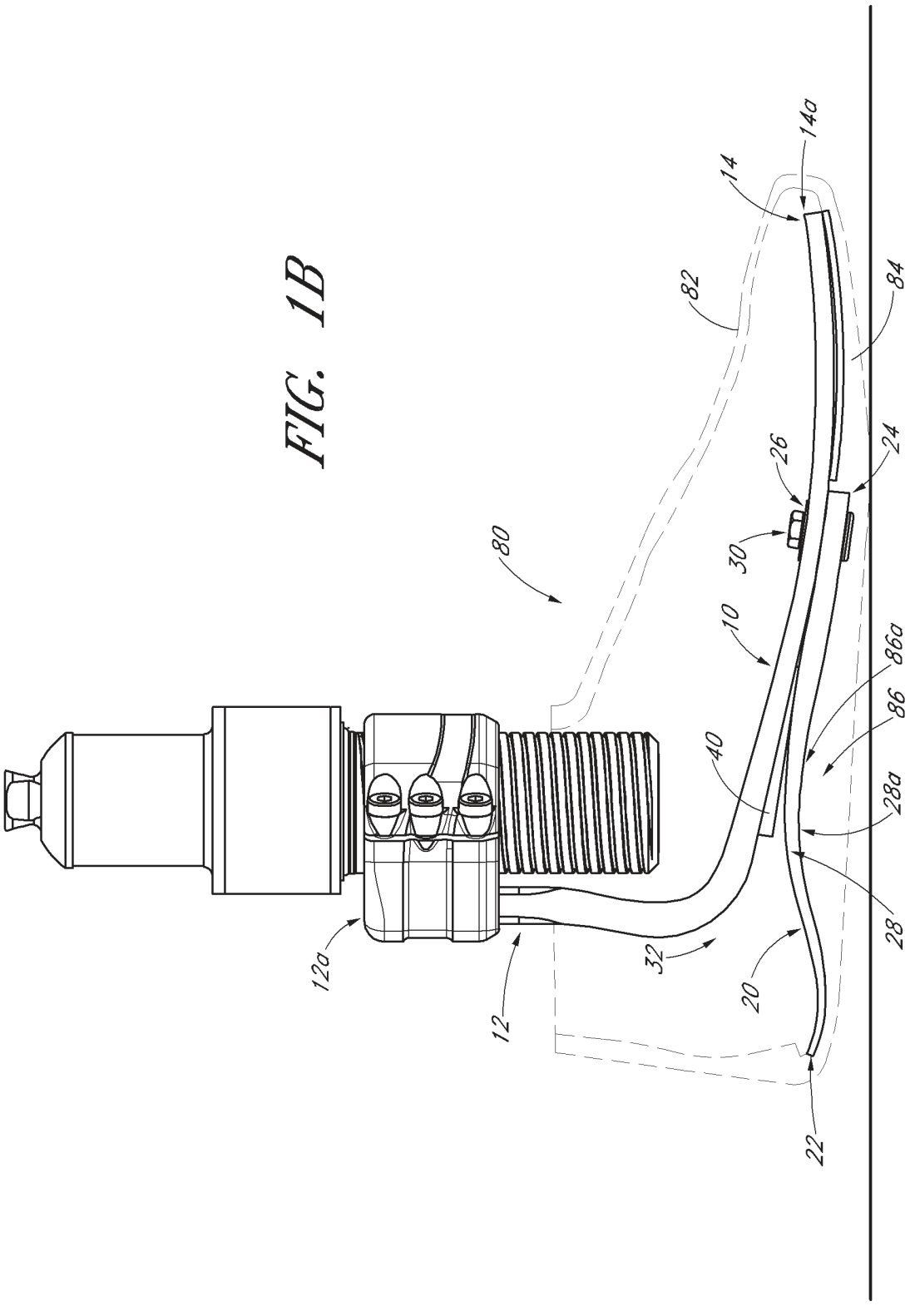

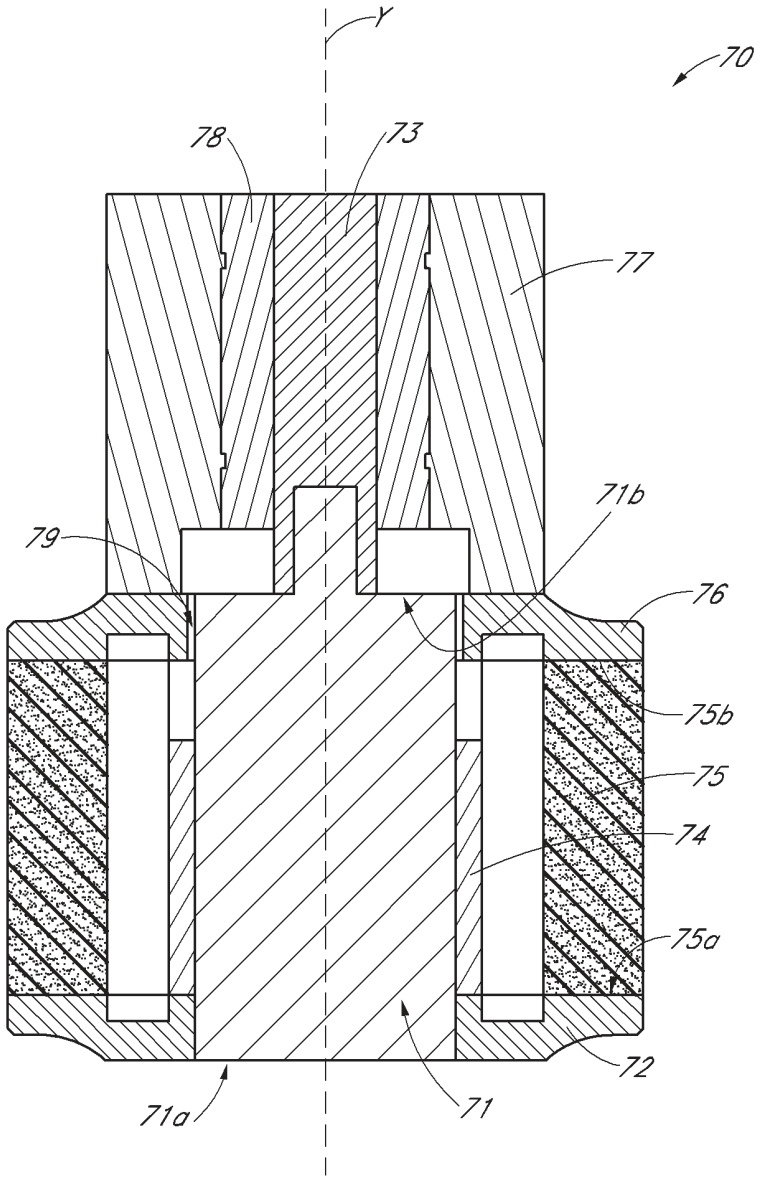

FIG. 2

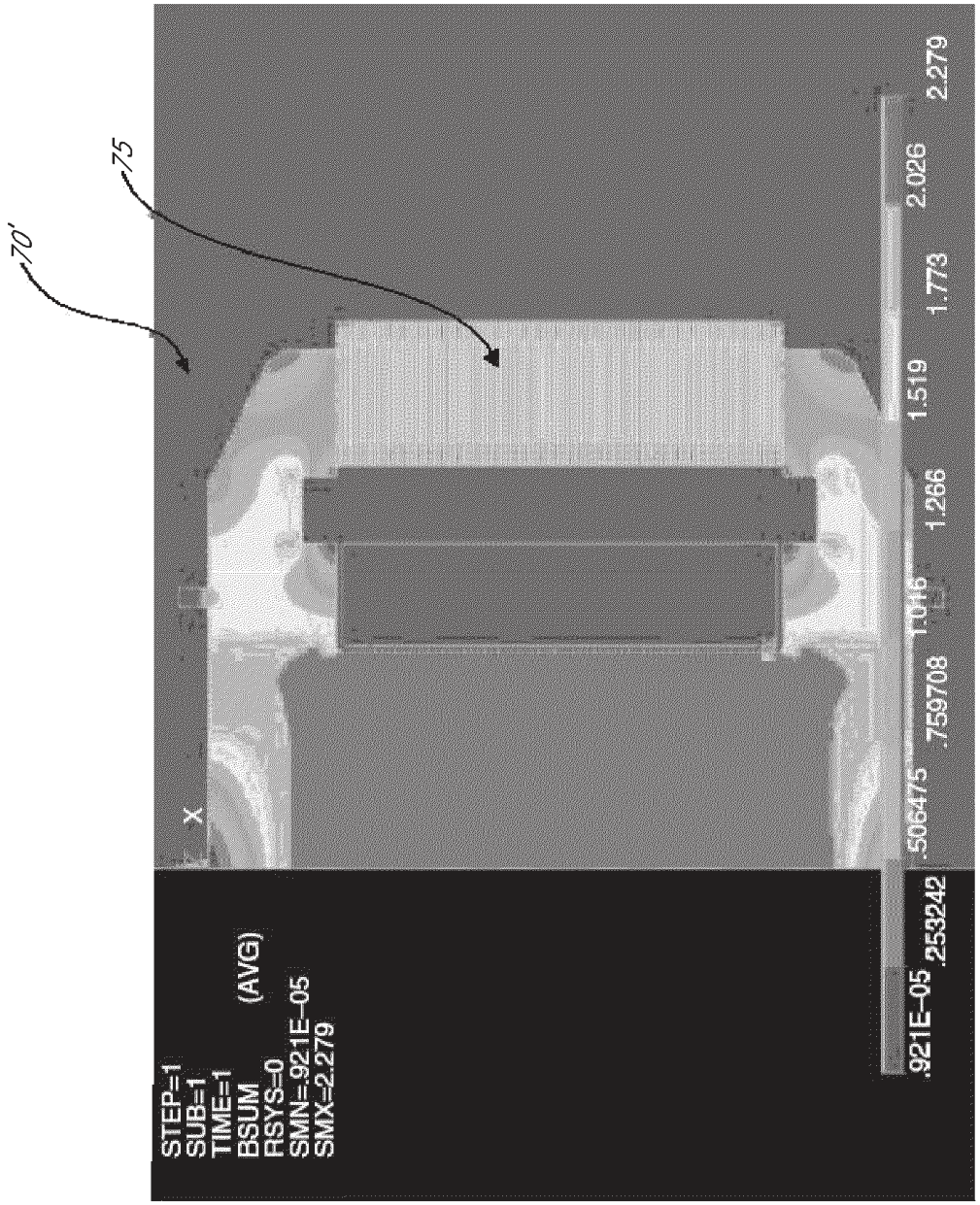
70'
75
STEP=1
SUB=1
TIME=1
BSUM (AVG)
RSYS=0
SMN=.921E-05
SMX=2.279
.921E-05
.253242
.506475
.759708
1.013
1.266
1.519
1.773
2.026
2.279

FIG. 3

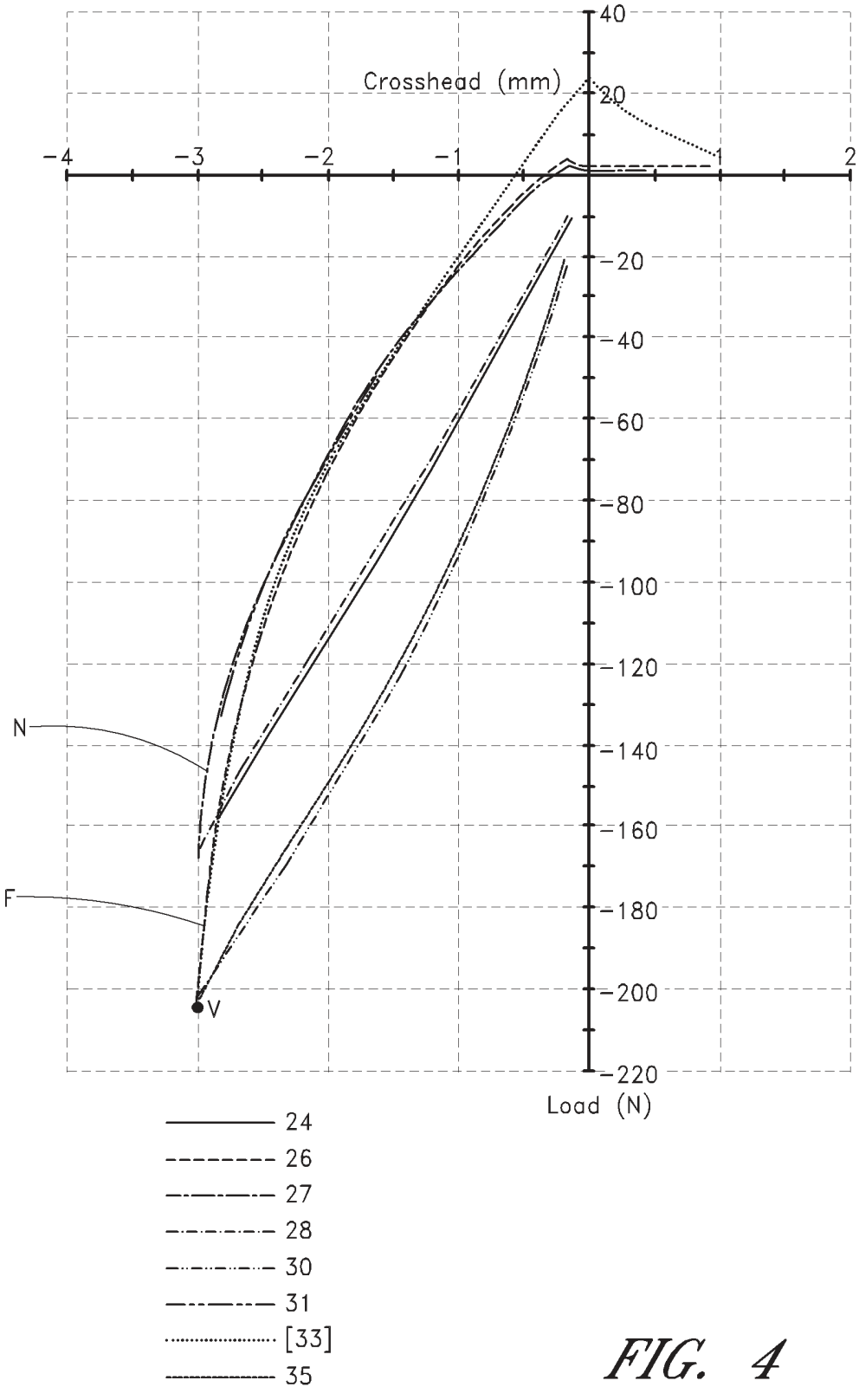
Crosshead (mm)
40
20
-4
-3
-2
-1
1
2
-20
-40
-60
-80
-100
-120
-140
-160
-180
-200
-220
Load (N)
N
F
V
24
26
27
28
30
31
[33]
35

FIG. 4

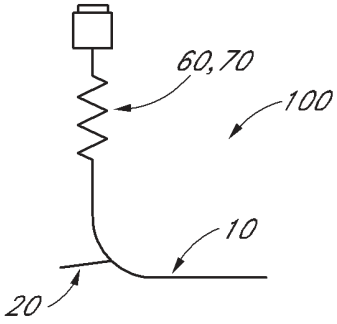

FIG. 5A

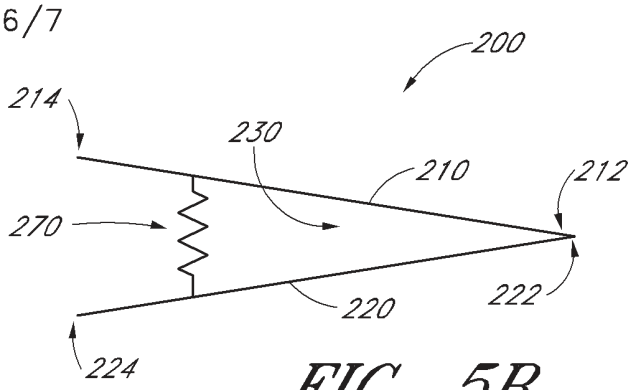

FIG. 5B

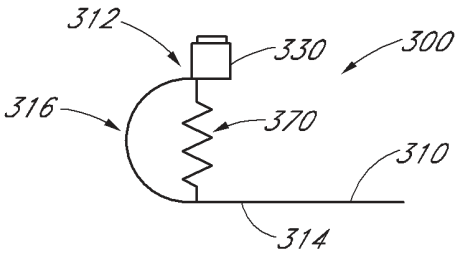

FIG. 5C

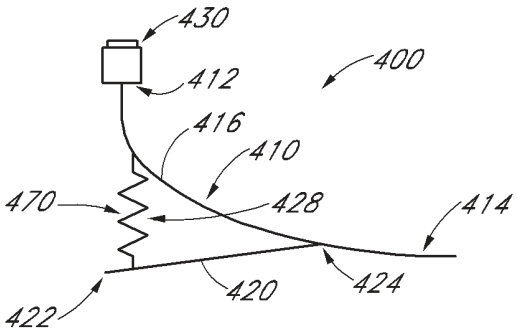

FIG. 5D

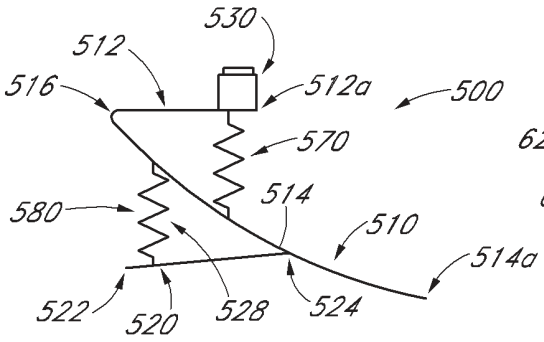

FIG. 5E

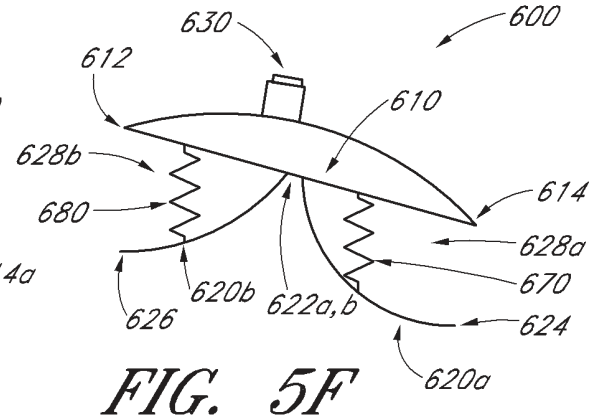

FIG. 5F

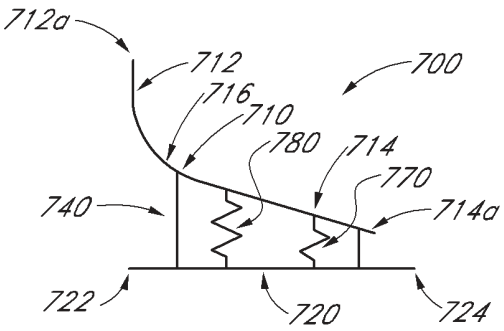

FIG. 5G

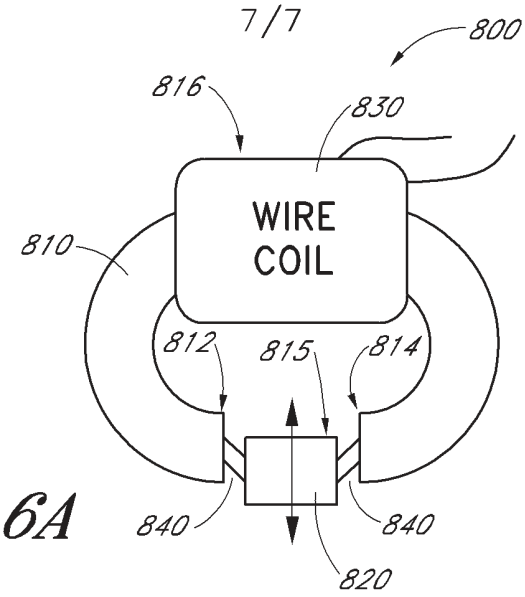

FIG. 6A

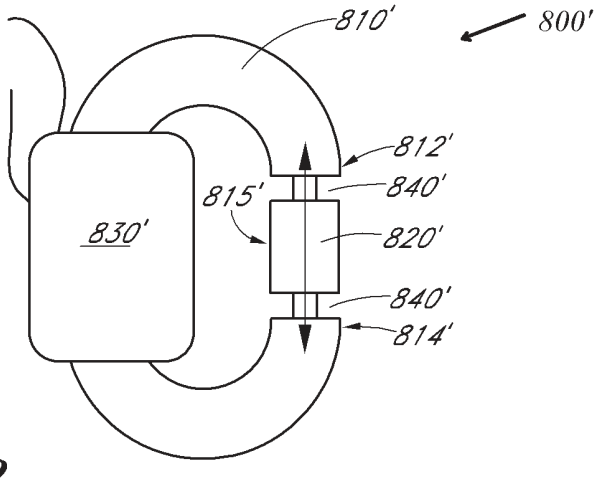

FIG. 6B

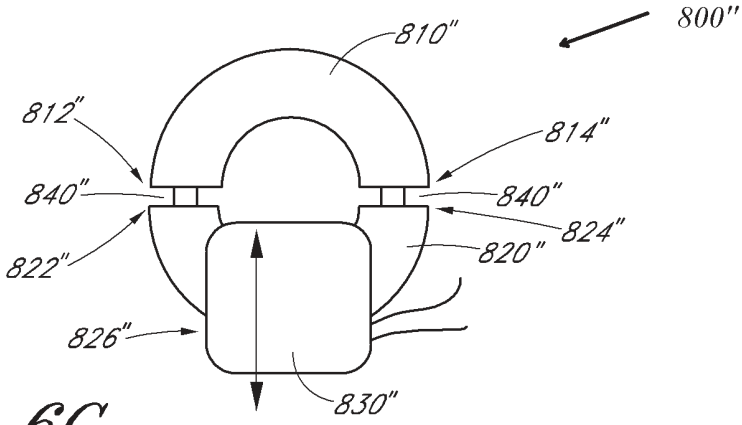

FIG. 6C